**Roles and Regulation of the Lipid Kinase, Vps34**

by

Noah Steinfeld

A dissertation submitted in partial fulfillment
of the requirements for the degree of
Doctor of Philosophy
(Cellular and Molecular Biology)
in the University of Michigan
2021

Doctoral Committee:

Professor Lois S. Weisman, Chair
Professor Robert S. Fuller
Associate Professor Ajit P. Joglekar
Professor Daniel J. Klionsky
Professor Kristen J. Verhey

“I cannot remember the books I have read any more than the meals I have eaten; even so, they have made me.”

Ralph Waldo Emerson

Noah Steinfeld

steinoah@umich.edu

ORCID iD: 0000-0003-1668-522X

## ACKNOWLEDGEMENTS

I would like to thank Dr. Lois Weisman for her mentorship throughout the years and for her trust to give me the flexibility to explore different areas of biology. She helped to guide me through the good and bad times and never gave up on me.

I would like to thank the members of my thesis committee, Dr. Robert Fuller, Dr. Ajit Joglekar, Dr. Dan Klionsky, and Dr. Kristen Verhey, for their helpful and insightful discussion and feedback over the years. I especially would like to thank Dr. Ajit Joglekar for his helpful discussions of quantifying colocalization.

I would like to thank members of the Weisman lab, past and present: Dr. Michael Lang, Dr. Junya Hasegawa, Dr. Sai Srinivas Panapakkam Giridharan, Dr. Guangming Luo, Dr. Ron Benyair, Dr. Pilar Rivero Rios, Lily Hahn, Annie Zhang, Alim Habib, and Monica Blazevic. Their knowledge, advice, support, and positive attitude made it fun to come to lab every day. I am especially grateful for Dr. Beth Strunk for being my first mentor in the lab, for answering a million questions, big and small, and always being supportive of my ideas. I would like to thank Dr. Sara Wong for being an aspirational role model of an older graduate student and helping me with yeast biology again and again. I would like to thank Emily Kauffman for making the lab run smoothly and doing a hundred little things to make my life in lab a little easier. Thank you also to the undergraduate and

high school students I had the pleasure of working with, Anna Morrison, Diogenes Lopez-Urioso, and Sarah Zhao, for bringing a great attitude and energy to the lab. You all taught me so much and I am excited to watch your scientific careers blossom. I especially want to thank Anna Morrison, who did an incredible amount of work with me and was reliable, enthusiastic, and dedicated.

I would like to thank our collaborators in the Klionsky lab, Dan Klionsky and his graduate students Vik Lahiri and Shree Padma Metur, for their advice and hard work on the autophagy portion of our paper. Their expertise was invaluable in the completion of that study. I would also like to thank a number of scientists for sharing reagents that were critical for my research including Dr. Ming Li, Dr. Mara Duncan, Dr. Christopher Burd, and Dr. Fulvio Reggiori. I would like to thank Joseph Dickens of Consulting for Statistics, Computing, and Analytics Research at the University of Michigan for his help performing statistical analysis on the degradation of Mup1-GFP.

I would like to thank the Program in Biomedical Sciences, the Cellular and Molecular Biology Program, the Life Sciences Institute, and the Rackham Graduate School for their support. Thank you to Margarita Bekiares, Pat Ocelnik, Lauren Perl, Nancy Hobbes, April Miller, Sue Clements, and Maggie Herron for their administrative support. I would like to thank Dr. Robert Fuller, Dr. Manoj Puthenveedu, Dr. Kenneth Cadigan, Dr. Kathleen Collins, and Dr. Vernon Carruthers for their leadership and support through the Cellular and Molecular Biology Program.

I would like to thank Dr. Naveen Bangia and Dr. Asoke Mal for taking a chance on me and giving me my first opportunities to work in a biology lab as a high school student. I would like to thank Dr. Mark Hochstrasser and his students, Dr. Bebiana Sá Moura and Dr. Nicole Eisele, for introducing me to yeast research and for their patience with me as I learned, as well as Dr. Robert Tomko who taught me that working in a science lab can be fun.

Most of all, I would like to thank my friends and family for their love and support for all these years. To my Mom, Dad, and my brother Ezra for always being there. To Alyssa, Katelyn, and Mark for all the time we spent on CDB 530 homework, football Saturdays, and intramural volleyball. To my former roommates, Ben and Will, for watching a lot of basketball and for being easy to live with. Finally, thank you especially to Abby for being patient while I was finishing graduate school and for uprooting your life to live in Ann Arbor during the pandemic. Without your help, support, inspiration, and love, it would have taken a lot longer to finish my dissertation.

## TABLE OF CONTENTS


ACKNOWLEDGEMENTS ii

LIST OF FIGURES vii

LIST OF TABLES x

ABSTRACT xi

CHAPTER I: Introduction 1

Phosphoinositide lipids 1

Identifying the yeast PI 3-kinase, Vps34, in *S. cerevisiae* 3

The pseudokinase, Vps15, is required for PI3P synthesis 4

Vps34 and Vps15 act within at least two large regulatory complexes 5

Structural insights into the PI 3-kinase complexes 7

Turnover of PI3P in yeast 8

PI3P regulates a number of downstream pathways in yeast 9

PI3P is converted into other PPI lipids 9

PI3P is required for multiple retrograde transport pathways 9

PI3P is required for ESCRT function 12

PI3P in the fusion of vesicles to the vacuole 13

PI3P is required for multiple steps in autophagy 13

PI3P plays a poorly understood role in pheromone signaling 15

Poorly understood phenotypes of *vps34Δ* cells 16

References 22
CHAPTER II: Elevating PI3P Drives Select Downstream Membrane Trafficking Pathways 30
Introduction 30
Results and Discussion 31
Generation of hyperactive Vps34 mutants 31
Hyperactive Vps34 increases retrograde transport of Atg27 35
Hyperactive Vps34 does not affect ESCRT-dependent degradation of amino acid transporters Ypq1 or Mup1 37
Hyperactive Vps34 inhibits a late step in autophagy 39
Conclusions 45
References 73
CHAPTER III: Future Directions 77
Evidence for another PI 3-kinase in yeast 77
Gleaning mechanistic insights into the regulation of Vps34 78
Additional screens to identify hyperactive mutants in PI 3-kinase complex components 79
Evidence and potential roles for a third Vps34-containing complex 81
A method of identifying the members of a third PI 3-kinase complex 84
Testing hyperactive Vps34 mutants in mammalian cells 85
References 98
CHAPTER IV: Methods 101
References 111

## LIST OF FIGURES


Figure 1.1 Interconversion of PPIs by PPI kinases and phosphatases in mammals and yeast 17

Figure 1.2 A model of Vps34 activation 18

Figure 1.3 Summary of the phenotypes observed in cells with PI 3-kinase complex proteins knocked out 19

Figure 1.4 Schematic illustrating the two known PI 3-kinase complexes in yeast and their functions 20

Figure 1.5 Schematic indicating several PI3P-dependent intracellular trafficking pathways in yeast 21

Figure 2.1 Generation of hyperactive Vps34 mutants 50

Figure 2.2 Generation of hyperactive Vps34 mutants based on a high-resolution structure of the Vps34-Vps15-Vps30-Vps38 complex 52

Figure 2.3 Generation of hyperactive Vps34 mutants via a mutant screen 54

Figure 2.4 Hyperactive Vps34-EDC does not affect the protein levels or localization of Vps34 56

Figure 2.5 Hyperactive Vps34-EDC does not affect the localization of some members of the PI(3,5)$P_2$ kinase complex 58

Figure 2.6 Hyperactive Vps34 increases retrograde transport of Atg27 60

Figure 2.7 Hyperactive Vps34 increases retrograde transport of Atg27 62

Figure 2.8 Hyperactive Vps34 does not affect ESCRT-dependent degradation of amino acid transporters Ypq1 or Mup1 64
Figure 2.9 Hyperactive Vps34 inhibits a late step in autophagy 66
Figure 2.10 Hyperactive Vps34 inhibits a late step in autophagy 68
Figure 2.11 Hyperactive Vps34 inhibits a late step in autophagy 70
Figure 2.12 Hyperactive Vps34-EDC may lead to a modest decrease in homotypic vacuole fusion 72
Figure 3.1 Knockout of Vps34 may not lead to a complete loss of PI3P in yeast 88
Figure 3.2 Only some hyperactive Vps34 mutations rescue growth of the K759D mutant 89
Figure 3.3 All hyperactive Vps34 mutants tested are able to rescue growth of a *vps30Δ* yeast strain on 15mM $ZnSO_4$ at 33°C 90
Figure 3.4 New screening conditions for hyperactive mutations in Vps34 91
Figure 3.5 Mutations in Vps34 plasmids that were isolated from colonies that rescue growth of *vps30Δ* cells grown at 33°C on plates containing 15mM $ZnSO_4$ 92
Figure 3.6 Crystal structure of the helical and kinase domains of Vps34, indicating residues identified in the hyperactive Vps34 mutant screen 93
Figure 3.7 Vps34 mutations based on mutants obtained from a hyperactive mutant screen do not elevate PI3P 94
Figure 3.8 PI 3-kinase Complex II is required for proper Mrl1-Envy localization 95

Figure 3.9 While Vps34 and Vps15 are necessary for internalization of Ypq1-SBP-EGFP, neither PI 3-kinase Complex I or II is required 96

Figure 3.10 Yeast Vps34 mutations at residues that correspond with mutations in human p110α that were listed multiple times in the COSMIC database do not elevate PI3P 97

## LIST OF TABLES


| | | |
|---|---|---|
| Table 4.1 | Yeast strains used in this study | 109 |
| Table 4.2 | Yeast plasmids used in this study | 110 |

## ABSTRACT

Lipids serve as structural components of biological membranes. Additionally, a small subset of lipids serve as signaling molecules. Phosphoinositide (PPI) lipids are a class of lipids that are low in abundance, but nonetheless control a variety of signal transduction pathways and play crucial roles in cellular homeostasis. PPI species are generated by phosphorylation of phosphatidylinositol (PI) on the 3, 4, or 5 position of its inositol ring head group in every combination to yield a total of seven PPI species. The levels of these lipids are dynamically regulated by PPI lipid kinases and phosphatases that interconvert PPI lipids in response to stimuli. The generation of a specific PPI species on a membrane leads to the recruitment of distinct effector proteins that can then perform downstream functions.

The dynamic regulation of PPI lipids suggests that in addition to being required for specific pathways, changes in PPI lipids may drive downstream processes. Most of the downstream functions of PPI lipids have been identified in studies that use knockout or knockdown of PPI kinases to deplete a specific PPI lipid and thereby test the necessity for that PPI species in a process. However, little is known about the impact of elevating phosphoinositides. Understanding the impact of elevating phosphoinositides is critical as the levels of PPI lipids can be dynamically elevated in response to stimuli.

To test this hypothesis, we elevated phosphatidylinositol-3-phosphate (PI3P) levels by generating hyperactive alleles of the yeast phosphatidylinositol 3-kinase, Vps34. We find that hyperactive Vps34 has complex effects on cellular function. Hyperactive Vps34 drives phosphatidylinositol 3,5 bisphosphate ($PI(3,5)P_2$) synthesis during hyperosmotic shock and retrograde transport from the vacuole. This demonstrates that elevating PI3P can accelerate some pathways and is rate limiting in those pathways. We also show that hyperactive Vps34 does not affect ESCRT (endosomal sorting complexes required for transport) function at endosomes or on the vacuole. Thus, elevating PI3P does not always increase the overall rate of a complex pathway. We also show that elevating PI3P can delay a pathway. Hyperactive Vps34 does not affect the induction of autophagy, but inhibits late steps in autophagy, in part via a delay in disassembly of the autophagy machinery from the surface of mature autophagosomes and also a delay in fusion of autophagosomes with the vacuole. This latter defect is likely due to a more general defect in vacuole fusion, as evidenced by an increase in the number of vacuole lobes per cell, which is consistent with a defect in homotypic vacuole fusion.

Overall, these studies suggest that stimulus-induced elevation of PI3P levels regulates some, but not all, PI3P-dependent membrane trafficking pathways and that phosphoinositide lipids are commonly rate-limiting in pathways where they are required. Because the hyperactive Vps34 mutations we have identified are conserved in the mammalian Vps34 homolog PIK3C3, we think it is likely that these mutations in PIK3C3 will elevate PI3P. Thus, in the future, this work provides a roadmap to test the downstream effects of elevating PI3P in mammalian systems.

# CHAPTER I

## Introduction[1]

### Phosphoinositide lipids

Lipids are generally structural components of a biological membrane. In addition, a small subset of lipids can also act as signaling molecules. Phosphoinositide (PPI) signaling lipids are a low abundance class of molecules that control a variety of signal transduction pathways and play crucial roles in cellular homeostasis. PPI species are generated by phosphorylation of phosphatidylinositol (PI) on the 3, 4, or 5 position of its inositol ring head group in every combination to yield a total of seven PPI species. All seven species can be detected in mammalian cell types, whereas only four are readily detectable in *Saccharomyces cerevisiae*. In cells, the levels of these lipids are dynamically regulated by PPI lipid kinases and phosphatases that interconvert PPI lipids in response to stimuli (Strahl and Thorner, 2007; Sasaki *et al.*, 2009; Balla, 2013; Shisheva *et al.*, 2015; Wallroth and Haucke, 2018; Dickson and Hille, 2019) (Figure 1.1). The dynamic regulation of PPI lipids is best demonstrated during hyperosmotic shock in *S. cerevisiae*, which leads to a transient 15 to 20-fold elevation in

[1] Sections of this chapter are adapted from a published paper: Steinfeld, N., Lahiri, V., Morrison, A., Metur, S.P., Klionsky, D.J., and Weisman, L.S. (2021). Elevating PI3P drives select downstream membrane trafficking pathways. Mol Biol Cell 32, 143-156.

phosphatidylinositol 3,5 bisphosphate ($PI(3,5)P_2$) via activation of the PI3P 5-kinase, Fab1 (Duex *et al.*, 2006). The changes in PPIs are controlled spatially by the specific localization of lipid kinases and phosphatases, and temporally via specific activation of these enzymes.

The generation of specific PPI species on membranes recruits distinct effector proteins that regulate downstream pathways (reviewed in (Schink *et al.*, 2016)). An assumption in the field is that these PPI lipids are coordinated to control complicated multi-step pathways. However, this is generally difficult to document. One pathway where coordination occurs is in the interconversion of PPI lipids regulating clathrin-mediated endocytosis (CME) in mammals (reviewed in (Kaksonen and Roux, 2018)). CME begins with the generation of $PI(4,5)P_2$ from PI4P by PIPK1 on the plasma membrane (Barbieri *et al.*, 2001; Di Paolo *et al.*, 2004), leading to the recruitment of a number of critical clathrin adaptors, including AP-2 (Rohde *et al.*, 2002; Padron *et al.*, 2003), CALM (Ford *et al.*, 2001; Itoh *et al.*, 2001), and other clathrin adaptors and proteins that induce membrane curvature (reviewed in (Posor *et al.*, 2015)). The recruitment of synaptojanin isoform p170 is then thought to turnover $PI(4,5)P_2$ to PI4P (Perera *et al.*, 2006), enabling the phosphorylation of PI4P to $PI(3,4)P_2$ by PI3KC2A (Posor *et al.*, 2013). $PI(3,4)P_2$ is believed to then further recruit SNX9, leading to increased membrane curvature and dynamin recruitment (Schoneberg *et al.*, 2017). Following vesicle fission, another synaptojanin isoform, p145, is recruited, dephosphorylating the remaining $PI(4,5)P_2$ to PI (Perera *et al.*, 2006), while at the same time, $PI(3,4)P_2$ recruits auxilin-HSC70 machinery to disassemble clathrin from the surface of vesicles (Lemmon, 2001;

Massol *et al.*, 2006). Finally, OCRL1 turns over the remaining PI(4,5)$P_2$ to PI (Cauvin *et al.*, 2016) and phosphoinositol 4-phosphatase converts PI(3,4)$P_2$ to PI3P, completing CME and giving the newly formed vesicle an endosomal identity (Zoncu *et al.*, 2009). These intricately regulated pathways in mammalian systems are simplified in yeast, as yeast contain only 4 PPI lipids: PI3P, which can be converted into PI(3,5)$P_2$, and PI4P, which can be converted into PI(4,5)$P_2$. This simplified yeast system provides some advantages over mammalian systems, most importantly that it is easier to manipulate the levels of a single PPI lipid without affecting the levels of other PPI lipids.

**Identifying the yeast PI 3-kinase, Vps34, in *S. cerevisiae***

PI3P was first identified as biochemically distinct from PI4P in fibroblasts using anion exchange on an HPLC (Whitman *et al.*, 1988) and soon after was found to be present in yeast as well (Auger *et al.*, 1989). PI 3-kinase activity was then rapidly purified from rat liver (Carpenter *et al.*, 1990), bovine brain (Otsu *et al.*, 1991), and fibroblasts (Escobedo *et al.*, 1991) and attributed to a 110 kDa protein. The sequence of this 100 kDa protein was determined and found to have significant homology to the *S. cerevisiae* Vps34 protein (Hiles *et al.*, 1992). In *vps34Δ* cells, no PI3P could be detected, suggesting that Vps34, is the sole enzyme responsible for generating PI3P from PI in yeast (Schu *et al.*, 1993). *In vitro*, Vps34 is unable to use PI4P or PI4,5$P_2$ as a substrate, suggesting that its kinase activity is specific to PI (Stack and Emr, 1994).

**The pseudokinase, Vps15, is required for PI3P synthesis**

Before it was characterized as a PI 3-kinase, Vps34 was first isolated from a screen selecting for mutants that mislocalize a vacuolar carboxypeptidase Y (CPY)-invertase fusion protein from the vacuole to the cell surface and were additionally found to exhibit severe defects in delivery of Proteinase A (PrA) and Proteinase B (PrB) to the vacuole (Robinson *et al.*, 1988). Additionally, *vps34Δ* cells exhibited temperature sensitive growth, sensitivity to osmotic stress, and defective vacuole inheritance, while maintaining relatively normal vacuole morphology (Herman and Emr, 1990). Of the other identified Vps mutants, only Vps15 exhibited the same phenotypes as Vps34, suggesting that Vps34 and Vps15 could act in the same step of the vacuole protein sorting pathway (Banta *et al.*, 1988; Herman *et al.*, 1991a; Herman *et al.*, 1991b). Soon after, Vps15 and Vps34 were found to interact by immunoprecipitation and chemical crosslinking (Stack *et al.*, 1993). Moreover, similar to *vps34Δ* cells, *vps15Δ* cells do not produce detectable levels of PI3P (Stack *et al.*, 1993).

The precise mechanism by which Vps15 regulates Vps34 kinase activity is not agreed upon. Vps15 is myristoylated at its N-terminus, though mutating the Vps15 myristoylation site does not lead to a defect in CPY maturation unless combined with other mutations (Herman *et al.*, 1991b). Due to its sequence conservation, Vps15 was first proposed to be a protein kinase (Herman *et al.*, 1991a). Point mutations in conserved amino acids in the Vps15 kinase domain led to defects in sorting of CPY similar to those observed in *vps15Δ* cells (Herman *et al.*, 1991a). Additionally, these point mutants abolished phosphorylation of Vps15 in cells, raising the possibility that

Vps15 is autophosphorylated (Herman *et al.*, 1991a). However, it has also been speculated that Vps15 is a pseudokinase since it has nontypical residues in critical catalytic elements, including an HGD motif rather than HRD in the catalytic loop and a DFA motif instead of DFG for magnesium ion binding in the activation loop (Rostislavleva *et al.*, 2015). Furthermore, Vps15 lacks an obvious ATP binding loop.

More recently, Vps15 has been proposed to regulate Vps34 activity in part via changes in the contact of the Vps34 helical and kinase domains (HELCAT) with the Vps15 pseudokinase domain (Stjepanovic *et al.*, 2017). In the inactive conformation, the Vps34 HELCAT domain contacts the Vps15 scaffold. During activation, the Vps34 HELCAT domain has been proposed to release contact with Vps15 and allow Vps34 to access its PI substrate (Figure 1.2). In support of this hypothesis, a ‘‘leashed’’ construct that prevented the HELCAT domain from releasing contact with Vps15 blocked Vps34 enzyme activity *in vitro* (Stjepanovic *et al.*, 2017). While it is clear that Vps15 acts as both a positive and negative regulator of Vps34 kinase function, many questions of the precise role Vps15 plays in regulating Vps34 remain.

**Vps34 and Vps15 act within at least two large regulatory complexes**

In addition to Vps34 and Vps15, PI 3-kinase activity is regulated by at least two large complexes. Vps34 and another regulator, Vps38, were identified as interactors of Vps30 through pulldown of Vps30 and mass spectrometry of its interactors (Kihara *et al.*, 2001). Further analysis by immunoprecipitation of Vps30 and western blot revealed that Vps30 also interacts with Vps15 and a previously reported Vps30 interactor, Atg14

(Kametaka *et al.*, 1998), suggesting that Vps30 acts as a member of at least one Vps34-Vps15 complex (Kihara *et al.*, 2001). Further analysis revealed that immunoprecipitation of Atg14 pulled down Vps34, Vps15, and Vps30, but not Vps38, while immunoprecipitation of Vps38 pulled down Vps34, Vps15, and Vps30, but not Atg14. This result indicates that Vps38 and Atg14 are present in two different PI 3-kinase complexes (Kihara *et al.*, 2001).

Consistent with Vps38 and Atg14 being part of separate complexes, phenotypic analysis revealed that while *vps38Δ* cells were deficient in CPY maturation and *atg14Δ* cells were deficient in autophagy and aminopeptidase I (API) maturation, *vps30Δ*, *vps15Δ*, and *vps34Δ* cells were deficient in all three processes (Kihara *et al.*, 2001) (Figure 1.3). Thus, the Atg14-containing complex I is required for autophagy, while Vps38-containing complex II is required for CPY maturation. Vps38 and Atg14 are thought to specify the subcellular localization of the PI 3-kinase complexes. The localization of Vps34 and Vps30, but not Vps15, to autophagosomes is Atg14-dependent, while the localization to puncta believed to be endosomes is Vps38-dependent (Obara *et al.*, 2006).

More recently, immunoprecipitation of Vps34 and mass spectrometry of its interactors revealed a novel interactor, Atg38 (Araki *et al.*, 2013). Immunoprecipitation of Atg38 and western blot revealed that Atg38 interacts with Vps34, Vps15, Vps30, and Atg14, but not Vps38, demonstrating that Atg38 is a member of complex I. In *atg38Δ* cells, Atg14 still interacts with Vps30, but no longer interacts with Vps34 or Vps15, indicating that

Atg38 is required to hold complex I together (Araki *et al.*, 2013). Complexes I and II are diagrammed in Figure 1.4.

**Structural insights into the PI 3-kinase complexes**

Our understanding of the shape and organization of the PI 3-kinase complexes has been bolstered by a 4.4 Å crystal structure of the yeast PI 3-kinase complex II (Rostislavleva *et al.*, 2015). This structure has an overall Y-shape with the tips of both arms of the Y binding to a membrane. Vps34 and Vps15 are intertwined on one arm so that the pseudokinase domain of Vps15 interacts with the lipid-binding region of the Vps34 kinase domain, suggesting that this structure is of an inactive conformation of the complex. On the other arm, Vps30 and Vps38 form a parallel heterodimer and bind the membrane via the Vps30 BARA domain (Huang *et al.*, 2012; Noda *et al.*, 2012). In the middle, the Vps34 C2 domain is the keystone to the organization of the complexes, interacting with all of the complex II subunits.

A lower resolution electron microscopy structural analysis of complex I without Atg38 revealed that the PI 3-kinase complex adopts a number of conformations (Stjepanovic *et al.*, 2017). The most common of these conformations closely resembles the conformation of the crystal structure of complex II. Electron microscopy also revealed a “dislodged” conformation that is proposed to be the active conformation of the complex (Stjepanovic *et al.*, 2017). In this conformation, the HELCAT domain of Vps34 does not contact Vps15, which is believed to allow Vps34 to access its PI substrate (Figure 1.2).

**Turnover of PI3P in yeast**

In yeast, the turnover of phosphoinositide lipids is controlled by a number of phosphoinositide phosphatases. These phosphatases fall broadly into two categories: those with homology to Sac1 (Guo *et al.*, 1999; Hughes *et al.*, 2000) and those with homology to myotubularin (Taylor *et al.*, 2000). With the exception of Fig4, which specifically dephosphorylates the 5-position of PI(3,5)$P_2$ *in vitro* (Rudge *et al.*, 2004), phosphatases with homology to Sac1 appear to act on a number of phosphoinositide species (Guo *et al.*, 1999; Hughes *et al.*, 2000; Foti *et al.*, 2001). The promiscuous nature of these Sac1 family phosphatases makes them difficult to study, as they are partially redundant with each other. Furthermore, it is difficult to attribute phenotypes observed in Sac1 family mutants to a change in just one phosphoinositide species.

*S. cerevisiae* contain one phosphatase with homology to myotubularin, Ymr1. *In vitro*, Ymr1 specifically dephosphorylates PI3P to PI (Taylor *et al.*, 2000). In cells, deletion of Ymr1 led to a modest ~15% increase in PI3P levels, though overexpression of Ymr1 on a 2μ plasmid led to a 25% decrease in PI3P levels (Parrish *et al.*, 2004). Interestingly, when combined with deletion of a Sac1 family phosphatase, Sjl3 (Inp53), *ymr1Δsjl3Δ* cells accumulate approximately 2.5 times the PI3P present in wild-type cells with minimal changes to other phosphoinositides (Parrish *et al.*, 2004). These cells exhibited a number of defects including vacuole fragmentation, along with defects in CPY, API, and carboxypeptidase S (CPS) maturation (Parrish *et al.*, 2004). These results demonstrate the importance turnover of PI3P plays in regulating cell homeostasis.

**PI3P regulates a number of downstream pathways in yeast**

The PI3P dependence of downstream processes is most often established by testing whether the process occurs in PI 3-kinase complex component knockouts, commonly Vps34. In many cases, the PI3P-dependence of a process has been attributed specifically to one of the two known PI 3-kinase complexes by testing whether the process is disrupted in Vps38 or Atg14 knockout cells. In this manner, a number of PI3P-dependent cellular processes have been identified in yeast (Figure 1.5).

*PI3P is converted into other PPI lipids*

Because PPI lipids are interconverted by phosphorylation and dephosphorylation, in mammalian systems, the production of PI3P can lead to downstream changes in a number of PPI lipid species. However, in a simplified yeast system, PI3P can only be phosphorylated at the 5-position to $PI(3,5)P_2$ (Gary *et al.*, 1998). Thus, Vps34 mutants that do not produce PI3P also do not produce $PI(3,5)P_2$ (Dove *et al.*, 1997).

*PI3P is required for multiple retrograde transport pathways*

Within the endocytic pathway, transport is thought of as moving towards the so-called terminal compartment, the vacuole. Multiple retrograde transport steps for movement away from the vacuole have been shown to require PI3P. The yeast retromer functions in retrograde transport of transmembrane sorting receptors from endosomes back to the Golgi (Seaman *et al.*, 1997; Seaman *et al.*, 1998). Defects in retromer function result in the aberrant delivery of Vps10, a yeast mannose-6 phosphate receptor, to the vacuolar membrane (Cooper and Stevens, 1996; Seaman *et al.*, 1997). Vps10 acts as a sorting

receptor for the soluble vacuolar hydrolase, CPY (Westphal *et al.*, 1996). Thus, when Vps10 is mislocalized to the vacuole, delivery of CPY to the vacuole is disrupted (Paravicini *et al.*, 1992). Interestingly, the delivery of other soluble vacuolar hydrolases, PrA and PrB, to the vacuole is not affect by mutations in the retromer (Paravicini *et al.*, 1992), despite the fact that Vps10 also acts as a sorting receptor for both PrA (Westphal *et al.*, 1996). This result suggests that other retrograde transport mechanisms may be involved in the delivery of PrA and PrB to the vacuole.

Retromer function requires PI3P as PI3P recruits retromer components, Vps5 and Vps17 to membranes (Burda *et al.*, 2002). Vps5 and Vps17 are sorting nexins that contain a BAR domain (SNX-BAR) that also contain PI3P-binding PX domains (Yu and Lemmon, 2001). These SNX-BAR proteins help to coordinate membrane deformation and cargo selection in vesicle formation (van Weering *et al.*, 2010). *vps34Δ*, *vps15Δ*, *vps30Δ*, and *vps38Δ* cells all exhibit a defect in CPY maturation, indicating that PI 3-kinase complex II is required for retromer function (Kihara *et al.*, 2001). Interestingly, while Vps30 and Vps38 are not required for the maturation of PrA and PrB, Vps34 and Vps15 are required (Kihara *et al.*, 2001) (Figure 1.3). These results suggest that Vps34/Vps15 maintain some functions independent of complexes I and II. Most likely, Vps34/Vps15 either maintain kinase function without other members of a kinase complex or function within an as yet uncharacterized third yeast PI 3-kinase complex.

Until recently, retrograde transport from the vacuole had only been demonstrated for an artificial cargo, retention sequence-alkaline phosphatase (RS-ALP), which fused a

retromer retrieval signal to ALP (Pho8 in yeast) (Bryant *et al.*, 1998). However, more recently, a SNX-BAR protein, Snx4, has been implicated in a retrograde transport pathway for retrieval of proteins from the vacuole to endosomes (Ma *et al.*, 2017; Suzuki and Emr, 2018). Snx4 functions as a heterodimer with Snx41 or Atg20/Snx42 (Hettema *et al.*, 2003). PI3P is required for proper Snx4 localization and is necessary for Snx4-dependent retrograde transport (Nice *et al.*, 2002; Suzuki and Emr, 2018). Atg27 is the first identified physiological substrate for Snx4-dependent retrograde transport from the vacuole and is also a client protein for retromer-dependent retrograde transport. Interestingly, there are conflicting reports on which Snx4 heterodimer is required for retrograde transport of Atg27. Some reports suggest that either the Snx4/Snx41 or Snx4/Snx42 can support retrograde transport of Atg27 (Suzuki and Emr, 2018), while others report that the Snx4/Snx41 heterodimer, but not the Snx4/Snx42 heterodimer can support retrograde transport of Atg27 (Ma *et al.*, 2017). Following its synthesis, Atg27 is delivered from the Golgi to the vacuole via the AP-3 pathway (Segarra *et al.*, 2015). From the vacuole, Atg27 undergoes retrograde transport to endosomes in a Snx4-dependent manner (Ma *et al.*, 2017; Suzuki and Emr, 2018). Finally, from endosomes, Atg27 undergoes retromer-dependent retrograde transport back to the Golgi (Suzuki and Emr, 2018). Due to the cyclic nature of its transport, changes in Atg27 localization can signify changes in the rates of these retrograde transport steps. For example, treatment with Rapamycin has been shown to induce transport of Atg27 away from the vacuole in a Snx4-dependent manner (Ma *et al.*, 2017). Similar to Atg27, RS-ALP is delivered to the vacuole in an AP-3-dependent manner (Bryant *et al.*, 1998). Interestingly, unlike retrieval of Atg27 from the vacuole (Suzuki and Emr, 2018), retrieval

of RS-ALP from the vacuole membrane requires $PI(3,5)P_2$ (Bryant *et al.*, 1998), suggesting that these two substrates undergo retrograde trafficking by distinct pathways.

*PI3P is required for ESCRT function*

Function of the endosomal sorting complexes required for transport (ESCRT) pathway also depends on PI3P. The multi-complex ESCRT machinery bends membranes away from the cytoplasm and plays important roles at endosomes in the biogenesis of multi-vesicular bodies (MVBs) (reviewed in (Piper and Katzmann, 2007)). Transmembrane ESCRT client proteins are first ubiquitinated, which enables their recognition and binding to the ESCRT complex. Once the cargo proteins are bound, the ESCRT complex generates vesicles via inward budding into lumen of the organelle, and the cargoes are ultimately delivered to the vacuole. ESCRT is required for the delivery of the vacuolar hydrolase CPS to the vacuolar lumen (Odorizzi *et al.*, 1998; Katzmann *et al.*, 2001). Precursor CPS is a type-II transmembrane protein that moves through the secretory pathway to endosomes, where ubiquitination marks CPS for ESCRT-dependent selective sorting into the invaginating vesicles of the MVB (Spormann *et al.*, 1992; Katzmann *et al.*, 2001). When MVBs fuse with the vacuole, CPS is delivered to the vacuolar lumen and is cleaved by proteinase A to its mature form that is soluble within the vacuolar lumen. Defects in ESCRT function result in an inability to form MVBs and aberrant delivery of CPS to the vacuolar limiting membrane (Odorizzi *et al.*, 1998). ESCRT-0 functions by binding ubiquitinated ESCRT client proteins and recruiting ESCRT-I to membranes. Vps34 is required for proper localization of the ESCRT-0

subunit Vps27, which contains a PI3P-binding FYVE domain (Katzmann *et al.*, 2003). Interestingly, Fab1, the PI3P 5-kinase, is also reported to be required for the delivery of CPS to the vacuolar lumen (Odorizzi *et al.*, 1998), suggesting that PI(3,5)$P_2$ may be involved in ESCRT function via an unknown mechanism. Surprisingly, neither Vps30 or Vps38 are required for the delivery of CPS to the vacuolar lumen (Burda *et al.*, 2002), which may suggest that ESCRT function is a complex I and II-independent role for Vps34. More recently, ESCRT and PI3P have also been found to function directly on the vacuole, generating vesicles via inward budding into the vacuole lumen for the selective degradation of vacuole membrane proteins (Li *et al.*, 2015; Zhu *et al.*, 2017).

*PI3P in the fusion of vesicles to the vacuole*

Additionally, PI3P is required for fusion of vesicles with the vacuole, and homotypic vacuole fusion. This is due in part to the direct binding of the SNARE Vam7 (Cheever *et al.*, 2001; Fratti and Wickner, 2007) and the heterodimeric GEF subunits Mon1 and Ccz1 (Cabrera *et al.*, 2014) to PI3P. Moreover, Vps34-dependent generation of PI3P is required for the vacuole association of many additional proteins required for vacuole fusion (Lawrence *et al.*, 2014).

*PI3P is required for multiple steps in autophagy*

It has long been known that defects in PI 3-kinase complex I block autophagy in yeast (Kihara *et al.*, 2001). Early in autophagy, PI3P recruits Atg18 to the phagophore (Dove *et al.*, 2004; Obara *et al.*, 2008) where it interacts with Atg2 and tethers pre-autophagosomal membranes to the endoplasmic reticulum, allowing Atg2 to transport

lipids to promote autophagosome biogenesis (Rieter *et al.*, 2013; Kotani *et al.*, 2018; Valverde *et al.*, 2019). More recently, PI3P has also been implicated in later steps of autophagy. Following autophagosome formation, Ymr1, a myotubularin family protein and putative PI3P phosphatase (Taylor *et al.*, 2000; Parrish *et al.*, 2004) is crucial for autophagosome fusion with the vacuole. Deletion of *YMR1* causes a failure of key autophagy machinery including Atg18 to dissociate from mature autophagosomes. This leads to accumulation of autophagosomes in the cytoplasm (Cebollero *et al.*, 2012) and suggests that turnover of PI3P is crucial for this process. PI3P also has a positive role in a late step in autophagy. *In vitro* studies indicate that fusion of autophagosomes with the vacuole requires PI3P and likely acts by recruiting the Rab GTPase Ypt7, which in turn recruits the HOPS tethering complex (Bas *et al.*, 2018). Thus, while PI3P is required for some steps in autophagy, impeding turnover of PI3P inhibits the resolution of autophagosomes.

Cytoplasm-to-vacuole targeting (Cvt) is a constitutive and specific form of autophagy that uses autophagosome-like vesicles for selective transport of the vacuolar hydrolase API (Yoshihisa and Anraku, 1989; Klionsky *et al.*, 1992; Harding *et al.*, 1996). While much of the autophagy machinery also functions in CVT, some autophagy proteins are dispensable for CVT and vice-versa (Harding *et al.*, 1996). While PI 3-kinase complex I is required for both processes (Kihara *et al.*, 2001) (Figure 1.3), PI3P has been proposed to have different functions in autophagy and CVT. Atg27 was identified as a PI3P-binding protein that binds to PI3P via a basic KKPAKK motif. Mutation of this motif blocked CVT function, but had much more minor effects on autophagy (Wurmser and

Emr, 2002). However, because of a sequencing error, the true amino acid sequence of Atg27 contains an additional 75 amino acids at the N-terminus. These additional amino acids mean that rather than being a type II transmembrane protein as previously reported (Wurmser and Emr, 2002), Atg27 is a type I transmembrane protein (Yen *et al.*, 2007). This means that the proposed PI3P binding site in full length Atg27 would not be exposed to the cytosolic side of the membrane. Furthermore, full length Atg27 did not require PI3P for correct localization nor did it require the KKPAKK motif (Yen *et al.*, 2007). Additionally, the KKPAKK motif was found to be dispensable for CVT and autophagy function (Yen *et al.*, 2007). Together, these results suggest that binding PI3P is not required for Atg27 function.

*PI3P plays a poorly understood role in pheromone signaling*

*vps34Δ* and *vps15Δ* cells, but not *vps30Δ*, *vps38Δ*, or *atg14Δ* cells exhibit a defect in pheromone signaling (Slessareva *et al.*, 2006). Vps34 and Vps15 both bind directly to Gpa1, a G protein alpha subunit involved in pheromone response, with Vps15 binding preferentially to unactivated Gpa1 and Vps34 preferentially binding activated Gpa1 (Slessareva *et al.*, 2006). Interestingly, expression of a constitutively active Gpa1 allele, Gpa1-Q323L leads to increased production of PI3P (Slessareva *et al.*, 2006), one of the few known methods of elevating PI3P levels in yeast. These results are consistent with Gpa1 stimulating Vps34 PI 3-kinase activity. It still remains unclear, however, how Vps34 modulates pheromone responsiveness. It is unlikely that this pheromone responsiveness phenotype is due to a defect in membrane trafficking, as other Vps mutants do not exhibit defects in pheromone signaling (Slessareva *et al.*, 2006).

*Poorly understood phenotypes of vps34Δ cells*

*vps34Δ* cells exhibit phenotypes that aren't completely explained by the known function of Vps34. Vps34 was identified in a screen for growth sensitivity on plates containing ethanol (Takahashi *et al.*, 2001). The same study found that Vps34 and the other identified ethanol sensitive mutants also exhibited sensitivity to Calcofluor white and Zymolyase, indicative of a defect in cell wall integrity (Takahashi *et al.*, 2001). Ethanol sensitivity is correlated with temperature sensitivity (Aguilera and Benitez, 1986) and *vps34Δ* cells are also known to have a growth defect at 37°C (Herman and Emr, 1990; Takahashi *et al.*, 2001). Interestingly, while *vps34Δ* and *vps15Δ* cells exhibit a growth defect at 37°C, *vps30Δ*, *vps38Δ*, and *atg14Δ* cells do not (Kihara *et al.*, 2001) (Figure 1.3). These defects in cell wall integrity and ethanol and temperature-sensitivity are not easily explained by the known function of Vps34 and may potentially point to a complex I and II-independent role for Vps34/Vps15. Overall, while much is known about the roles that PI3P plays in yeast, much still remains to be discovered. Here, I focus on manipulating the levels of PI3P in yeast and understanding the downstream consequences.

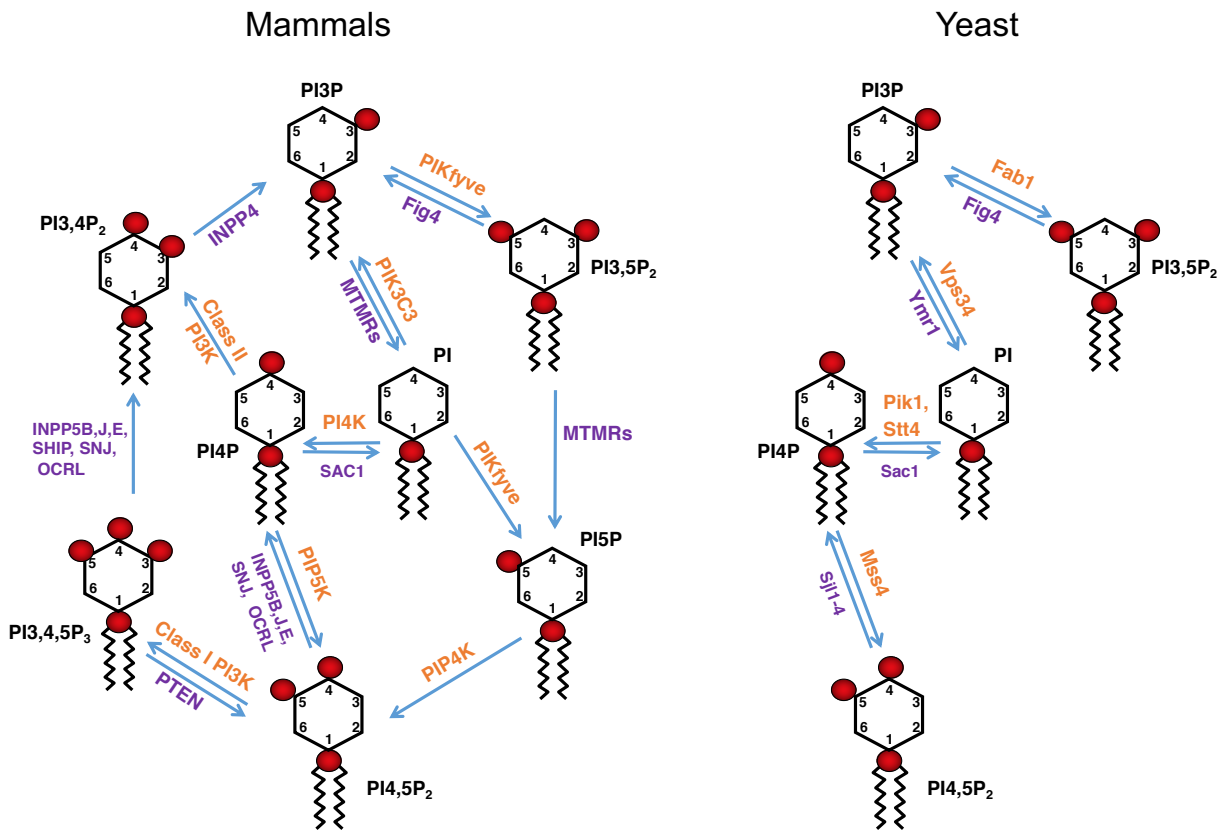


**Figure 1.1: Interconversion of PPIs by PPI kinases and phosphatases in mammals and yeast.** PPIs are generated by the action of phosphoinositide kinases and phosphatases in mammals (left) and yeast (right). These reactions are confined to membrane subdomains where these phosphoinositide modifying enzymes reside (reviewed in (Strahl and Thorner, 2007; Sasaki *et al.*, 2009; Balla, 2013; Shisheva *et al.*, 2015; Wallroth and Haucke, 2018; Dickson and Hille, 2019)). These reactions yield mono-phosphates (phosphatidylinositol-3-phosphate (PI3P), phosphatidylinositol-4-phosphate (PI4P), phosphatidylinositol-5-phosphate (PI5P)), bis-phosphates (phosphatidylinositol-3,4-bisphosphate ($PI3,4P_2$), phosphatidylinositol-3,5-bisphosphate ($PI(3,5)P_2$), phosphatidylinositol-4,5-bisphosphate ($PI4,5P_2$)), and tris-phosphate (phosphatidylinositol-3,4,5-trisphosphate ($PI3,4,5P_3$)). Red circles represent phosphate groups.

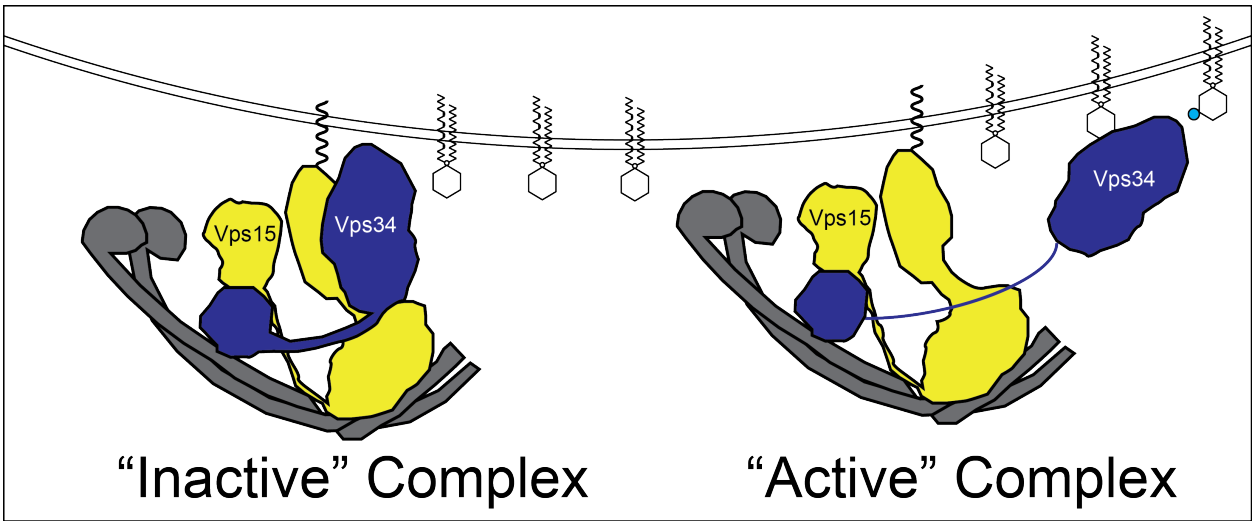


**Figure 1.2: A model of Vps34 activation.** Vps34 is proposed to be regulated in part via changes in contact of the Vps34 HELCAT domain with Vps15. In the inactive conformation, the Vps34 HELCAT domain contacts the Vps15 scaffold. During activation, the Vps34 HELCAT domain is proposed to alter the contact with Vps15 and allow Vps34 to access its PI substrate (Stjepanovic *et al.*, 2017).

| | WT | Δ*vps15* | Δ*vps34* | Δ*vps30* | Δ*apg14* | Δ*vps38* |
|---|---|---|---|---|---|---|
| Autophagy | + | − | − | − | − | + |
| API | + | − | − | − | − | + |
| CPY | + | − | − | − | + | − |
| PrA | + | − | − | + | + | + |
| PrB | + | − | − | + | + | + |
| Growth at 37°C | + | − | − | + | + | + |

**Figure 1.3: Summary of the phenotypes observed in cells with PI 3-kinase complex proteins knocked out.** PI 3-kinase complex proteins were knocked out individually and tested for a number of phenotypes including vacuolar delivery and maturation of Aminopeptidase I (API), carboxypeptidase Y (CPY), and Proteinase A and B (PrA and PrB). Additionally, autophagy was assessed by measuring the autophagy-dependent processing of alkaline phosphatase Pho8Δ60 (Noda *et al.*, 1995). The ability of the cells to grow at 37°C was also tested. Table is reproduced from (Kihara *et al.*, 2001).

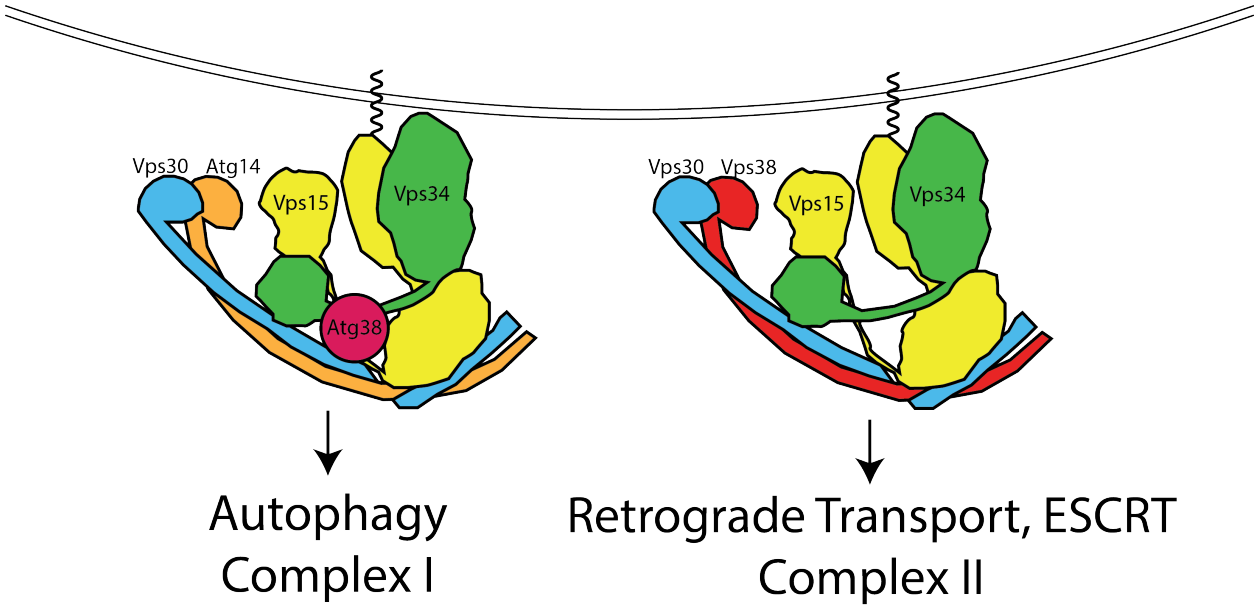


**Figure 1.4: Schematic illustrating the two known PI 3-kinase complexes in yeast and their functions.** Vps34 acts in at least two large regulatory complexes. Vps15, a member of both complexes is absolutely required for PI3P synthesis. In addition to Vps34 and Vps15, both known complexes contain Vps30. Complex I, which includes Atg14 and Atg38, is required for autophagy, whereas complex II, which includes Vps38, is required for retromer and ESCRT function.

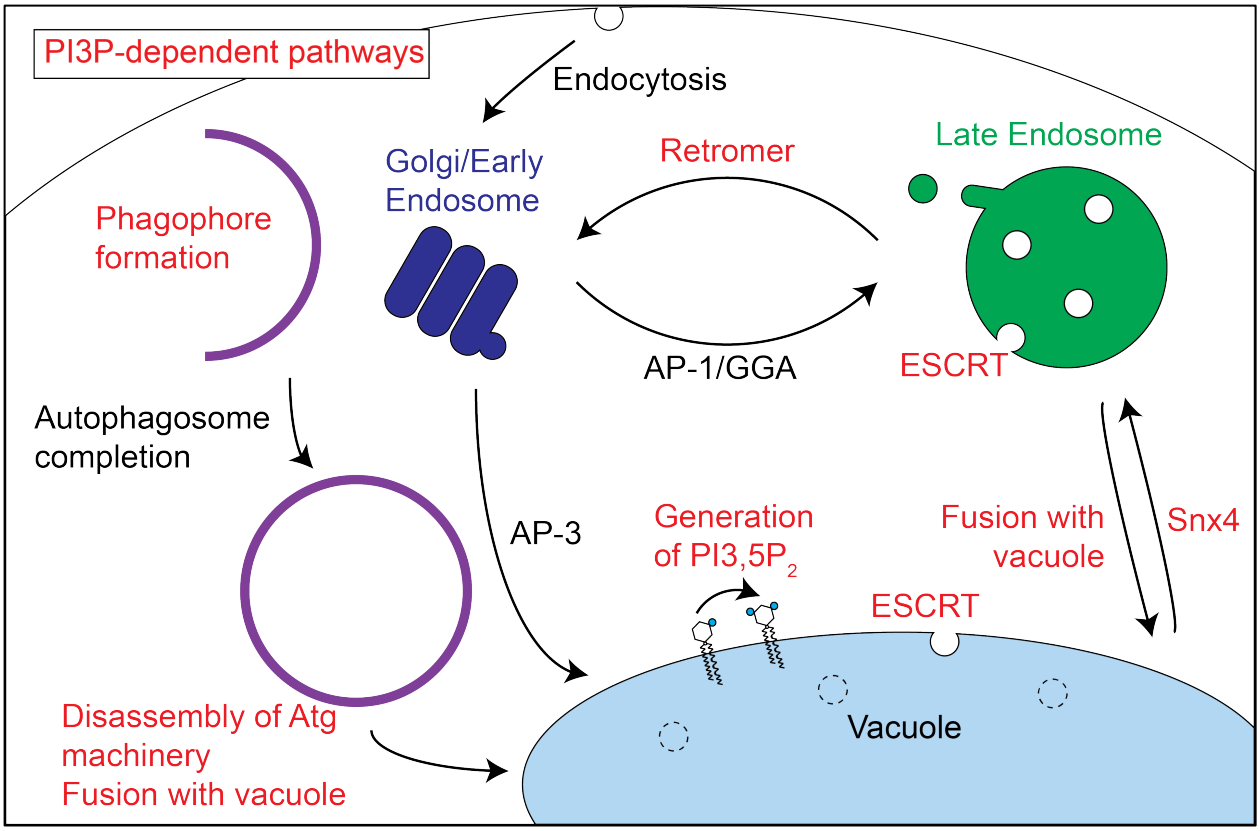


**Figure 1.5: Schematic indicating several PI3P-dependent intracellular trafficking pathways in yeast.** PI3P serves as the substrate for $PI(3,5)P_2$. PI3P is also required for Snx4-dependent retrograde transport from the vacuole and retromer-dependent retrograde transport from endosomes. ESCRT function at late endosomes and the vacuole is also dependent on PI3P. Furthermore, PI3P is required for phagophore formation during the initiation of autophagy. PI3P is then removed prior to the disassembly of some autophagy proteins from the surface of mature autophagosomes. In addition, fusion of autophagosomes and other vesicles with the vacuole, as well as homotypic vacuole fusion (not shown), are PI3P-dependent pathways. PI3P also plays a role in pheromone signaling (not shown).

## References


Aguilera, A., and Benitez, T. (1986). Ethanol-sensitive mutants of Saccharomyces cerevisiae. Arch Microbiol *143*, 337-344.

Araki, Y., Ku, W.C., Akioka, M., May, A.I., Hayashi, Y., Arisaka, F., Ishihama, Y., and Ohsumi, Y. (2013). Atg38 is required for autophagy-specific phosphatidylinositol 3-kinase complex integrity. J Cell Biol *203*, 299-313.

Auger, K.R., Carpenter, C.L., Cantley, L.C., and Varticovski, L. (1989). Phosphatidylinositol 3-kinase and its novel product, phosphatidylinositol 3-phosphate, are present in Saccharomyces cerevisiae. J Biol Chem *264*, 20181-20184.

Balla, T. (2013). Phosphoinositides: tiny lipids with giant impact on cell regulation. Physiol Rev *93*, 1019-1137.

Banta, L.M., Robinson, J.S., Klionsky, D.J., and Emr, S.D. (1988). Organelle assembly in yeast: characterization of yeast mutants defective in vacuolar biogenesis and protein sorting. J Cell Biol *107*, 1369-1383.

Barbieri, M.A., Heath, C.M., Peters, E.M., Wells, A., Davis, J.N., and Stahl, P.D. (2001). Phosphatidylinositol-4-phosphate 5-kinase-1beta is essential for epidermal growth factor receptor-mediated endocytosis. J Biol Chem *276*, 47212-47216.

Bas, L., Papinski, D., Licheva, M., Torggler, R., Rohringer, S., Schuschnig, M., and Kraft, C. (2018). Reconstitution reveals Ykt6 as the autophagosomal SNARE in autophagosome-vacuole fusion. J Cell Biol.

Bryant, N.J., Piper, R.C., Weisman, L.S., and Stevens, T.H. (1998). Retrograde traffic out of the yeast vacuole to the TGN occurs via the prevacuolar/endosomal compartment. J Cell Biol *142*, 651-663.

Burda, P., Padilla, S.M., Sarkar, S., and Emr, S.D. (2002). Retromer function in endosome-to-Golgi retrograde transport is regulated by the yeast Vps34 PtdIns 3-kinase. J Cell Sci *115*, 3889-3900.

Cabrera, M., Nordmann, M., Perz, A., Schmedt, D., Gerondopoulos, A., Barr, F., Piehler, J., Engelbrecht-Vandre, S., and Ungermann, C. (2014). The Mon1-Ccz1 GEF activates the Rab7 GTPase Ypt7 via a longin-fold-Rab interface and association with PI3P-positive membranes. J Cell Sci *127*, 1043-1051.

Carpenter, C.L., Duckworth, B.C., Auger, K.R., Cohen, B., Schaffhausen, B.S., and Cantley, L.C. (1990). Purification and characterization of phosphoinositide 3-kinase from rat liver. J Biol Chem *265*, 19704-19711.

Cauvin, C., Rosendale, M., Gupta-Rossi, N., Rocancourt, M., Larraufie, P., Salomon, R., Perrais, D., and Echard, A. (2016). Rab35 GTPase Triggers Switch-like Recruitment

of the Lowe Syndrome Lipid Phosphatase OCRL on Newborn Endosomes. Curr Biol *26*, 120-128.

Cebollero, E., van der Vaart, A., Zhao, M., Rieter, E., Klionsky, D.J., Helms, J.B., and Reggiori, F. (2012). Phosphatidylinositol-3-phosphate clearance plays a key role in autophagosome completion. Curr Biol *22*, 1545-1553.

Cheever, M.L., Sato, T.K., de Beer, T., Kutateladze, T.G., Emr, S.D., and Overduin, M. (2001). Phox domain interaction with PtdIns(3)P targets the Vam7 t-SNARE to vacuole membranes. Nat Cell Biol *3*, 613-618.

Cooper, A.A., and Stevens, T.H. (1996). Vps10p cycles between the late-Golgi and prevacuolar compartments in its function as the sorting receptor for multiple yeast vacuolar hydrolases. J Cell Biol *133*, 529-541.

Di Paolo, G., Moskowitz, H.S., Gipson, K., Wenk, M.R., Voronov, S., Obayashi, M., Flavell, R., Fitzsimonds, R.M., Ryan, T.A., and De Camilli, P. (2004). Impaired PtdIns(4,5)P2 synthesis in nerve terminals produces defects in synaptic vesicle trafficking. Nature *431*, 415-422.

Dickson, E.J., and Hille, B. (2019). Understanding phosphoinositides: rare, dynamic, and essential membrane phospholipids. Biochem J *476*, 1-23.

Dove, S.K., Cooke, F.T., Douglas, M.R., Sayers, L.G., Parker, P.J., and Michell, R.H. (1997). Osmotic stress activates phosphatidylinositol-3,5-bisphosphate synthesis. Nature *390*, 187-192.

Dove, S.K., Piper, R.C., McEwen, R.K., Yu, J.W., King, M.C., Hughes, D.C., Thuring, J., Holmes, A.B., Cooke, F.T., Michell, R.H., et al. (2004). Svp1p defines a family of phosphatidylinositol 3,5-bisphosphate effectors. EMBO J *23*, 1922-1933.

Duex, J.E., Nau, J.J., Kauffman, E.J., and Weisman, L.S. (2006). Phosphoinositide 5-phosphatase Fig 4p is required for both acute rise and subsequent fall in stress-induced phosphatidylinositol 3,5-bisphosphate levels. Eukaryot Cell *5*, 723-731.

Escobedo, J.A., Navankasattusas, S., Kavanaugh, W.M., Milfay, D., Fried, V.A., and Williams, L.T. (1991). cDNA cloning of a novel 85 kd protein that has SH2 domains and regulates binding of PI3-kinase to the PDGF beta-receptor. Cell *65*, 75-82.

Ford, M.G., Pearse, B.M., Higgins, M.K., Vallis, Y., Owen, D.J., Gibson, A., Hopkins, C.R., Evans, P.R., and McMahon, H.T. (2001). Simultaneous binding of PtdIns(4,5)P2 and clathrin by AP180 in the nucleation of clathrin lattices on membranes. Science *291*, 1051-1055.

Foti, M., Audhya, A., and Emr, S.D. (2001). Sac1 lipid phosphatase and Stt4 phosphatidylinositol 4-kinase regulate a pool of phosphatidylinositol 4-phosphate that functions in the control of the actin cytoskeleton and vacuole morphology. Mol Biol Cell *12*, 2396-2411.

Fratti, R.A., and Wickner, W. (2007). Distinct targeting and fusion functions of the PX and SNARE domains of yeast vacuolar Vam7p. J Biol Chem *282*, 13133-13138.

Gary, J.D., Wurmser, A.E., Bonangelino, C.J., Weisman, L.S., and Emr, S.D. (1998). Fab1p is essential for PtdIns(3)P 5-kinase activity and the maintenance of vacuolar size and membrane homeostasis. J Cell Biol *143*, 65-79.

Guo, S., Stolz, L.E., Lemrow, S.M., and York, J.D. (1999). SAC1-like domains of yeast SAC1, INP52, and INP53 and of human synaptojanin encode polyphosphoinositide phosphatases. J Biol Chem *274*, 12990-12995.

Harding, T.M., Hefner-Gravink, A., Thumm, M., and Klionsky, D.J. (1996). Genetic and phenotypic overlap between autophagy and the cytoplasm to vacuole protein targeting pathway. J Biol Chem *271*, 17621-17624.

Herman, P.K., and Emr, S.D. (1990). Characterization of VPS34, a gene required for vacuolar protein sorting and vacuole segregation in Saccharomyces cerevisiae. Mol Cell Biol *10*, 6742-6754.

Herman, P.K., Stack, J.H., DeModena, J.A., and Emr, S.D. (1991a). A novel protein kinase homolog essential for protein sorting to the yeast lysosome-like vacuole. Cell *64*, 425-437.

Herman, P.K., Stack, J.H., and Emr, S.D. (1991b). A genetic and structural analysis of the yeast Vps15 protein kinase: evidence for a direct role of Vps15p in vacuolar protein delivery. EMBO J *10*, 4049-4060.

Hettema, E.H., Lewis, M.J., Black, M.W., and Pelham, H.R. (2003). Retromer and the sorting nexins Snx4/41/42 mediate distinct retrieval pathways from yeast endosomes. EMBO J *22*, 548-557.

Hiles, I.D., Otsu, M., Volinia, S., Fry, M.J., Gout, I., Dhand, R., Panayotou, G., Ruiz-Larrea, F., Thompson, A., Totty, N.F., et al. (1992). Phosphatidylinositol 3-kinase: structure and expression of the 110 kd catalytic subunit. Cell *70*, 419-429.

Huang, W., Choi, W., Hu, W., Mi, N., Guo, Q., Ma, M., Liu, M., Tian, Y., Lu, P., Wang, F.L., et al. (2012). Crystal structure and biochemical analyses reveal Beclin 1 as a novel membrane binding protein. Cell Res *22*, 473-489.

Hughes, W.E., Woscholski, R., Cooke, F.T., Patrick, R.S., Dove, S.K., McDonald, N.Q., and Parker, P.J. (2000). SAC1 encodes a regulated lipid phosphoinositide phosphatase, defects in which can be suppressed by the homologous Inp52p and Inp53p phosphatases. J Biol Chem *275*, 801-808.

Itoh, T., Koshiba, S., Kigawa, T., Kikuchi, A., Yokoyama, S., and Takenawa, T. (2001). Role of the ENTH domain in phosphatidylinositol-4,5-bisphosphate binding and endocytosis. Science *291*, 1047-1051.

Kaksonen, M., and Roux, A. (2018). Mechanisms of clathrin-mediated endocytosis. Nat Rev Mol Cell Biol *19*, 313-326.

Kametaka, S., Okano, T., Ohsumi, M., and Ohsumi, Y. (1998). Apg14p and Apg6/Vps30p form a protein complex essential for autophagy in the yeast, Saccharomyces cerevisiae. J Biol Chem *273*, 22284-22291.

Katzmann, D.J., Babst, M., and Emr, S.D. (2001). Ubiquitin-dependent sorting into the multivesicular body pathway requires the function of a conserved endosomal protein sorting complex, ESCRT-I. Cell *106*, 145-155.

Katzmann, D.J., Stefan, C.J., Babst, M., and Emr, S.D. (2003). Vps27 recruits ESCRT machinery to endosomes during MVB sorting. J Cell Biol *162*, 413-423.

Kihara, A., Noda, T., Ishihara, N., and Ohsumi, Y. (2001). Two distinct Vps34 phosphatidylinositol 3-kinase complexes function in autophagy and carboxypeptidase Y sorting in Saccharomyces cerevisiae. J Cell Biol *152*, 519-530.

Klionsky, D.J., Cueva, R., and Yaver, D.S. (1992). Aminopeptidase I of Saccharomyces cerevisiae is localized to the vacuole independent of the secretory pathway. J Cell Biol *119*, 287-299.

Kotani, T., Kirisako, H., Koizumi, M., Ohsumi, Y., and Nakatogawa, H. (2018). The Atg2-Atg18 complex tethers pre-autophagosomal membranes to the endoplasmic reticulum for autophagosome formation. Proc Natl Acad Sci U S A *115*, 10363-10368.

Lawrence, G., Brown, C.C., Flood, B.A., Karunakaran, S., Cabrera, M., Nordmann, M., Ungermann, C., and Fratti, R.A. (2014). Dynamic association of the PI3P-interacting Mon1-Ccz1 GEF with vacuoles is controlled through its phosphorylation by the type 1 casein kinase Yck3. Mol Biol Cell *25*, 1608-1619.

Lemmon, S.K. (2001). Clathrin uncoating: Auxilin comes to life. Curr Biol *11*, R49-52.

Li, M., Rong, Y., Chuang, Y.S., Peng, D., and Emr, S.D. (2015). Ubiquitin-dependent lysosomal membrane protein sorting and degradation. Mol Cell *57*, 467-478.

Ma, M., Burd, C.G., and Chi, R.J. (2017). Distinct complexes of yeast Snx4 family SNX-BARs mediate retrograde trafficking of Snc1 and Atg27. Traffic *18*, 134-144.

Massol, R.H., Boll, W., Griffin, A.M., and Kirchhausen, T. (2006). A burst of auxilin recruitment determines the onset of clathrin-coated vesicle uncoating. Proc Natl Acad Sci U S A *103*, 10265-10270.

Nice, D.C., Sato, T.K., Stromhaug, P.E., Emr, S.D., and Klionsky, D.J. (2002). Cooperative binding of the cytoplasm to vacuole targeting pathway proteins, Cvt13 and Cvt20, to phosphatidylinositol 3-phosphate at the pre-autophagosomal structure is required for selective autophagy. J Biol Chem *277*, 30198-30207.

Noda, N.N., Kobayashi, T., Adachi, W., Fujioka, Y., Ohsumi, Y., and Inagaki, F. (2012). Structure of the novel C-terminal domain of vacuolar protein sorting 30/autophagy-related protein 6 and its specific role in autophagy. J Biol Chem *287*, 16256-16266.

Noda, T., Matsuura, A., Wada, Y., and Ohsumi, Y. (1995). Novel system for monitoring autophagy in the yeast Saccharomyces cerevisiae. Biochem Biophys Res Commun *210*, 126-132.

Obara, K., Sekito, T., Niimi, K., and Ohsumi, Y. (2008). The Atg18-Atg2 complex is recruited to autophagic membranes via phosphatidylinositol 3-phosphate and exerts an essential function. J Biol Chem *283*, 23972-23980.

Obara, K., Sekito, T., and Ohsumi, Y. (2006). Assortment of phosphatidylinositol 3-kinase complexes--Atg14p directs association of complex I to the pre-autophagosomal structure in Saccharomyces cerevisiae. Mol Biol Cell *17*, 1527-1539.

Odorizzi, G., Babst, M., and Emr, S.D. (1998). Fab1p PtdIns(3)P 5-kinase function essential for protein sorting in the multivesicular body. Cell *95*, 847-858.

Otsu, M., Hiles, I., Gout, I., Fry, M.J., Ruiz-Larrea, F., Panayotou, G., Thompson, A., Dhand, R., Hsuan, J., Totty, N., et al. (1991). Characterization of two 85 kd proteins that associate with receptor tyrosine kinases, middle-T/pp60c-src complexes, and PI3-kinase. Cell *65*, 91-104.

Padron, D., Wang, Y.J., Yamamoto, M., Yin, H., and Roth, M.G. (2003). Phosphatidylinositol phosphate 5-kinase Ibeta recruits AP-2 to the plasma membrane and regulates rates of constitutive endocytosis. J Cell Biol *162*, 693-701.

Paravicini, G., Horazdovsky, B.F., and Emr, S.D. (1992). Alternative pathways for the sorting of soluble vacuolar proteins in yeast: a vps35 null mutant missorts and secretes only a subset of vacuolar hydrolases. Mol Biol Cell *3*, 415-427.

Parrish, W.R., Stefan, C.J., and Emr, S.D. (2004). Essential role for the myotubularin-related phosphatase Ymr1p and the synaptojanin-like phosphatases Sjl2p and Sjl3p in regulation of phosphatidylinositol 3-phosphate in yeast. Mol Biol Cell *15*, 3567-3579.

Perera, R.M., Zoncu, R., Lucast, L., De Camilli, P., and Toomre, D. (2006). Two synaptojanin 1 isoforms are recruited to clathrin-coated pits at different stages. Proc Natl Acad Sci U S A *103*, 19332-19337.

Piper, R.C., and Katzmann, D.J. (2007). Biogenesis and function of multivesicular bodies. Annu Rev Cell Dev Biol *23*, 519-547.

Posor, Y., Eichhorn-Gruenig, M., Puchkov, D., Schoneberg, J., Ullrich, A., Lampe, A., Muller, R., Zarbakhsh, S., Gulluni, F., Hirsch, E., et al. (2013). Spatiotemporal control of endocytosis by phosphatidylinositol-3,4-bisphosphate. Nature *499*, 233-237.

Posor, Y., Eichhorn-Grunig, M., and Haucke, V. (2015). Phosphoinositides in endocytosis. Biochim Biophys Acta *1851*, 794-804.

Rieter, E., Vinke, F., Bakula, D., Cebollero, E., Ungermann, C., Proikas-Cezanne, T., and Reggiori, F. (2013). Atg18 function in autophagy is regulated by specific sites within its beta-propeller. J Cell Sci *126*, 593-604.

Robinson, J.S., Klionsky, D.J., Banta, L.M., and Emr, S.D. (1988). Protein sorting in Saccharomyces cerevisiae: isolation of mutants defective in the delivery and processing of multiple vacuolar hydrolases. Mol Cell Biol *8*, 4936-4948.

Rohde, G., Wenzel, D., and Haucke, V. (2002). A phosphatidylinositol (4,5)-bisphosphate binding site within mu2-adaptin regulates clathrin-mediated endocytosis. J Cell Biol *158*, 209-214.

Rostislavleva, K., Soler, N., Ohashi, Y., Zhang, L., Pardon, E., Burke, J.E., Masson, G.R., Johnson, C., Steyaert, J., Ktistakis, N.T., et al. (2015). Structure and flexibility of the endosomal Vps34 complex reveals the basis of its function on membranes. Science *350*, aac7365.

Rudge, S.A., Anderson, D.M., and Emr, S.D. (2004). Vacuole size control: regulation of PtdIns(3,5)P2 levels by the vacuole-associated Vac14-Fig4 complex, a PtdIns(3,5)P2-specific phosphatase. Mol Biol Cell *15*, 24-36.

Sasaki, T., Takasuga, S., Sasaki, J., Kofuji, S., Eguchi, S., Yamazaki, M., and Suzuki, A. (2009). Mammalian phosphoinositide kinases and phosphatases. Prog Lipid Res *48*, 307-343.

Schink, K.O., Tan, K.W., and Stenmark, H. (2016). Phosphoinositides in Control of Membrane Dynamics. Annu Rev Cell Dev Biol *32*, 143-171.

Schoneberg, J., Lehmann, M., Ullrich, A., Posor, Y., Lo, W.T., Lichtner, G., Schmoranzer, J., Haucke, V., and Noe, F. (2017). Lipid-mediated PX-BAR domain recruitment couples local membrane constriction to endocytic vesicle fission. Nat Commun *8*, 15873.

Schu, P.V., Takegawa, K., Fry, M.J., Stack, J.H., Waterfield, M.D., and Emr, S.D. (1993). Phosphatidylinositol 3-kinase encoded by yeast VPS34 gene essential for protein sorting. Science *260*, 88-91.

Seaman, M.N., Marcusson, E.G., Cereghino, J.L., and Emr, S.D. (1997). Endosome to Golgi retrieval of the vacuolar protein sorting receptor, Vps10p, requires the function of the VPS29, VPS30, and VPS35 gene products. J Cell Biol *137*, 79-92.

Seaman, M.N., McCaffery, J.M., and Emr, S.D. (1998). A membrane coat complex essential for endosome-to-Golgi retrograde transport in yeast. J Cell Biol *142*, 665-681.

Segarra, V.A., Boettner, D.R., and Lemmon, S.K. (2015). Atg27 tyrosine sorting motif is important for its trafficking and Atg9 localization. Traffic *16*, 365-378.

Shisheva, A., Sbrissa, D., and Ikonomov, O. (2015). Plentiful PtdIns5P from scanty PtdIns(3,5)P2 or from ample PtdIns? PIKfyve-dependent models: Evidence and speculation (response to: DOI 10.1002/bies.201300012). Bioessays *37*, 267-277.

Slessareva, J.E., Routt, S.M., Temple, B., Bankaitis, V.A., and Dohlman, H.G. (2006). Activation of the phosphatidylinositol 3-kinase Vps34 by a G protein alpha subunit at the endosome. Cell *126*, 191-203.

Spormann, D.O., Heim, J., and Wolf, D.H. (1992). Biogenesis of the yeast vacuole (lysosome). The precursor forms of the soluble hydrolase carboxypeptidase yscS are associated with the vacuolar membrane. J Biol Chem *267*, 8021-8029.

Stack, J.H., and Emr, S.D. (1994). Vps34p required for yeast vacuolar protein sorting is a multiple specificity kinase that exhibits both protein kinase and phosphatidylinositol-specific PI 3-kinase activities. J Biol Chem *269*, 31552-31562.

Stack, J.H., Herman, P.K., Schu, P.V., and Emr, S.D. (1993). A membrane-associated complex containing the Vps15 protein kinase and the Vps34 PI 3-kinase is essential for protein sorting to the yeast lysosome-like vacuole. EMBO J *12*, 2195-2204.

Stjepanovic, G., Baskaran, S., Lin, M.G., and Hurley, J.H. (2017). Vps34 Kinase Domain Dynamics Regulate the Autophagic PI 3-Kinase Complex. Mol Cell *67*, 528-534 e523.

Strahl, T., and Thorner, J. (2007). Synthesis and function of membrane phosphoinositides in budding yeast, Saccharomyces cerevisiae. Biochim Biophys Acta *1771*, 353-404.

Suzuki, S.W., and Emr, S.D. (2018). Membrane protein recycling from the vacuole/lysosome membrane. J Cell Biol *217*, 1623-1632.

Takahashi, T., Shimoi, H., and Ito, K. (2001). Identification of genes required for growth under ethanol stress using transposon mutagenesis in Saccharomyces cerevisiae. Mol Genet Genomics *265*, 1112-1119.

Taylor, G.S., Maehama, T., and Dixon, J.E. (2000). Myotubularin, a protein tyrosine phosphatase mutated in myotubular myopathy, dephosphorylates the lipid second messenger, phosphatidylinositol 3-phosphate. Proc Natl Acad Sci U S A *97*, 8910-8915.

Valverde, D.P., Yu, S., Boggavarapu, V., Kumar, N., Lees, J.A., Walz, T., Reinisch, K.M., and Melia, T.J. (2019). ATG2 transports lipids to promote autophagosome biogenesis. J Cell Biol *218*, 1787-1798.

van Weering, J.R., Verkade, P., and Cullen, P.J. (2010). SNX-BAR proteins in phosphoinositide-mediated, tubular-based endosomal sorting. Semin Cell Dev Biol *21*, 371-380.

Wallroth, A., and Haucke, V. (2018). Phosphoinositide conversion in endocytosis and the endolysosomal system. J Biol Chem *293*, 1526-1535.

Westphal, V., Marcusson, E.G., Winther, J.R., Emr, S.D., and van den Hazel, H.B. (1996). Multiple pathways for vacuolar sorting of yeast proteinase A. J Biol Chem *271*, 11865-11870.

Whitman, M., Downes, C.P., Keeler, M., Keller, T., and Cantley, L. (1988). Type I phosphatidylinositol kinase makes a novel inositol phospholipid, phosphatidylinositol-3-phosphate. Nature *332*, 644-646.

Wurmser, A.E., and Emr, S.D. (2002). Novel PtdIns(3)P-binding protein Etf1 functions as an effector of the Vps34 PtdIns 3-kinase in autophagy. J Cell Biol *158*, 761-772.

Yen, W.L., Legakis, J.E., Nair, U., and Klionsky, D.J. (2007). Atg27 is required for autophagy-dependent cycling of Atg9. Mol Biol Cell *18*, 581-593.

Yoshihisa, T., and Anraku, Y. (1989). Nucleotide sequence of AMS1, the structure gene of vacuolar alpha-mannosidase of Saccharomyces cerevisiae. Biochem Biophys Res Commun *163*, 908-915.

Yu, J.W., and Lemmon, M.A. (2001). All phox homology (PX) domains from Saccharomyces cerevisiae specifically recognize phosphatidylinositol 3-phosphate. J Biol Chem *276*, 44179-44184.

Zhu, L., Jorgensen, J.R., Li, M., Chuang, Y.S., and Emr, S.D. (2017). ESCRTs function directly on the lysosome membrane to downregulate ubiquitinated lysosomal membrane proteins. Elife *6*.

Zoncu, R., Perera, R.M., Balkin, D.M., Pirruccello, M., Toomre, D., and De Camilli, P. (2009). A phosphoinositide switch controls the maturation and signaling properties of APPL endosomes. Cell *136*, 1110-1121.

# CHAPTER II

## Elevating PI3P Drives Select Downstream Membrane Trafficking Pathways[2]

### Introduction

Phosphoinositide (PPI) lipids are signaling molecules that play critical roles in multiple cellular processes. Most studies of how PPI lipids regulate downstream pathways use knockout or knockdown of PPI kinases to deplete a specific PPI lipid and thereby test the necessity for that PPI species in a process (Kihara *et al.*, 2001). However, there are very few reports on the impact of elevating phosphoinositides. Understanding the impact of elevating phosphoinositides is critical as the levels of PPI lipids are dynamically regulated by PPI lipid kinases and phosphatases in response to stimuli (Balla, 2013). For example, during hyperosmotic shock in *S. cerevisiae*, there is a transient 15 to 20-fold elevation in phosphatidylinositol-3,5-bisphosphate ($PI(3,5)P_2$) (Duex *et al.*, 2006a). The dynamic regulation of PPI lipids suggests that in addition to being required for specific pathways, changes in PPI lipids may drive downstream processes.

[2] This chapter is adapted from a published paper: Steinfeld, N., Lahiri, V., Morrison, A., Metur, S.P., Klionsky, D.J., and Weisman, L.S. (2021). Elevating PI3P drives select downstream membrane trafficking pathways. Mol Biol Cell 32, 143-156.

Here, we test this hypothesis directly by manipulating the levels of phosphatidylinositol 3-phosphate (PI3P), which is dynamically regulated in yeast (Duex *et al.*, 2006a). We report the generation and use of hyperactive mutations in Vps34 and the discovery that PI3P drives select pathways, including synthesis of $PI(3,5)P_2$ during hyperosmotic shock and retrograde transport of Atg27. In these cases, the PI3P-dependent step is rate limiting. We also show that hyperactive Vps34 does not affect ESCRT function at endosomes or on the vacuole. Thus, elevating PI3P does not always increase the overall rate of a complex pathway. We also show that elevating PI3P can delay a pathway. Hyperactive Vps34 does not affect the induction of autophagy, but inhibits late steps in autophagy, in part via a delay in disassembly of the autophagy machinery from the surface of mature autophagosomes and also a delay in fusion of autophagosomes with the vacuole. This latter defect is likely due to a more general defect in vacuole fusion, as evidenced by an increase in the number of vacuole lobes per cell, which is consistent with a defect in homotypic vacuole fusion. Overall, our studies suggest that stimulus-induced elevation of PI3P regulates some, but not all, PI3P-dependent membrane trafficking pathways and that phosphoinositide lipids are commonly rate-limiting in pathways where they are required.

## Results and Discussion

### *Generation of hyperactive Vps34 mutants*

To test the hypothesis that changes in PPI levels drive downstream processes, we devised a strategy for specifically elevating PI3P. PI3P was an attractive target because several downstream PI3P-dependent processes have been identified in yeast (Figure

2.1A). Additionally, the existing 4.4 Å crystal structure of the yeast PI 3-kinase complex allowed us to predict amino acid changes that would increase PI3P levels (Rostislavleva *et al.*, 2015). Moreover, the crystal structure also allowed us to map the location of amino acid changes responsible for the hyperactivity of the Vps34 mutants identified in our screen.

We found that overexpression of Vps34 alone or together with Vps15 caused a modest, 13%, increase in PI3P levels despite robust overexpression (Figure 2.2A and B). This result suggests either that overexpression of additional subunits of the Vps34 complex are required for increased Vps34 function or that Vps34 kinase activity is negatively regulated.

To achieve more robust elevation of PI3P levels, we tested whether point mutations in Vps34 would yield a hyperactive enzyme. Vps34 activity is proposed to be regulated in part via changes in the contact of the Vps34 helical and kinase domains (HELCAT) with the Vps15 pseudokinase domain (Figure 2.1B) (Stjepanovic *et al.*, 2017). In the inactive conformation, the Vps34 HELCAT domain contacts the Vps15 scaffold. During activation, the Vps34 HELCAT domain is proposed to alter its contact with Vps15 and allow Vps34 to access its PI substrate. Based on the structure of the PI 3-kinase complex, we introduced point mutations in Vps34 along its contact site with Vps15 (Figure 2.2C). We tested eight Vps34 point mutants and identified two mutations, R283E and A287D, that robustly increased PI3P by 36 and 27%, respectively (Figure 2.2D).

Combining R283E and A287D, but not other mutations along the Vps34 HELCAT-Vps15 interface, elevated PI3P levels by approximately 40% (Figure 2.2E). These two mutants are on an alpha-helix N-terminal to the helical domain of Vps34 and face Vps15 (Figure 2.1C). Identification of these hyperactive Vps34 mutants provides further evidence that altered contact between the Vps34 HELCAT domain and Vps15 promotes Vps34 kinase activity.

We also performed an unbiased genetic screen for hyperactive Vps34 mutants using a method similar to one used to generate hyperactive mutations in the PI3P 5-kinase, Fab1 (Duex *et al.*, 2006b; Lang *et al.*, 2017). We generated a hypomorphic Vps34-K759D allele, which has a mutation in the activation loop of Vps34 and found that it lowers PI3P levels to approximately 20% of wild-type Vps34. We then performed random PCR mutagenesis on the C-terminal half of Vps34-K759D (Figure 2.3A). Mutagenized plasmids were tested for their ability to rescue growth in *vps34Δ* cells grown on rapamycin at 33°C. From 22 independently isolated mutants, we identified nine unique point mutations. Five of these mutations elevate PI3P levels. The best of these mutations, Y501C, elevated PI3P approximately 40% (Figure 2.1C, 2.3C). Interestingly, each of the five mutated residues are located on either the alpha-C helix of the Vps34 kinase domain or an adjacent helix of the helical domain (Figure 2.3B). Conformational changes in the alpha-C helix are critical for regulating kinase function (Taylor *et al.*, 2015). We hypothesize these hyperactive mutants favor an active conformation of the alpha-C helix. It is not known whether these are regulatory sites on the native enzyme. We determined that combining the R283E and A287D mutant with

Y501C (Vps34-EDC) elevates PI3P by approximately 60%, which is higher than either mutant alone (Figure 2.1D). The Vps34-EDC mutant does not change Vps34 protein levels (Figure 2.4A and B), nor does it change the localization of Vps34 within the cell as measured by the amount of Envy-Vps34 that co-localizes with the vacuole (Figure 2.4C and D). This suggests that the distribution of PI3P in the cell is most likely unchanged by the hyperactive mutant.

PI3P is the substrate for the PI3P 5-kinase Fab1, which generates $PI(3,5)P_2$ (Gary *et al.*, 1998). We tested whether elevation of PI3P via hyperactive Vps34 leads to an elevation of $PI(3,5)P_2$. At basal conditions, no statistically significant increase in $PI(3,5)P_2$ levels was detected (Figure 2.1E). However, when hyperosmotic shock was used to induce a transient elevation of $PI(3,5)P_2$ (Duex *et al.*, 2006a), the presence of hyperactive Vps34 mutants resulted in further elevation of $PI(3,5)P_2$ (Figure 2.1F). Note that while PI3P levels decrease during hyperosmotic shock, hyperactive Vps34 mutants still elevate PI3P above wild-type levels (Figure 2.3D). Thus, hyperactive Vps34 drives elevation of $PI(3,5)P_2$ during hyperosmotic shock. We ruled out several potential mechanisms by which hyperactive Vps34 might elevate $PI(3,5)P_2$. We determined that hyperactive Vps34-EDC does not change the amount of Fab1-Envy that co-localizes with the vacuole (Figure 2.5A and B). Additionally, there was no change in the amount of Fab1 complex member Fig4 (Botelho *et al.*, 2008) that colocalizes with the vacuole (Figure 2.5C and D). These results suggest that hyperactive Vps34 does not result in increased recruitment of the Fab1 complex to membranes. Moreover, the increase in $PI(3,5)P_2$ is likely not due to inhibition of Fig4, the $PI(3,5)P_2$ 5-phosphatase (Gary *et al.*, 2002).

Catalytically dead Fig4 mutants exhibit a mild increase in $PI(3,5)P_2$ under basal conditions, yet a decrease in $PI(3,5)P_2$ at 10 min following hyperosmotic shock (Duex *et al.*, 2006b; Strunk *et al.*, 2020). Thus, the increase in $PI(3,5)P_2$ caused by Vps34-EDC most likely occurs because of increased availability of PI3P, which may provide more substrate for Fab1 and/or activate Fab1. Note that the additional $PI(3,5)P_2$ provided during hyperosmotic shock by hyperactive Vps34-EDC does not affect the growth of yeast cells following hyperosmotic shock (Figure 2.5E).

*Hyperactive Vps34 increases retrograde transport of Atg27*

Atg27 is a cargo for PI3P-dependent Snx4- and retromer-dependent retrograde transport. Following its synthesis, Atg27 is delivered from the Golgi to the vacuole via the AP-3 pathway (Segarra *et al.*, 2015). From the vacuole, Atg27 undergoes retrograde transport to endosomes in a Snx4-dependent manner (Ma *et al.*, 2017; Suzuki and Emr, 2018). From endosomes, Atg27 undergoes retrograde transport back to the Golgi via the retromer (Suzuki and Emr, 2018). Due to the cyclic nature of its transport, changes in Atg27 localization signify changes in the rates of each of these transport steps.

We tested whether hyperactive Vps34 increases the rate of retrograde transport of Atg27 from the vacuole to endosomes and/or Golgi. In wild-type cells, Atg27-2xGFP was primarily localized to the vacuole (Figure 2.6A) with a few Golgi (Figure 2.6D) and endosomal (Figure 2.6F) puncta. Notably, in the presence of Vps34-EDC, Atg27-2xGFP was more punctate (Figure 2.6A) and fewer hyperactive Vps34-EDC cells had Atg27-2xGFP visible on the vacuole (Figure 2.6B). Moreover, on a per cell basis, less Atg27-

2xGFP colocalized with the vacuole (Figure 2.6C). Blocking retrograde transport from the vacuole by deletion of *SNX4* suppressed Atg27-2xGFP traffic from the vacuole (Figure 2.6A-C). These results suggest that hyperactive Vps34-EDC accelerates the Snx4 and/or retromer pathways.

The loss of Atg27-2xGFP localization to the vacuole is likely not caused by impairment of the AP-3-dependent anterograde delivery of Atg27 to the vacuole. We tested the localization of another AP-3 client protein Yck3 (Sun *et al.*, 2004) and found that it was delivered to the vacuole in the presence of Vps34-EDC (Figure 2.7A), indicating that Vps34-EDC does not cause a defect in AP-3 function.

We tested whether the additional Atg27-2xGFP puncta present in Vps34-EDC correspond to Golgi and/or endosomes. We found that expression of Vps34-EDC resulted in a higher percentage of the total cellular Atg27-2xGFP that colocalizes with the Golgi marker, Sec7-mCherry (Figure 2.6D and E). There was no statistically significant difference between Vps34-EDC-expressing cells compared to wild-type with respect to the total cellular Atg27-2xGFP signal that colocalized with endosome marker Vps8-mCherry (Figure 2.6F and G). Accumulation of Atg27-2xGFP in the Golgi is consistent with the hypothesis that hyperactive Vps34-EDC leads to increases in both Snx4- and retromer-dependent retrograde transport of Atg27.

We tested whether deletion of the retromer subunit *VPS35* suppresses the increased Atg27-2xGFP localization to the Golgi caused by Vps34-EDC. Consistent with the

retromer being required for accelerated retrograde transport of Atg27, in *vps35*Δ cells, there was no difference in Atg27-2xGFP localization to the Golgi between wild-type Vps34 and Vps34-EDC (Figure 2.7B and C). However, surprisingly, *vps35*Δ cells exhibited increased localization of Atg27-2xGFP to the Golgi compared to wild-type cells. This result was unexpected since a previous study reported that Atg27 accumulates on endosomes in *vps35*Δ cells with less Atg27 on Golgi (Suzuki and Emr, 2018), which fits with the view that the retromer functions in retrograde traffic of proteins from endosomes to the Golgi. However, this previous study is complicated by the fact that experiments were performed following 1 h of treatment with rapamycin. Because rapamycin inhibits protein synthesis in yeast (Barbet *et al.*, 1996), we reasoned that rapamycin treatment may have masked a defect in AP-3-dependent anterograde delivery of Atg27 to the vacuole, leading to accumulation of Atg27 in the Golgi. However, deletion of *VPS35* does not appear to affect AP-3 function, as another AP-3 client protein Yck3 is delivered to the vacuole in *vps35*Δ cells (Figure 2.7D). Thus, under basal conditions, trafficking of Atg27 in *vps35*Δ cells is more complex than previously appreciated. Together, these results suggest that, in yeast, elevating PI3P drives retrograde transport from the vacuole, and leaves open the possibility that retrograde traffic from endosomes to the Golgi is accelerated as well.

*Hyperactive Vps34 does not affect ESCRT-dependent degradation of amino acid transporters Ypq1 or Mup1*

ESCRT function is regulated by PI3P and plays a crucial role in trafficking select transmembrane proteins to the vacuole for degradation, including the vacuolar cationic

amino acid transporter Ypq1 (Li *et al.*, 2015; Zhu *et al.*, 2017). Following withdrawal of lysine, Ypq1 is ubiquitinated and internalized inside the vacuole by the ESCRT machinery where it is degraded.

Using western blot analysis, we tested whether hyperactive Vps34-EDC accelerates ESCRT-dependent degradation of Ypq1 following withdrawal of lysine by measuring Ypq1-GFP levels normalized to Vph1. We found that degradation of Ypq1-GFP was not affected by Vps34-EDC (Figure 2.8A and B), suggesting that elevating PI3P does not affect ESCRT function in the degradation of Ypq1.

We also tested a second ESCRT substrate, the plasma membrane methionine transporter Mup1 (Teis *et al.*, 2008). Mup1 accumulates on the plasma membrane when cells are starved for methionine. When methionine is reintroduced to cells, Mup1 is ubiquitinated, endocytosed, delivered to endosomes, and internalized by ESCRT into multi-vesicular bodies, which then fuse with the vacuole where Mup1 is degraded (Menant *et al.*, 2006; Teis *et al.*, 2008). Thus, to test ESCRT function, we measured Mup1-GFP levels normalized to Pgk1 following re-addition of methionine.

Similar to what was observed with Ypq1, there were no statistically significant differences in the rate of Mup1 degradation between wild-type and hyperactive Vps34-EDC following re-addition of methionine (Figure 2.8C and D). The half-life of Mup1-GFP following re-addition of methionine was calculated to be 33.7 min (SEM 2.39 min) with wild-type Vps34, and 30.8 min (SEM 2.61 min) with Vps34-EDC. This experiment

indicates that elevating PI3P does not affect ESCRT function in the degradation of Mup1. Overall, in contrast to the retrograde transport of Atg27, elevating PI3P does not accelerate ESCRT function on the vacuole or endosomes, demonstrating that elevating PI3P does not always increase the overall rate of a complex pathway.

*Hyperactive Vps34 inhibits a late step in autophagy*

PI3P is involved in multiple steps of autophagy, including autophagosome biogenesis, disassembly of the autophagy machinery from the surface of mature autophagosomes, and the fusion of mature autophagosomes with the vacuole. As part of our analysis, we investigated each of these steps. A combination of autophagy induction and flux was assessed by determining the levels of lipidated Atg8 (Atg8–PE) (Klionsky *et al.*, 2016). Atg8 (LC3 and GABARAP subfamilies in mammals) is a ubiquitin-like protein. The expression of *ATG8* is strongly induced after autophagy induction, following which Atg8 is conjugated to phosphatidylethanolamine (PE) on the phagophore membrane (Ichimura *et al.*, 2000). Following phagophore expansion and closure and before autophagosome-vacuole fusion, Atg8–PE on the cytoplasmic surface of the resulting autophagosome is cleaved from the membrane. The lumenal surface of the autophagosome, however, contains Atg8–PE that is trapped within the autophagosome. This pool of Atg8–PE can be monitored as autophagic cargo because, following fusion with the vacuole, this pool of Atg8–PE is degraded in the vacuolar lumen. Consequently, the steady-state level of Atg8–PE after autophagy induction is a function of both its generation and its degradation in the vacuole.

Treating cells with the serine protease inhibitor PMSF blocks the vacuolar degradation of Atg8–PE, facilitating the measurement of autophagy induction independent of Atg8–PE turnover. Following 1 h of autophagy stimulation by nitrogen starvation, no difference in Atg8–PE levels could be detected between strains expressing Vps34-WT and Vps34-EDC in the presence of PMSF (Figure 2.9A and B), suggesting that the extent of autophagy induction was unchanged by hyperactive Vps34-EDC. Similarly, in the presence of PMSF, no difference in Atg8–PE levels could be detected between strains expressing Vps34-WT and Vps34-EDC at either 15 or 30 min following nitrogen starvation (Figure 2.9C and D). These results suggest that autophagy initiation requires, but is not driven by PI3P.

As a second independent measure of the induction of autophagy, we investigated the transcriptional upregulation of critical autophagy genes, *ATG1*, *ATG7*, and *ATG9*, whose expression is elevated during nitrogen starvation (Delorme-Axford and Klionsky, 2018). We found no differences in mRNA levels between Vps34-WT and Vps34-EDC following 30 min of nitrogen starvation (Figure 2.10A), suggesting that hyperactive Vps34 does not affect the transcription of autophagy genes.

Whereas the levels of Atg8–PE are very similar between Vps34-WT and Vps34-EDC following starvation in the presence of PMSF, comparing Atg8–PE levels in the absence of PMSF reveals that Vps34-EDC partially blocks autophagy flux. In the absence of PMSF, degradation of Atg8–PE can occur after autophagosome fusion with the vacuole. Following 1 h of nitrogen starvation in the absence of PMSF, Atg8–PE protein levels

were markedly lower in Vps34-WT compared to Vps34-EDC (Figure 2.9A and B). The observation that no difference in Atg8–PE levels were detected between Vps34-WT and Vps34-EDC in the presence of PMSF, but that Atg8–PE was lower in Vps34-WT in the absence of PMSF, indicates that hyperactive Vps34 partially inhibits vacuolar delivery and degradation of Atg8–PE.

To further characterize the defect in a late step of autophagy, we examined the dynamics of autophagosome biogenesis using GFP-tagged Atg8 as a marker. Hyperactive Vps34-EDC results in an increased number of GFP-Atg8 puncta in cells following 30 min of nitrogen starvation (Figure 2.10B and C). This result is consistent with either an increase in the induction of autophagy and/or with the inhibition of a late step in autophagy. Using time-lapse microscopy of GFP-Atg8 puncta, we measured the lifetime of GFP-Atg8 puncta in strains expressing either Vps34-WT or Vps34-EDC. GFP-Atg8 puncta in the presence of Vps34-WT persisted for 9 min, consistent with previous studies (Cebollero *et al.*, 2012). In contrast, GFP-Atg8 puncta in the presence of Vps34-EDC persisted for 13.5 min (Figure 2.9E and F). These results suggest that the resolution of autophagosomes is delayed by hyperactive Vps34. Further evidence of this inhibition is observed by measuring the degradation of GFP-Atg8 via the appearance of proteolytically resistant free GFP by immunoblot analysis. Expression of hyperactive Vps34-EDC resulted in a reduction in the appearance of free GFP following 1 and 2 h of nitrogen starvation (Figure 2.11A and B), indicating a reduction in autophagy flux.

To explore whether yet higher elevation of PI3P levels would further reduce autophagy flux, we enhanced the elevation of PI3P by combining the Vps34-EDC mutant with a knockout of the *YMR1* gene, encoding a putative PI3P phosphatase. We found that the Vps34-EDC *ymr1Δ* mutant elevated PI3P by 105%, compared to 53% by Vps34-EDC alone and 28% by a *ymr1Δ* mutant alone (Figure 2.11C). Deletion of *YMR1* in our strain background more robustly elevated PI3P levels than previously reported (Parrish *et al.*, 2004), and the increase in PI3P levels caused by *YMR1* deletion was more evident in the presence of Vps34-EDC. Notably, the double Vps34-EDC *ymr1Δ* mutant inhibited autophagy flux considerably more than either mutation alone as measured by degradation of GFP-Atg8 by immunoblot analysis (Figure 2.11A and B). These results strongly indicate an inverse correlation between autophagy flux and an increase in cellular PI3P. Furthermore, the turnover of PI3P on autophagosomes may be critical for the successful completion of a late step in autophagy.

Prior to the fusion of mature autophagosomes with the vacuole, some autophagy proteins, including the PI3P-binding protein Atg18, must be removed from the autophagosome surface (Cebollero *et al.*, 2012). Removal of proteins from the surface of autophagosomes likely requires depletion of PI3P via the PI3P phosphatase Ymr1 (Cebollero *et al.*, 2012). Conversely, *in vitro* studies suggest that PI3P is required for the fusion of the autophagosome with the vacuole (Bas *et al.*, 2018). Thus, we tested whether the expression of hyperactive Vps34-EDC had an impact on the displacement of Atg18 from the autophagosome surface and/or the fusion of autophagosomes with the vacuole.

To specifically test displacement of Atg18 from the autophagosome surface independent of autophagosome-vacuole fusion, we blocked autophagosome-vacuole fusion by deleting the vacuolar t-SNARE Vam3 (Cebollero *et al.*, 2012). We assessed the disassembly of Atg18 after 1 h of nitrogen starvation, by determining the percentage of GFP-Atg8-positive autophagosomes that colocalized with surface Atg18-RFP. In *vam3Δ* cells, hyperactive Vps34-EDC leads to a 10% increase in the percentage of GFP-Atg8 puncta that colocalize with Atg18-RFP (Figure 2.11D and E). This result suggests that hyperactive Vps34-EDC leads to a defect in the dissociation of autophagy proteins from mature autophagosomes.

We also tested whether there was a defect in autophagosome fusion with the vacuole in a strain with wild-type Vam3. After 1 h of nitrogen starvation we measured the percentage of GFP-Atg8-positive autophagosomes that colocalize with Atg18-RFP. In this experiment, both disassembly of Atg18-RFP from the autophagosome surface and autophagosome-vacuole fusion can occur. A defect in autophagosome-vacuole fusion will result in the persistence of GFP-Atg8 puncta that do not colocalize with Atg18-RFP, and thus a decrease in the colocalization between GFP-Atg8 and Atg18-RFP. Indeed, we found that hyperactive Vps34-EDC caused a 9% decrease in the percentage of GFP-Atg8 puncta that colocalize with Atg18-RFP (Figure 2.11D and E). Note that the 10% defect in disassembly of Atg18-RFP from autophagosomes that was observed in the *vam3Δ* cells likely also occurs in the wild-type *VAM3* strain. Thus, this result suggests that Vps34-EDC leads to an approximately 20% defect in fusion of

autophagosomes with the vacuole. Additionally, the total number of GFP-Atg8 puncta observed in *vam3Δ* cells did not change between wild-type and hyperactive Vps34-EDC (Figure 2.10D). Because autophagosomes are not turned over in *vam3Δ* cells, this result provides further evidence that hyperactive Vps34-EDC does not affect the induction of autophagy, indicating that differences in autophagy induction are not responsible for changes in the colocalization of GFP-Atg8 and Atg18-RFP. Note that Atg18 protein levels were not different between wild-type and Vps34-EDC under nutrient-rich conditions or following nitrogen starvation (Figure 2.10E and F).

Together, our results suggest that whereas hyperactive Vps34-EDC has no effect on the induction of autophagy, it results in a decrease in autophagic flux in part via defects in both disassembly of the autophagy machinery from the surface of mature autophagosomes and fusion of autophagosomes with the vacuole. However, the 10% defect in disassembly of autophagy proteins from autophagosomes and the 20% defect in autophagosome-vacuole fusion do not fully account for the observed defect in autophagic flux. Autophagic flux, as measured by Atg8–PE levels, lifetime of Atg8 puncta, or degradation of GFP-Atg8 indicated a defect in the range of 50-70%. Thus, there are likely additional steps in the resolution of autophagy that are affected by hyperactive Vps34-EDC. Interestingly, despite inhibiting autophagy, hyperactive Vps34-EDC does not affect the survival of yeast cells during long-term nitrogen starvation (Figure 2.10G), which suggests that Vps34-EDC cells maintain sufficient levels of autophagy function to allow for survival during chronic nitrogen starvation.

The finding that hyperactive Vps34-EDC causes a partial defect in autophagosome fusion with the vacuole, raises the possibility that there is a more global defect in fusion with the vacuole. A defect in vacuole-vacuole fusion would result in a more fragmented vacuole morphology. To assess homotypic vacuole fusion, we counted the number of vacuole lobes per cell, finding a small but significant 12% increase in vacuole lobes (Figure 2.12A-B). This difference was predominantly due to an approximately 40% decrease in the number of cells with a single vacuole (Figure 2.12C). While an increase in the number of vacuole lobes per cell could also be caused by an increase in vacuole fission, a modest impairment of fusion fits closely with the observed defect in autophagosome fusion with the vacuole.

*Conclusions*

Most studies of PPI lipids use knockdown, knockout, or drug inhibition of PPI kinases to test whether a specific PPI is essential for a pathway. However, this approach does not indicate whether a PPI lipid is a key regulator of the pathway of interest. The ability to generate mutations that robustly elevate a PPI lipid provides an effective tool to elucidate the regulatory roles of PPI lipids. The major advantage of the Vps34-EDC mutant was that it enabled specific and direct testing of the downstream effects of elevating PI3P. It should be noted that in these experiments, the Vps34-EDC plasmid is constitutively expressed and thus PI3P is constitutively elevated. This is in contrast with wild-type cells where stimulus-induced changes in phosphoinositides occur on the order of minutes (Duex *et al.*, 2006a). Cells may respond differently to chronic versus acute elevation of phosphoinositides. We determined that elevation of PI3P drives some

pathways, including synthesis of $PI(3,5)P_2$ during hyperosmotic shock, as well as retrograde transport of Atg27. These findings demonstrate that elevation of PI3P drives some downstream processes and that in these cases, the PI3P-dependent step is rate limiting. In contrast, hyperactive Vps34 does not affect ESCRT function, demonstrating that elevating PI3P does not always increase the overall rate of a complex pathway. Much like ESCRT function, induction of autophagy is not accelerated by hyperactive Vps34, though, conversely, autophagic flux is lowered by hyperactive Vps34, in part by delaying disassembly of the autophagy machinery from the surface of mature autophagosomes as well as a delay in fusion of autophagosomes with the vacuole. These results provide evidence that PI3P can also inhibit specific steps within a pathway. Thus, these studies suggest that stimulus-induced elevation of PI3P can positively or negatively regulate some PI3P-dependent membrane trafficking pathways, and that phosphoinositide lipids are commonly rate-limiting in pathways where they are required. Moreover, these findings suggest that stimulus-induced elevation of PPI lipids provides a way for stimuli to selectively regulate pathways.

It is interesting to speculate on the reasons that elevating PI3P differentially impacts PI3P-dependent pathways. Because hyperactive Vps34-EDC does not appear to affect the localization of Vps34 within the cell, it is unlikely that these differential effects are caused by differences in the subcellular distribution of PI3P. We had initially hypothesized that elevating PI3P would drive downstream PI3P-dependent pathways by enhancing the recruitment of PI3P-binding proteins to membrane subdomains and/or increasing substrate availability, thus allowing downstream processes to occur more

rapidly. However, as observed in some pathways, elevating PI3P sometimes does not affect the rate of a process. One possibility is that wild-type PI3P levels are sufficient to saturate a process, allowing for the recruitment of all the molecules of a PI3P-binding protein to a membrane subdomain or to provide an enzyme with sufficient substrate. The production of $PI(3,5)P_2$ appears to fit this model. When Fab1 is activated during hyperosmotic shock, hyperactive Vps34 resulted in elevated production of $PI(3,5)P_2$, likely due to increased PI3P substrate availability. However, when Fab1 is not as active at basal conditions, $PI(3,5)P_2$ levels are not significantly increased by hyperactive Vps34, suggesting that wild-type PI3P levels are sufficient to provide Fab1 with enough substrate to produce $PI(3,5)P_2$. It is also possible that within a complicated multi-step process, PI3P may act in a step that is not rate limiting. In the ESCRT pathway related to PI3P-dependent degradation of Mup1, it is possible that elevated PI3P may accelerate the PI3P-dependent step of Mup1 degradation, but this acceleration is not observed in the overall rate of the pathway because a different step, perhaps the ubiquitination or endocytosis of Mup1, is rate limiting.

We also observed that increased PI3P production inhibits late steps in autophagy. We speculate that late in autophagy, excess PI3P results in the aberrant accumulation of PI3P-binding proteins on the surface of autophagosomes that would normally be released. The accumulation of these proteins crowds out other critical proteins that need to be recruited for the fusion of autophagosomes with the vacuole. Another possibility is that excess PI3P can lead to the expansion of membrane subdomains and dilute PI3P effectors, rendering them less functional. Support for this model comes from

a previous report that *ymr1Δsjl3Δ* cells, which accumulate approximately 2.5 times the PI3P present in wild-type cells with minimal changes to other phosphoinositides, have defects in retromer and ESCRT function (Parrish *et al.*, 2004). While interpretation of these results is complicated by the fact that Sjl3 is reported to act on a number of phosphoinositide species (Guo *et al.*, 1999; Hughes *et al.*, 2000; Foti *et al.*, 2001), excess PI3P is mislocalized in *ymr1Δsjl3Δ* cells, leading to mislocalization of PI3P-binding proteins in the retromer and ESCRT pathways (Parrish *et al.*, 2004). The differences between these previously reported results and the results reported here raise the possibility that the downstream effects of elevating PI3P may depend on the magnitude of the increase in PI3P levels or may be indicative of the differences in inhibiting the turnover of a PPI lipid versus accelerating its production.

Previous reports of the downstream effects of elevating PPI lipid levels are limited. Beyond the results reported here, hyperactive mutations in Fab1 were generated in our lab (Duex *et al.*, 2006b; Lang *et al.*, 2017) as a means to determine mechanisms of Fab1 activation. However, the impact of these changes on downstream pathways has not yet been pursued. To our knowledge, the only other hyperactive mutations in PPI kinases that have been identified are in the mammalian $PI(4,5)P_2$ 3-kinases, including p110α (PIK3CA) (Rodriguez-Viciana *et al.*, 1996; Samuels *et al.*, 2004; Ikenoue *et al.*, 2005). In this context, most hyperactive mutations in p110α were identified in patient samples as mutations that occurred frequently in cancer (Samuels *et al.*, 2004). $PI(4,5)P_2$ 3-kinase activity is required for the heregulin-induced phosphorylation of BRCA1 and hyperactive p110α is sufficient to induced a downstream increase in the

phosphorylation of BRCA1 (Altiok *et al.*, 1999). Hyperactive p110α also induces downstream phosphorylation of p70 S6 kinase and 4E-binding protein 1 (Ikenoue *et al.*, 2005; Kang *et al.*, 2005). Furthermore, $PI(4,5)P_2$ 3-kinase activity is required for the phosphorylation of AKT and for the downstream proliferation of human thyrocytes that is induced by oncogenic mutant RAS (Gire *et al.*, 2000). While hyperactive p110α is sufficient to induce phosphorylation of AKT, it does not lead to downstream cell proliferation unless combined with activation of MAPK (Gire *et al.*, 2000). Like $PI(4,5)P_2$ 3-kinase activity, MAPK activation is necessary, but not sufficient for the proliferative response to mutant RAS (Gire *et al.*, 1999), demonstrating that both signals are needed for cell proliferation and that hyperactive p110α does not always increase the rate of a complex pathway. However, other activating mutations in p110α are reported to have the ability to induce oncogenic transformation of NIH 3T3, mammary epithelial cells, and chicken embryo fibroblasts (Ikenoue *et al.*, 2005; Isakoff *et al.*, 2005; Kang *et al.*, 2005), suggesting that different hyperactive p110α mutants may have differing effects on cell proliferation. Since most previous studies report that hyperactive PPI kinases upregulate downstream processes, our findings demonstrate that the effects of elevating PPI lipid levels are more complicated than previously appreciated and merit further study in the future.

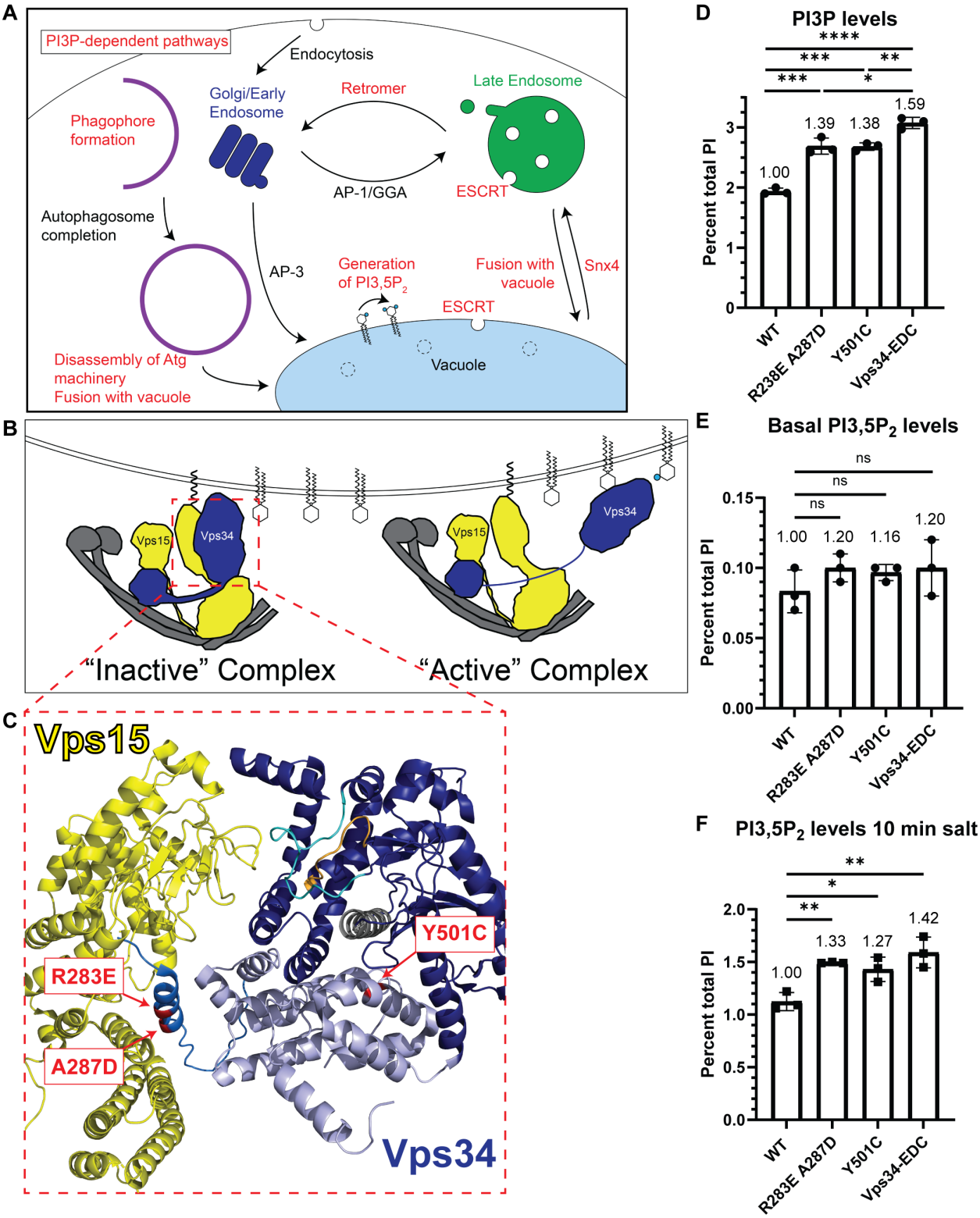


**Figure 2.1. Generation of hyperactive Vps34 mutants.** (A) Schematic indicating several PI3P-dependent intracellular trafficking pathways in yeast. PI3P serves as the substrate for PI(3,5)$P_2$. PI3P is also required for Snx4-dependent retrograde transport from the vacuole and retromer-dependent retrograde transport from endosomes.

ESCRT function at late endosomes and the vacuole is also dependent on PI3P. Furthermore, PI3P is required for phagophore formation during the initiation of autophagy, and PI3P is then removed prior to the disassembly of some autophagy proteins from the surface of mature autophagosomes. In addition, fusion of autophagosomes and other vesicles with the vacuole, as well as homotypic vacuole fusion (not shown), are PI3P-dependent pathways. (B) Vps34 is proposed to be regulated in part via changes in contact of the Vps34 HELCAT domain with Vps15. In the inactive conformation, the Vps34 HELCAT domain contacts the Vps15 scaffold. During activation, the Vps34 HELCAT domain is proposed to alter the contact with Vps15 and allow Vps34 to access its PI substrate (Stjepanovic *et al.*, 2017). (C) Crystal structure of the helical (light blue) and kinase (dark blue) domains of Vps34 and its contact with the pseudo-kinase domain of Vps15 (yellow) (Rostislavleva *et al.*, 2015). The three amino acid changes that comprise the Vps34-EDC hyperactive mutant are indicated (red). Two of these mutations, R283E and A287D, are on an alpha-helix N-terminal to the helical domain of Vps34 (neutral blue) and may hinder Vps34 HELCAT interaction with Vps15 and favor the active Vps34 conformation. The Y501C mutation is in the helical domain of Vps34 and faces the alpha-C helix (gray) of the kinase domain, nearby the activation (cyan) and catalytic (orange) loops of Vps34. (D-F) The Vps34 mutants R283E A287D and Y501C elevate PI3P levels. PI(3,5)$P_2$ levels are also elevated during hyperosmotic shock. Combining the mutants to Vps34-EDC further elevated PI3P levels and PI(3,5)$P_2$ levels. *vps34Δ* cells were transformed with a wild-type or mutant pRS416-Vps34 plasmid. PPI lipid levels were measured by metabolically labeling cells with myo-$^3$H-inositol for 16 h. Prior to harvest, indicated cultures were exposed to 10 min of hyperosmotic shock. PPI lipid head groups were separated by anion exchange and HPLC. n=3. Error bars indicate standard deviation. Unpaired t-test. ns=p>.05, *=p<.05, **=p<.01, ***=p<.001, ****=p<.0001.

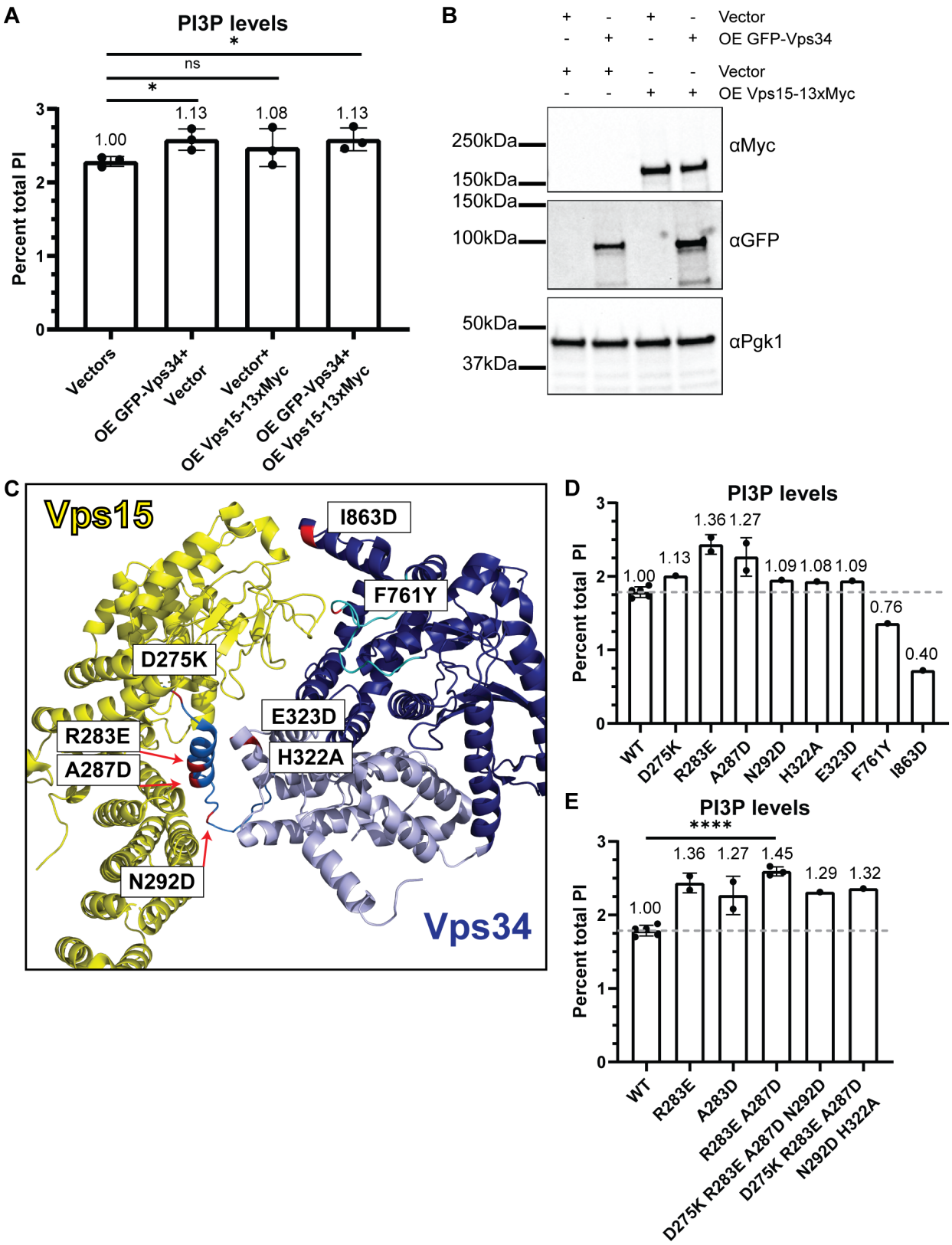


**Figure 2.2. Generation of hyperactive Vps34 mutants based on a high-resolution structure of the Vps34-Vps15-Vps30-Vps38 complex.** (A and B) Overexpression of

GFP-Vps34 and Vps15-13xMyc results in a modest 13% increase in PI3P levels. Wild-type yeast cells were transformed with pRS426-GFP-Vps34, pRS425-Vps15-13xMyc, or both plasmids together. PPI lipid levels were measured. In parallel, GFP-Vps34 and Vps15-13xMyc protein levels were analyzed via western blot to measure overexpression. Vps15-13xMyc was detected using anti-Myc antibody. GFP-Vps34 was detected with anti-GFP antibody. Pgk1 was used as a loading control. Representative of n=3. PPI lipid levels were measured by metabolically labeling cells with myo-$^{3}$H-inositol for 16 h, harvesting cells, and separating PPI lipid head groups by anion exchange and HPLC. n=3. Error bars indicate standard deviation. Unpaired t-test. ns=p>.05, *=p<.05. (C) Based on the crystal structure of the PI 3-kinase complex and the hypothesis that altering the contact between Vps34 HELCAT (helical in light blue kinase in dark blue) and Vps15 (yellow) would activate Vps34, we tested eight point mutants (red) in Vps34 for elevated PI3P levels (Rostislavleva *et al.*, 2015; Stjepanovic *et al.*, 2017). D275K, R283E, A287D, and N292D are on an alpha-helix N-terminal to the helical domain of Vps34 (neutral blue), E323D and H322A are in the helical domain, F761Y is in the activation loop (cyan), and I863D is in the kinase domain. (D and E) Of the mutants predicted to disrupt the interaction between Vps34 HELCAT and Vps15, PI3P levels are most elevated by R283E and A287D (D). Combination of R283E with A287D further elevated PI3P levels (E). However, combining R283E A287D with additional mutations did not further elevated PI3P levels (E). *vps34Δ* cells were transformed with a wild-type or mutant pRS416-Vps34 plasmid. PPI lipid levels were measured by metabolically labeling cells with myo-$^{3}$H-inositol for 16 h, harvesting cells, and separating PPI lipid head groups by anion exchange and HPLC. n=5 for WT, n=2 for R283E and A287D, n=3 for R283E A287D, n=1 for the rest. WT, R283E, and A287D data points are the same in D and E. Error bars indicate standard deviation. Unpaired t-test. ****=p<.0001.

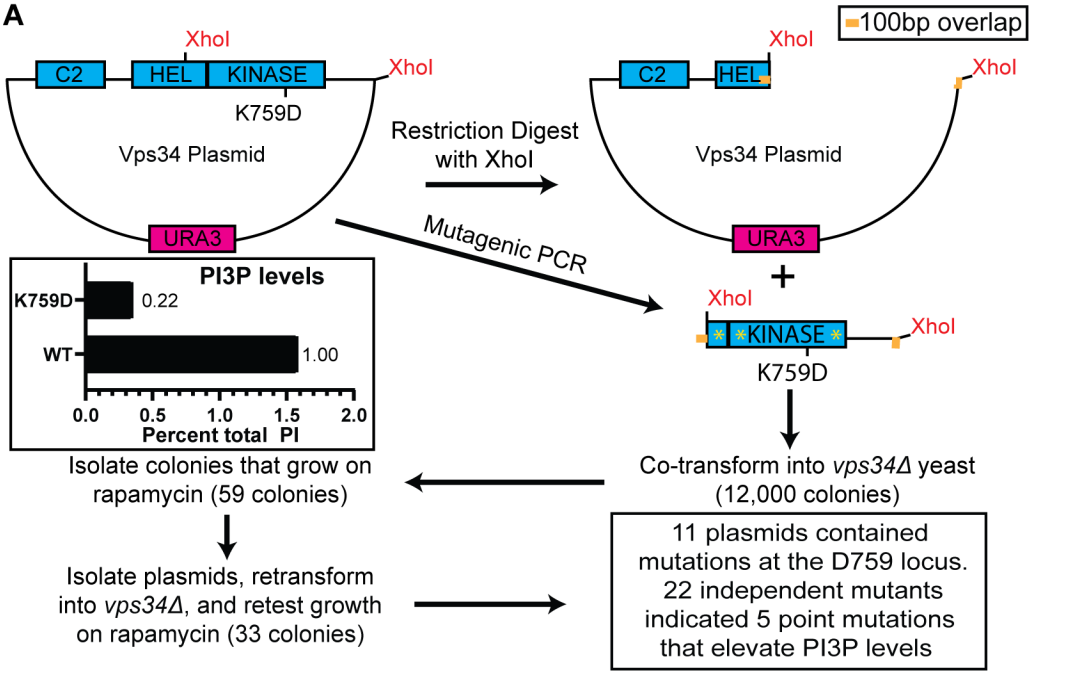
A
XhoI
C2
HEL
KINASE
XhoI
K759D
Vps34 Plasmid
URA3
Restriction Digest with XhoI
100bp overlap
XhoI
C2
HEL
XhoI
Vps34 Plasmid
URA3
Mutagenic PCR
PI3P levels
K759D
0.22
WT
1.00
0.0 0.5 1.0 1.5 2.0
Percent total PI
XhoI
KINASE
XhoI
K759D
Isolate colonies that grow on rapamycin (59 colonies)
Co-transform into vps34Δ yeast (12,000 colonies)
Isolate plasmids, retransform into vps34Δ, and retest growth on rapamycin (33 colonies)
11 plasmids contained mutations at the D759 locus. 22 independent mutants indicated 5 point mutations that elevate PI3P levels

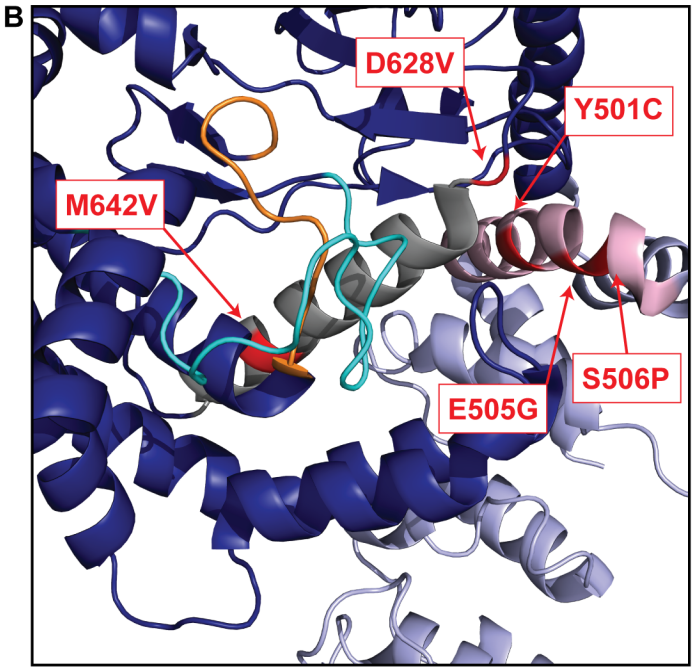
B
D628V
Y501C
M642V
S506P
E505G

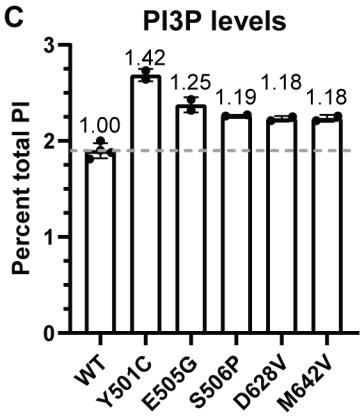
C
PI3P levels
Percent total PI
0
1
2
3
1.00
1.42
1.25
1.19
1.18
1.18
WT
Y501C
E505G
S506P
D628V
M642V

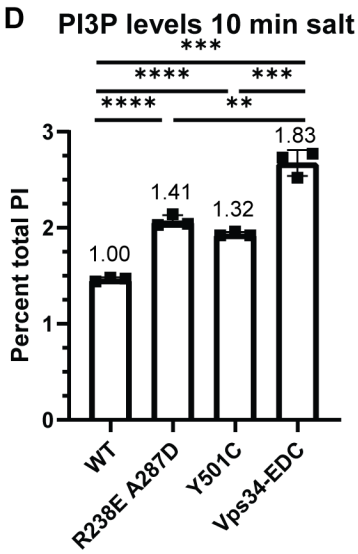
D
PI3P levels 10 min salt
***
****
***
****
**
Percent total PI
0
1
2
3
1.00
1.41
1.32
1.83
WT
R238E A287D
Y501C
Vps34-EDC

**Figure 2.3. Generation of hyperactive Vps34 mutants via a mutant screen.** (A) A screen for hyperactive mutations in Vps34 was designed to identify mutants that rescued growth of a hypomorphic Vps34 allele, Vps34-K759D, a mutation in the activation loop of Vps34 that lowers PI3P levels to 22% of wild-type. *vps34Δ* cells were transformed with pRS416-Vps34 or pRS416-Vps34-K759D plasmids. PPI lipid levels were measured by metabolically labeling cells with myo-$^{3}$H-inositol for 16 h, harvesting cells, and separating PPI lipid head groups by anion exchange and HPLC. n=1. The C-terminal half of Vps34 was PCR amplified using mutagenic Taq DNA polymerase and a Vps34 plasmid was cut with restriction enzyme, XhoI, to remove the region of Vps34 that was mutated. The plasmid backbone and mutated PCR fragment were co-transformed into *vps34Δ* cells. Two days following co-transformation, colonies were replica plated to plates containing 10 nM rapamycin and grown at 33°C. Mutant Vps34 plasmids were isolated from colonies that rescued growth on rapamycin at 33°C and retransformed into *vps34Δ* cells to confirm rescued growth on rapamycin at 33°C. Sanger sequencing was used to identify the mutations present in isolated plasmids. 22 independent mutants revealed nine unique point mutations. Of those nine mutations, changes at five of them were found to elevate PI3P levels. (B) Crystal structure of the helical (light blue) and kinase (dark blue) domains of Vps34, indicating five residues identified in the hyperactive Vps34 mutant screen (red). M642V and D628V are at opposite ends of the alpha-C helix (gray) of the kinase domain, nearby the activation (cyan) and catalytic (orange) loops of Vps34. Y501C, E505G, and S506P face the alpha-C helix on the same side of an alpha helix in the helical domain of Vps34 (light pink). (C) Of the mutants identified in the Vps34 hyperactive mutant screen, PI3P levels are most elevated by Y501C. *vps34Δ* cells were transformed with a wild-type or mutant pRS416-Vps34 plasmid. PPI lipid levels were measured by metabolically labeling cells with myo-$^{3}$H-inositol for 16 h, harvesting cells, and separating PPI lipid head groups by anion exchange and HPLC. n=4 for WT, n=2 for the rest. Error bars indicate standard deviation. (D) The Vps34 mutants R283E A287D and Y501C elevate PI3P levels during hyperosmotic shock. Combining the mutants to generate Vps34-EDC further elevated PI3P during hyperosmotic shock. *vps34Δ* cells were transformed with a wild-type or mutant pRS416-Vps34 plasmid. PPI lipid levels were measured by metabolically labeling cells with myo-$^{3}$H-inositol for 16 h. Prior to harvest, indicated cultures were exposed to 10 min of hyperosmotic shock. PPI lipid head groups were separated by anion exchange and HPLC. Data are from the same samples as Figure 2.1D-F. n=3. Error bars indicate standard deviation. Unpaired t-test. **=p<.01, ***=p<.001, ****=p<.0001.

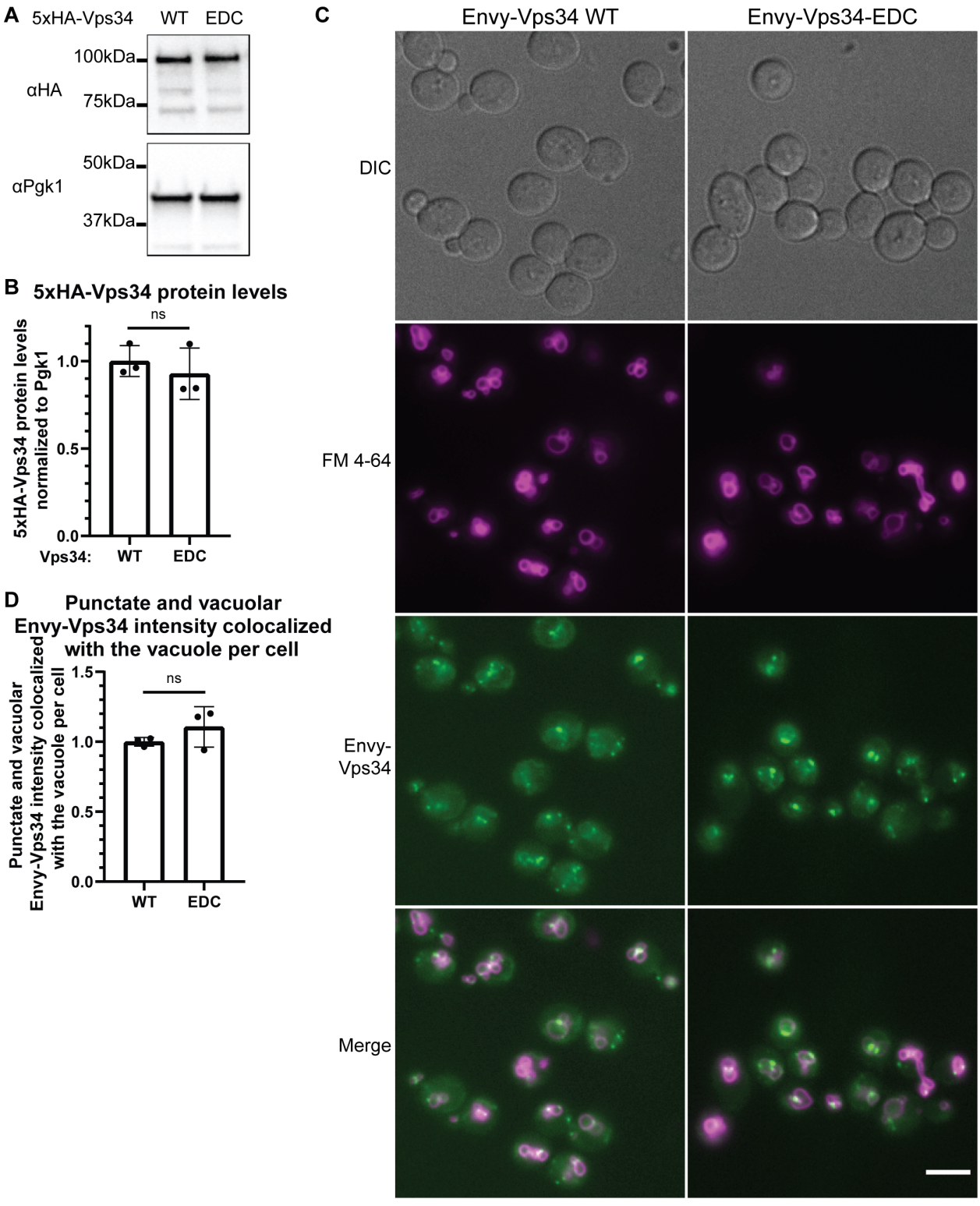


**Figure 2.4. Hyperactive Vps34-EDC does not affect the protein levels or localization of Vps34.** (A and B) Hyperactive Vps34-EDC does not change 5xHA-Vps34 protein levels. *vps34Δ* cells were transformed with pRS416-5xHA-Vps34 or pRS416-5xHA-Vps34-EDC. 5xHA-Vps34 protein levels were analyzed via western blot

using anti-HA antibody. 5xHA-Vps34 levels were normalized to Pgk1. Levels were then normalized to wild-type. Representative of n=3. Error bars indicate standard deviation. Unpaired t-test. ns=p>.05. (C and D) Hyperactive Vps34-EDC does not change the intensity of punctate and vacuolar Envy-Vps34 localized to the vacuole. *vps34Δ* cells were transformed with pRS416-Envy-Vps34 or pRS416-Envy-Vps34-EDC. After labeling with FM 4-64, cells were chased at 24°C for 3 h before imaging. DIC, differential interference contrast. Scale bar = 5 μm. The Envy-Vps34 signal that overlaps FM 4-64 was divided by the number of cells quantified. Quantification of at least 100 cells per n, n=3. The average of the wild-type samples was normalized to 1. Error bars indicate standard deviation. Unpaired t-test. ns=p>.05.

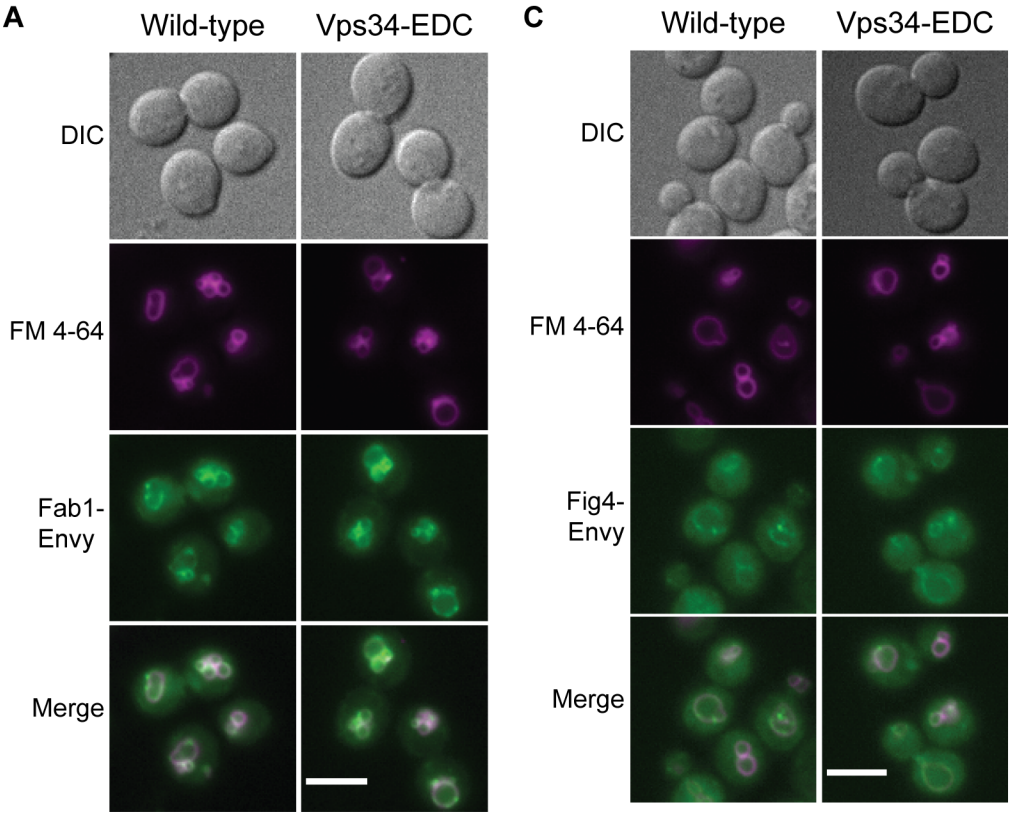
A
Wild-type
Vps34-EDC
DIC
FM 4-64
Fab1-Envy
Merge
C
Wild-type
Vps34-EDC
DIC
FM 4-64
Fig4-Envy
Merge

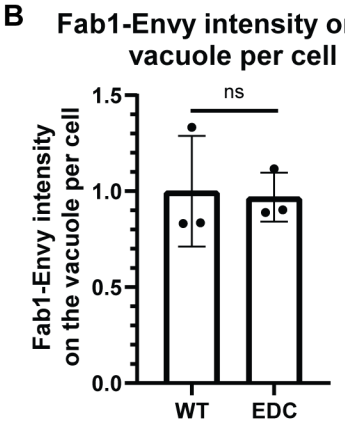
B
Fab1-Envy intensity on the vacuole per cell
Fab1-Envy intensity on the vacuole per cell
ns
1.5
1.0
0.5
0.0
WT
EDC

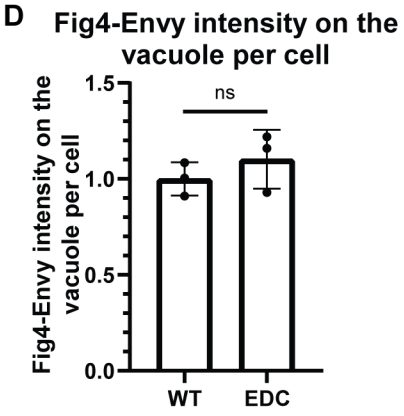
D
Fig4-Envy intensity on the vacuole per cell
Fig4-Envy intensity on the vacuole per cell
ns
1.5
1.0
0.5
0.0
WT
EDC

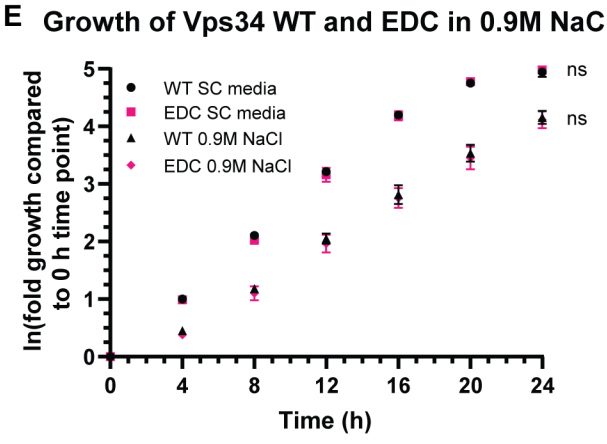
E
Growth of Vps34 WT and EDC in 0.9M NaCl
ln(fold growth compared to 0 h time point)
WT SC media
EDC SC media
WT 0.9M NaCl
EDC 0.9M NaCl
ns
ns
5
4
3
2
1
0
0
4
8
12
16
20
24
Time (h)

**Figure 2.5. Hyperactive Vps34-EDC does not affect the localization of some members of the PI(3,5)$P_2$ kinase complex.** (A and B) Hyperactive Vps34-EDC does not change the localization of Fab1-Envy to the vacuole. *vps34Δ* cells were transformed with pRS416-Fab1-Envy and pRS413-Vps34 or pRS413-Vps34-EDC. After labeling with FM 4-64, cells were chased at 24°C for 3 h before imaging. DIC, differential interference contrast. Scale bar = 5 µm. The Fab1-Envy signal that overlaps FM 4-64 was divided by the number of cells quantified. Quantification of at least 100 cells per n, n=3. The average of the wild-type samples was normalized to 1. Error bars indicate standard deviation. Unpaired t-test. ns=p>.05. (C and D) Hyperactive Vps34-EDC does not change the localization of Fig4-Envy to the vacuole. *vps34Δ* cells were transformed with pRS413-Fig4-Envy and pRS416-Vps34 or pRS416-Vps34-EDC. After labeling with FM 4-64, cells were chased at 24°C for 3 h before imaging. DIC, differential interference contrast. Scale bar = 5 µm. The Fig4-Envy signal that overlaps FM 4-64 was divided by the number of cells quantified. Quantification of at least 100 cells per n, n=3. The average of the wild-type samples was normalized to 1. Error bars indicate standard deviation. Unpaired t-test. ns=p>.05. (E) Hyperactive Vps34-EDC does not affect the growth of yeast cells following hyperosmotic shock. *vps34Δ* cells were transformed with pRS416-Vps34 or pRS416-Vps34-EDC. Cells were grown to mid-log phase in SC media and then diluted to equal concentrations. An equal volume of SC media or SC media with 1.8 M NaCl was added to the culture to begin the time-course. ODs were measured immediately following the addition of SC media or SC media with 1.8 M NaCl and then every 4 h for 24 h. The time zero OD measurement for each sample was normalized to 1. A natural logarithmic transformation was applied to the normalized ODs so that exponential growth is represented linearly. n=4. Error bars indicate standard deviation. Unpaired t-test between WT and EDC at each time point. ns=p>.05.

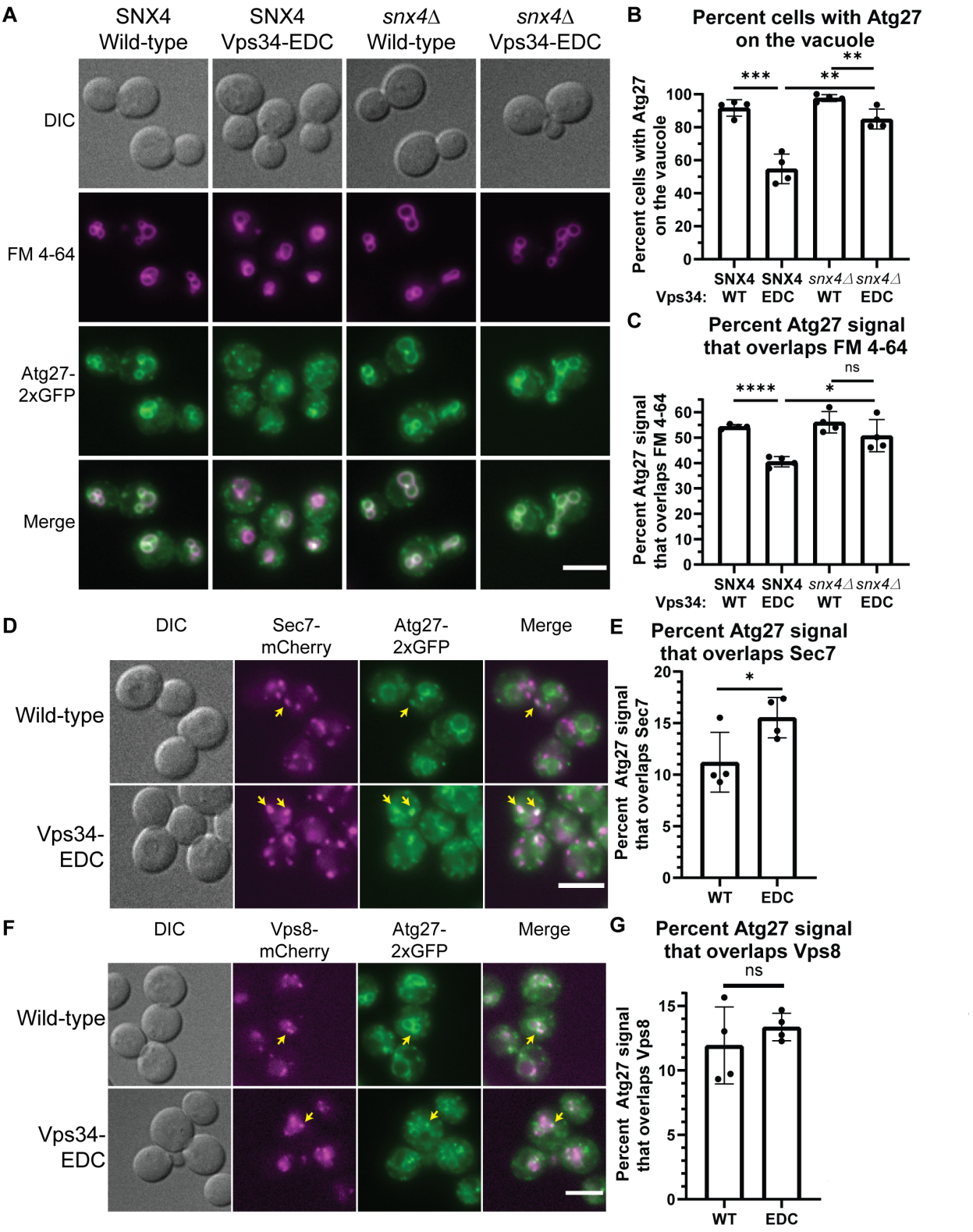


**Figure 2.6. Hyperactive Vps34 increases retrograde transport of Atg27.** (A-C) Hyperactive Vps34-EDC results in fewer cells that contain Atg27-2xGFP on the vacuole (FM 4-64, magenta) (B) and in less total Atg27-2xGFP colocalization with FM 4-64 (C).

Deletion of *SNX4* results in the retention of Atg27-2xGFP on the vacuole. *vps34Δ* or *vps34Δsnx4Δ* cells with Atg27-2xGFP integrated at the endogenous locus were transformed with pRS416-Vps34 or pRS416-Vps34-EDC. After labeling with FM 4-64, cells were chased at 24°C for 3 h before imaging. DIC, differential interference contrast. Scale bar = 5 μm. Cells were scored as either having Atg27-2xGFP visible on the vacuole (colocalization with FM 4-64) or present only in puncta. The scorer was blinded to the genotype of the cells being quantified (B). To measure Atg27-2xGFP localization on a population basis, the Atg27-2xGFP signal that overlaps FM 4-64 was divided by total Atg27-2xGFP signal (C). Quantification of at least 40 cells per n, n=4. Error bars indicate standard deviation. Unpaired t-test. ns=p>.05, *=p<.05, **=p<.01, ***=p<.001, ****=p<.0001. (D and E) Atg27-2xGFP partially colocalizes with the trans-Golgi (Sec7-mCherry). This colocalization increases in the presence of hyperactive Vps34-EDC. *vps34Δ* cells with Atg27-2xGFP and Sec7-mCherry integrated at the endogenous loci were transformed with pRS416-Vps34 or pRS416-Vps34-EDC. DIC, differential interference contrast. Scale bar = 5 μm. Examples of Atg27-2xGFP puncta that colocalize with Sec7-mCherry are indicated by yellow arrows. The Atg27-2xGFP signal that overlaps Sec7-mCherry was divided by total Atg27-2xGFP signal. Quantification of at least 40 cells per n, n=4. Error bars indicate standard deviation. Unpaired t-test. *=p<.05. (F and G) Atg27-2xGFP partially colocalizes with endosomes (Vps8-mCherry). This colocalization is not statistically different for hyperactive Vps34-EDC compared to wild-type. *vps34Δ* cells with Atg27-2xGFP and Vps8-mCherry integrated at the endogenous loci were transformed with pRS416-Vps34 or pRS416-Vps34-EDC. DIC, differential interference contrast. Scale bar = 5 μm. Examples of Atg27-2xGFP puncta that colocalize with Vps8-mCherry are indicated by yellow arrows. The Atg27-2xGFP signal that overlaps Vps8-mCherry was divided by total Atg27-2xGFP signal. Quantification of at least 40 cells per n, n=4. Error bars indicate standard deviation. Unpaired t-test. ns=p>.05.

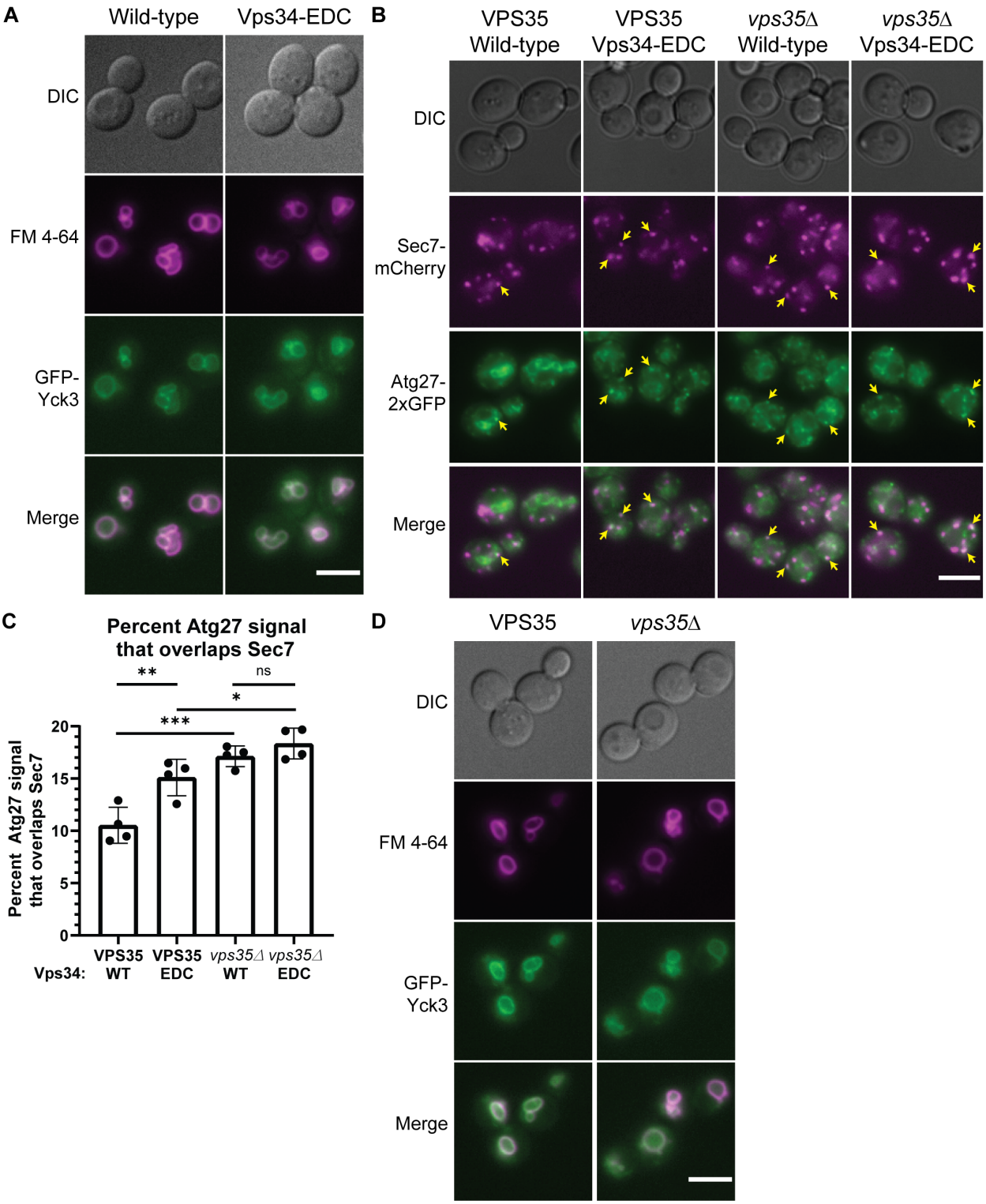


**Figure 2.7. Hyperactive Vps34 increases retrograde transport of Atg27.** (A) Hyperactive Vps34-EDC does not change the localization of the GFP-Yck3 kinase, an AP-3 client protein localized to the vacuole membrane. *vps34Δ* cells were co-transformed with pRS413-Vps34 or pRS413-Vps34-EDC and pRS416-GFP-Yck3. After labeling with FM 4-64, cells were chased at 24°C for 3 h before imaging. DIC,

differential interference contrast. Scale bar = 5 μm. At least 40 cells per n, n=3. (B and C) Atg27-2xGFP partially colocalizes with the trans-Golgi (Sec7-mCherry). This colocalization increases in the presence of hyperactive Vps34-EDC. In the absence of *VPS35*, Atg27-2xGFP colocalization with the trans-Golgi is unchanged between wild-type and Vps34-EDC. *vps34Δ* or *vps34Δ vps35Δ* cells with Atg27-2xGFP and Sec7-mCherry integrated at the endogenous loci were transformed with pRS416-Vps34 or pRS416-Vps34-EDC. DIC, differential interference contrast. Scale bar = 5 μm. Examples of Atg27-2xGFP puncta that colocalize with Sec7-mCherry are indicated by yellow arrows. The Atg27-2xGFP signal that overlaps Sec7-mCherry was divided by total Atg27-2xGFP signal. Quantification of at least 40 cells per n, n=4. Error bars indicate standard deviation. Unpaired t-test. ns=p>.05, *=p<.05, **=p<.01, ***=p<.001. (D) Deletion of *VPS35* does not change the localization of the GFP-Yck3 kinase, an AP-3 client protein localized to the vacuole membrane. Wild-type or *vps35*Δ cells were transformed with pRS416-GFP-Yck3. After labeling with FM 4-64, cells were chased at 24°C for 3 h before imaging. DIC, differential interference contrast. Scale bar = 5 μm. At least 40 cells per n, n=4.

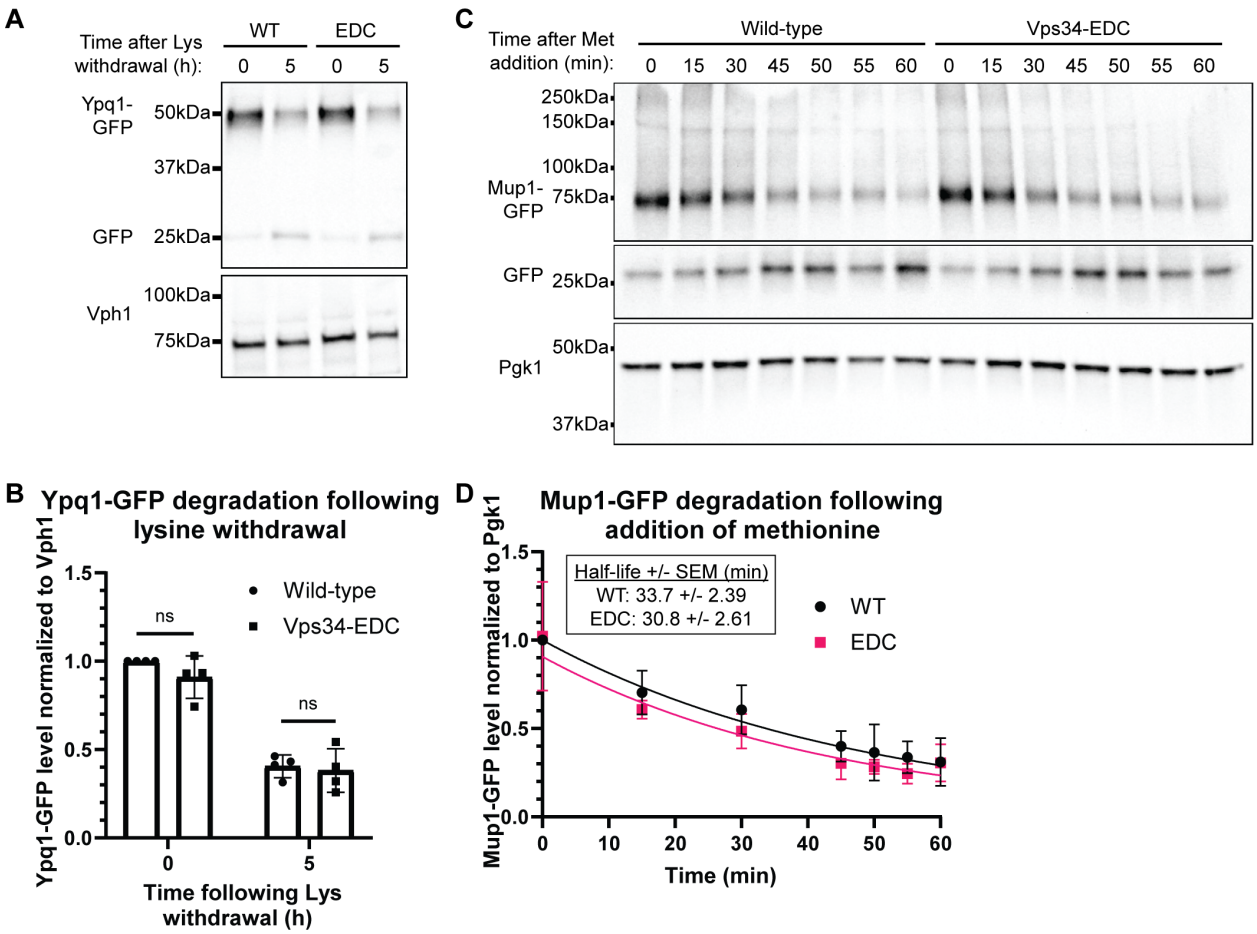


**Figure 2.8. Hyperactive Vps34 does not affect ESCRT-dependent degradation of amino acid transporters Ypq1 or Mup1.** (A and B) ESCRT-dependent internalization of Ypq1-GFP following the withdrawal of lysine is not statistically significantly different for hyperactive Vps34-EDC compared to wild-type. *vps34Δ* cells were transformed with pRS416-Vps34 or pRS416-Vps34-EDC and pRS414-Ypq1-GFP. To induce Ypq1-GFP internalization, cells were transferred to media lacking lysine. Samples were collected at 0 and 5 h following lysine withdrawal. Ypq1-GFP protein levels were analyzed via western blot using anti-GFP antibody and were normalized to Vph1. Levels were then normalized to wild-type at the zero time-point. Representative of n=4. Error bars indicate standard deviation. Unpaired t-test. ns=p>.05. (C and D) ESCRT-dependent internalization of Mup1-GFP following the addition of methionine is not statistically significantly different for hyperactive Vps34-EDC compared to wild-type. *vps34Δ* cells were transformed with pRS416-Vps34 or pRS416-Vps34-EDC and pRS414-Mup1-GFP. Cells were grown in media lacking methionine. To induce Mup1-GFP internalization, cells were transferred to media containing methionine. Samples were collected at the indicated time points following methionine addition. Mup1-GFP protein levels were analyzed via western blot using anti-GFP antibody and normalized to Pgk1. Levels were then normalized to wild-type at the zero time-point. Representative of n=4. Error bars indicate standard deviation. The degradation rate of Mup1-GFP was determined using a linear mixed effects model. The logarithmic transformation of Mup1-GFP levels was

modelled as a linear function of time and allowed to vary by genotype. Replicate-specific intercepts were included to account for residual correlation between protein levels within the same replicate. The difference in degradation rates between genotypes was not statistically significant (a 95% confidence interval of the genotype by time interaction contained 0). The equation generated by the linear mixed effects model is plotted (D). The half-life of Mup1-GFP following re-addition of methionine was calculated to be 33.7 min (SEM 2.39 min) with wild-type Vps34, and 30.8 min (SEM 2.61 min) with Vps34-EDC.

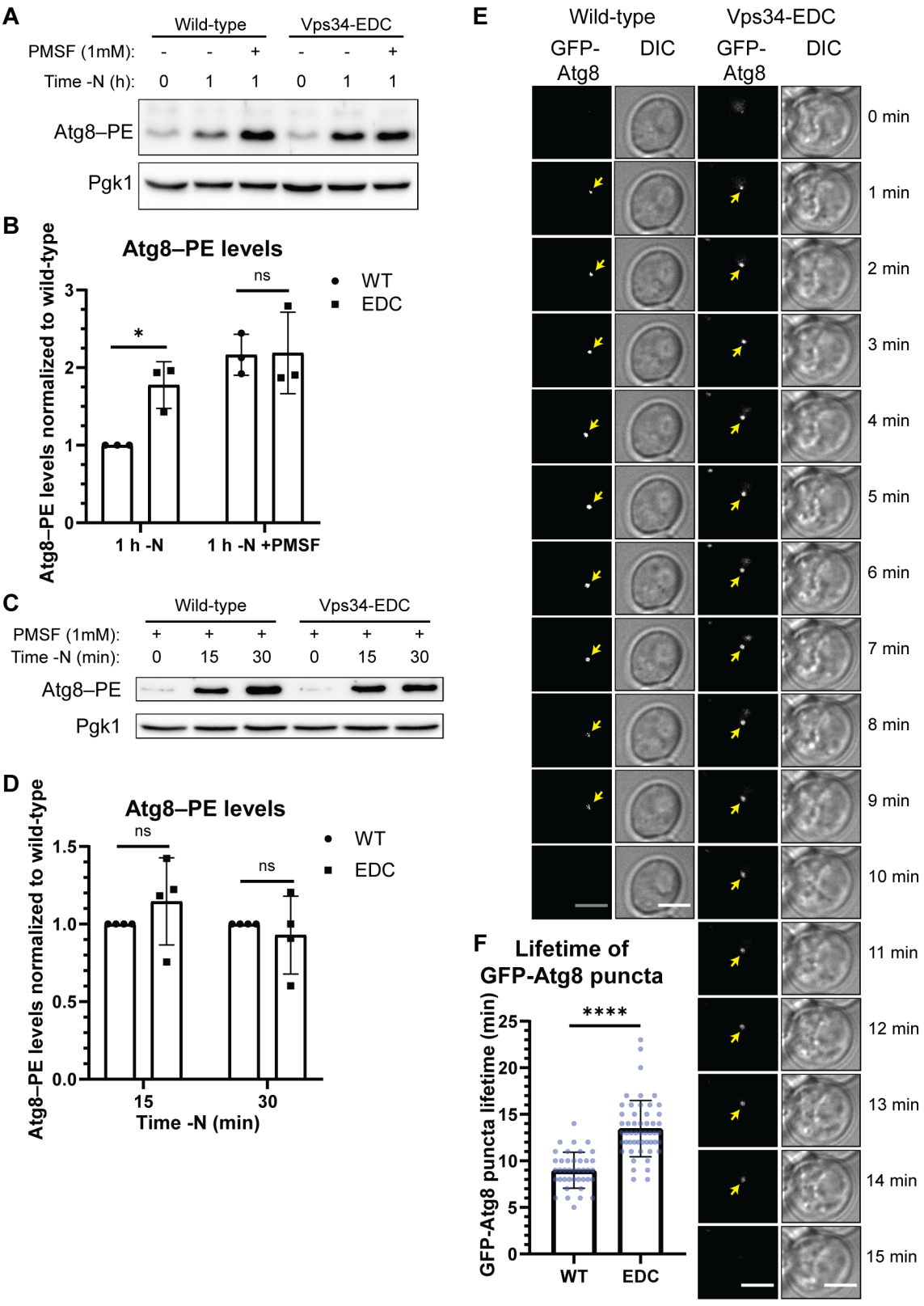


**Figure 2.9. Hyperactive Vps34 inhibits a late step in autophagy.** (A and B) Comparison of Atg8–PE protein levels in the absence and presence of PMSF, a protease inhibitor, suggests that Vps34-EDC inhibits a late step in autophagy, but does

not change the rate of autophagy induction. During autophagy, the levels of Atg8–PE are determined by both covalent attachment of phosphatidylethanolamine (PE) to Atg8 and by degradation of Atg8–PE once autophagosomes fuse with the vacuole. When degradation of Atg8–PE is inhibited by the serine protease inhibitor, PMSF, there was no difference in Atg8–PE levels in Vps34-WT compared to Vps34-EDC, suggesting that autophagy induction is unchanged by Vps34-EDC. However, in the absence of PMSF, Atg8–PE protein levels are elevated by hyperactive Vps34-EDC following 1 h of nitrogen starvation, suggesting that Vps34-EDC inhibits a late step in autophagy. *vps34Δ* cells were transformed with pRS416-Vps34 or pRS416-Vps34-EDC. Atg8–PE protein levels were analyzed via western blot using anti-Atg8 antibody. Atg8–PE levels were normalized to Pgk1. Levels were further normalized to wild-type at 1 h of nitrogen starvation. Representative of n=3. Error bars indicate standard deviation. Unpaired t-test. ns=p>.05, *=p<.05. (C and D) Following 15 and 30 min of nitrogen starvation, Atg8–PE protein levels are unchanged between hyperactive Vps34-EDC and wild-type when degradation of Atg8–PE is inhibited by the protease inhibitor, PMSF. This result suggests that Vps34-EDC does not affect autophagy induction. *vps34Δ* cells were transformed with pRS416-Vps34 or pRS416-Vps34-EDC. Atg8–PE protein levels were analyzed via western blot using anti-Atg8 antibody. Atg8–PE levels were normalized to Pgk1. Levels were further normalized to wild-type at 15 and 30 min following nitrogen starvation. Representative of n=4. Error bars indicate standard deviation. Unpaired t-test. ns=p>.05. (E and F) Hyperactive Vps34-EDC results in an increase in the lifetime of GFP-Atg8 puncta in cells. *vps34Δ* cells were co-transformed with pRS414-GFP-Atg8 and pRS416-Vps34 or pRS416-Vps34-EDC. Cells were imaged every minute for 26 min following 30 min of nitrogen starvation. 20 z-slices that were 0.2 μm apart were acquired at each time point. Single z-slice. DIC, differential interference contrast. Scale bar = 3.5 μm. GFP-Atg8 puncta were tracked over time with the lifetime of each puncta calculated as the time between the first and last frames the puncta were visible. Only GFP-Atg8 puncta that could be followed unambiguously over their lifetime were analyzed. For wild-type, n=40. For Vps34-EDC, n=52. Error bars indicate standard deviation. Unpaired t-test. ****=p<.0001.

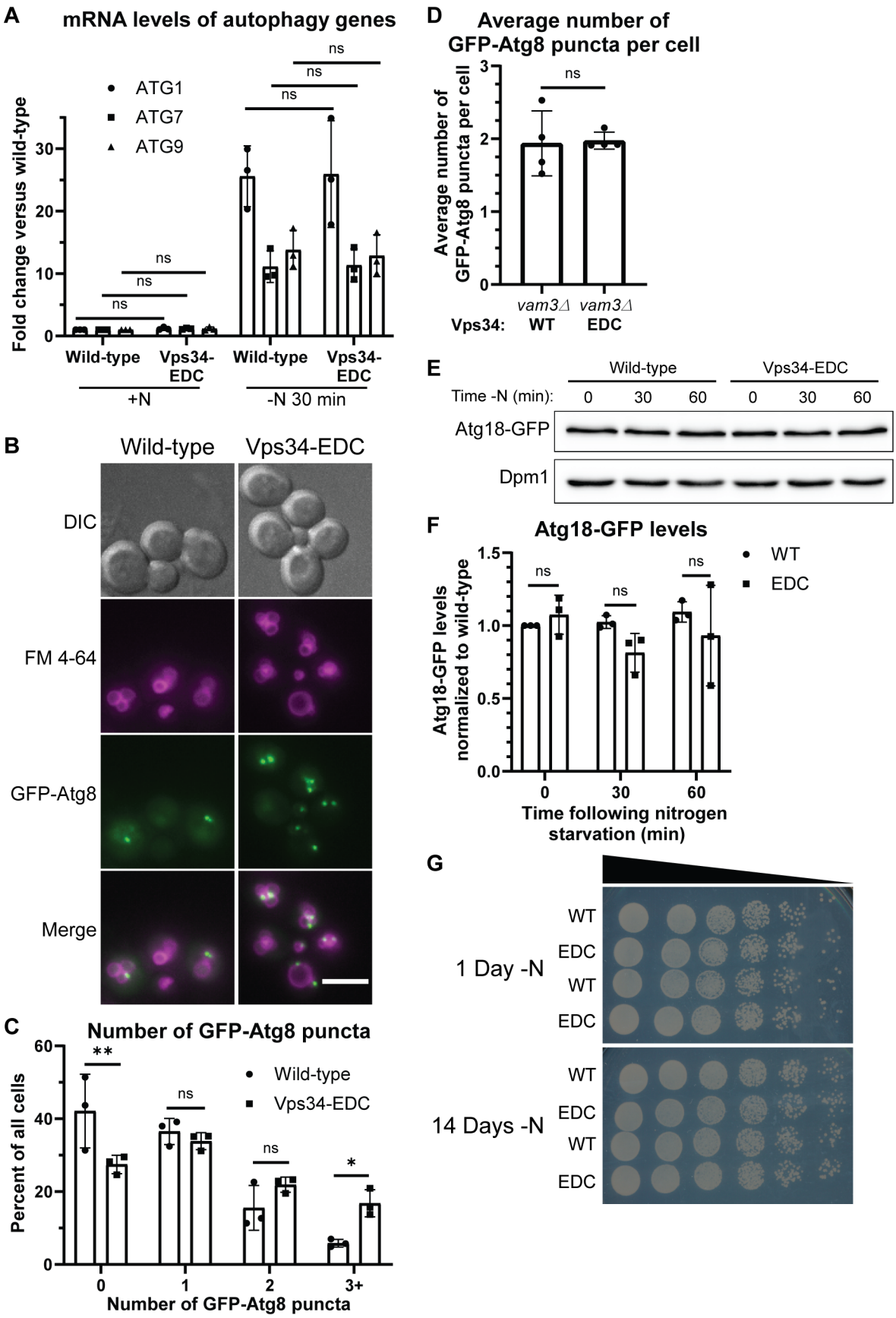
A
mRNA levels of autophagy genes
ATG1
ATG7
ATG9
Fold change versus wild-type
ns
Wild-type
Vps34-EDC
Wild-type
Vps34-EDC
+N
-N 30 min
B
Wild-type
Vps34-EDC
DIC
FM 4-64
GFP-Atg8
Merge
C
Number of GFP-Atg8 puncta
Wild-type
Vps34-EDC
Percent of all cells
**
*
Number of GFP-Atg8 puncta
D
Average number of GFP-Atg8 puncta per cell
Average number of GFP-Atg8 puncta per cell
vam3Δ
vam3Δ
Vps34:
WT
EDC
E
Wild-type
Vps34-EDC
Time -N (min):
Atg18-GFP
Dpm1
F
Atg18-GFP levels
Atg18-GFP levels normalized to wild-type
WT
EDC
Time following nitrogen starvation (min)
G
1 Day -N
14 Days -N
WT
EDC

**Figure 2.10. Hyperactive Vps34 inhibits a late step in autophagy.** (A) mRNA levels of *ATG1*, *ATG7*, and *ATG9* are unchanged between Vps34-EDC and wild-type, suggesting that Vps34-EDC does not affect the transcription of select autophagy genes. *vps34Δ* cells were transformed with pRS416-Vps34 or pRS416-Vps34-EDC. *ATG1*, *ATG7*, and *ATG9* mRNA transcript levels were measured by qRT-PCR in nitrogen rich conditions and following 30 min of nitrogen starvation. mRNA levels were normalized to wild-type in nitrogen rich conditions. n=3. Error bars indicate standard deviation. Unpaired t-test. ns=p>.05. (B and C) Hyperactive Vps34-EDC results in an increase in the number of GFP-Atg8 puncta in cells following 30 min of nitrogen starvation. *vps34Δ* cells were co-transformed with pRS414-GFP-Atg8 and pRS416-Vps34 or pRS416-Vps34-EDC. After labeling with FM 4-64, cells were chased at 24°C for 3 h before 9 z-slices that were 0.2 µm apart were imaged. Maximum intensity projection. DIC, differential interference contrast. Scale bar = 5 µm. GFP-Atg8 puncta were counted by a scorer who was blinded to the genotype of the cells being quantified. Quantification of at least 100 cells per n, n=3. Error bars indicate standard deviation. Two-way ANOVA and Dunnett's post-hoc test. ns=p>.05, *=p<.05, **=p<.01. (D) Hyperactive Vps34-EDC does not cause an increase in the number of GFP-Atg8 puncta in *vam3Δ* cells after 1 h of nitrogen starvation. This experiment is an alternative quantification of the experiment performed in Figure 2.11D and E. *vps34Δ vam3Δ* cells with Atg18-RFP integrated at the endogenous locus were transformed with pRS413-GFP-Atg8 and pRS416-Vps34 or pRS416-Vps34-EDC. GFP-Atg8 puncta were counted by a scorer who was blinded to the genotype of the cells being quantified. Cells without visible Atg18-RFP were excluded from quantification. Quantification of 100 cells per n, n=4. Error bars indicate standard deviation. Unpaired t-test. ns=p>.05. (E and F) Vps34-EDC does not change Atg18-GFP protein levels at basal conditions or during nitrogen starvation. *vps34Δ* cells were co-transformed with pRS413-Vps34 or pRS413-Vps34-EDC and pRS416-Atg18-GFP. Atg18-GFP protein levels were analyzed via western blot using anti-GFP antibody. Atg18-GFP levels were normalized to Dpm1. Levels were then normalized to wild-type at basal conditions. Representative of n=3. Error bars indicate standard deviation. Unpaired t-test. ns=p>.05. (G) Hyperactive Vps34-EDC does not affect the survival of yeast cells during long-term nitrogen starvation. *vps34Δ* cells were transformed with pRS416-Vps34 or pRS416-Vps34-EDC and grown to mid-log phase in SC media. Equal numbers of cells were collected and rinsed twice in nitrogen-starvation media before resuspending in nitrogen-starvation media. Following 1 day and 14 days of nitrogen starvation, equal volumes of culture were serially diluted 1:5 and spotted on SC plates. Plates were imaged following 3 days of yeast growth. 2 representative samples of n=4.

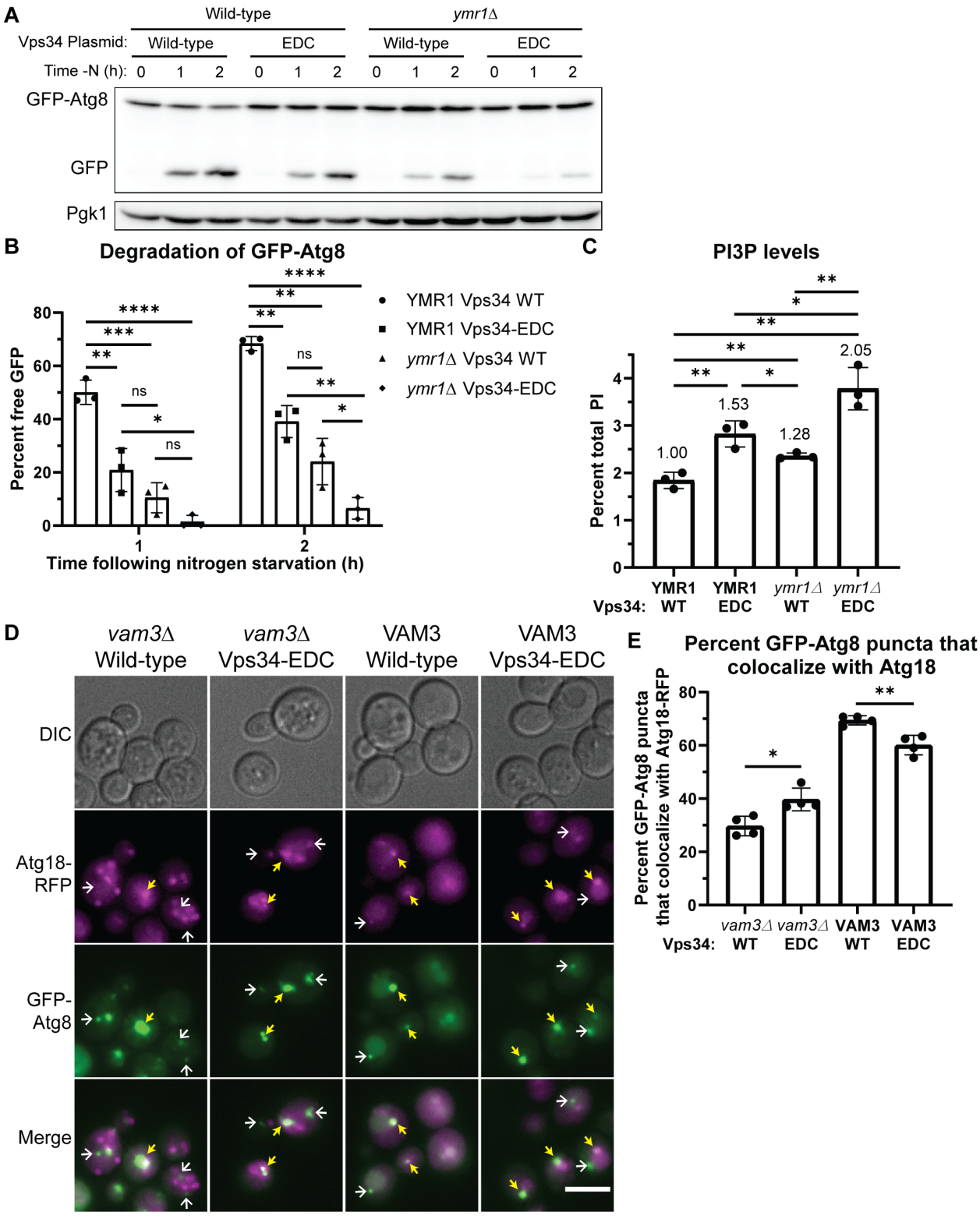


**Figure 2.11. Hyperactive Vps34 inhibits a late step in autophagy.** (A and B) The Vps34-EDC mutant or deletion of *YMR1* inhibits degradation of GFP-Atg8 following nitrogen starvation. Combining Vps34-EDC with a deletion of *YMR1* further inhibits degradation of GFP-Atg8, indicating a block in autophagy flux. *vps34Δ* or *vps34Δ ymr1Δ*

cells were co-transformed with pRS416-Vps34 or pRS416-Vps34-EDC and copper inducible pRS414-pCup1-GFP-Atg8. No exogenous copper was added during this experiment. GFP-Atg8 and GFP protein levels were analyzed via western blot using anti-GFP antibody. Free GFP levels were divided by the sum of GFP-Atg8 and free GFP and expressed as a percent. Representative of n=3. Error bars indicate standard deviation. Unpaired t-test. ns=p>.05, *=p<.05, **=p<.01, ***=p<.001, ****=p<.0001. (C) The Vps34-EDC mutant and deletion of the yeast myotubularin gene *YMR1* elevated PI3P levels. Combining Vps34-EDC with deletion of *YMR1* further elevated PI3P levels. *vps34Δ* or *vps34Δ ymr1Δ* cells were transformed with pRS416-Vps34 or pRS416-Vps34-EDC. PPI lipid levels were measured by metabolically labeling cells with myo-$^{3}$H-inositol for 16 h, harvesting cells, and separating PPI lipid head groups by anion exchange and HPLC. n=3. Error bars indicate standard deviation. Unpaired t-test. *=p<.05, **=p<.01. (D and E) Hyperactive Vps34-EDC leads to a defect in disassembly of the autophagy machinery from the surface of mature autophagosomes as well as a defect in fusion of autophagosomes with the vacuole. In the presence of Vam3, Vps34-EDC caused a small but statistically significant decrease in the percentage of GFP-Atg8 puncta that colocalize with Atg18-RFP after 1 h of nitrogen starvation. This suggests that Vps34-EDC leads to a minor defect in fusion of autophagosomes with the vacuole. However, in *vam3Δ* cells where fusion of autophagosomes with the vacuole is completely blocked, hyperactive Vps34-EDC leads to a small but statistically significant increase in the percentage of GFP-Atg8 puncta that colocalize with Atg18-RFP after 1 h of nitrogen starvation. This result suggests that Vps34-EDC also leads to a minor defect in the dissociation of key autophagy machinery from mature autophagosomes. *vps34Δ* or *vps34Δ vam3Δ* cells with Atg18-RFP integrated at the endogenous locus were transformed with pRS413-GFP-Atg8 and pRS416-Vps34 or pRS416-Vps34-EDC. Cells were imaged after 1 h of nitrogen starvation. DIC, differential interference contrast. Scale bar = 5 μm. Individual GFP-Atg8 puncta were scored on whether or not they colocalized with Atg18-RFP puncta. The scorer was blinded to the genotype of the cells being quantified. Cells without visible Atg18-RFP were excluded from quantification. Examples of GFP-Atg8 puncta that colocalize with Atg18-RFP are indicated by yellow arrows. Examples of GFP-Atg8 puncta that do not colocalize with Atg18-RFP are indicated by white arrows. Quantification of 100 cells per n, n=4. Error bars indicate standard deviation. Unpaired t-test. **=p<.01, ****=p<.0001.

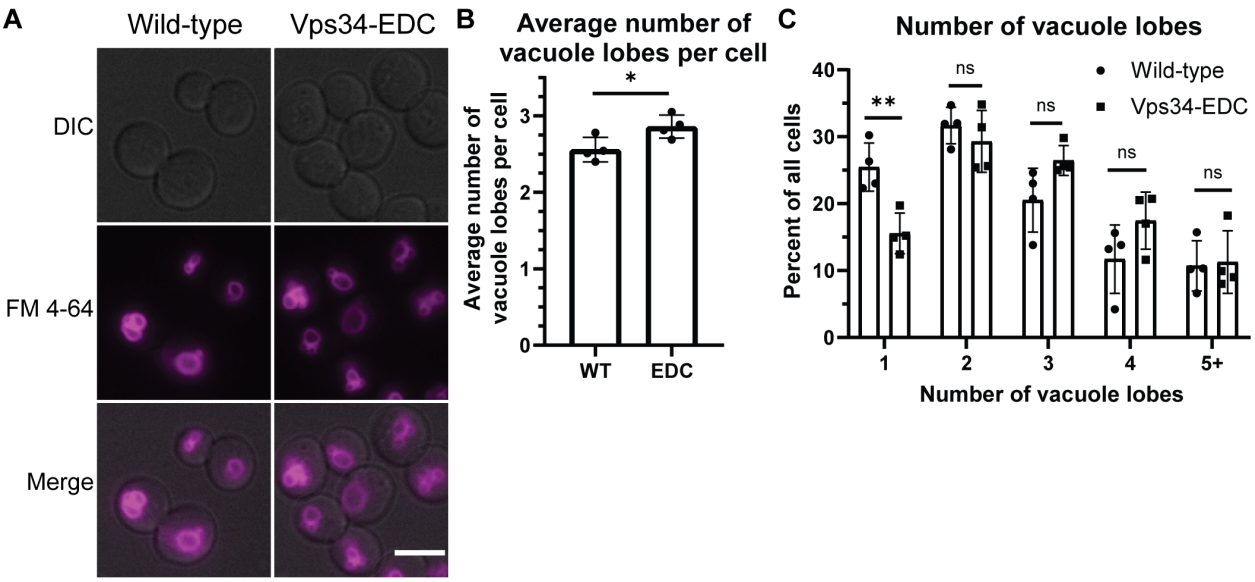


**Figure 2.12. Hyperactive Vps34-EDC may lead to a modest decrease in homotypic vacuole fusion.** (A-C) Hyperactive Vps34-EDC results in a 12% increase in the average number of vacuole lobes in a cell (B), which occurs primarily due to a decrease in the number of cells with 1 vacuole lobe (C). *vps34Δ* cells were transformed with pRS416-Vps34 or pRS416-Vps34-EDC. After labeling with FM 4-64, cells were chased at 24°C for 3 h before imaging. DIC, differential interference contrast. Scale bar = 5 µm. The number of vacuole lobes was counted by a scorer who was blinded to the genotype of the cells being quantified. Quantification of at least 100 cells per n, n=4. Error bars indicate standard deviation. Unpaired t-test (B). Two-way ANOVA and Dunnett's post-hoc test (C). ns=p>.05, *=p<.05, **=p<.01.

**References**

Altiok, S., Batt, D., Altiok, N., Papautsky, A., Downward, J., Roberts, T.M., and Avraham, H. (1999). Heregulin induces phosphorylation of BRCA1 through phosphatidylinositol 3-Kinase/AKT in breast cancer cells. J Biol Chem *274*, 32274-32278.

Balla, T. (2013). Phosphoinositides: tiny lipids with giant impact on cell regulation. Physiol Rev *93*, 1019-1137.

Barbet, N.C., Schneider, U., Helliwell, S.B., Stansfield, I., Tuite, M.F., and Hall, M.N. (1996). TOR controls translation initiation and early G1 progression in yeast. Mol Biol Cell *7*, 25-42.

Bas, L., Papinski, D., Licheva, M., Torggler, R., Rohringer, S., Schuschnig, M., and Kraft, C. (2018). Reconstitution reveals Ykt6 as the autophagosomal SNARE in autophagosome-vacuole fusion. J Cell Biol.

Botelho, R.J., Efe, J.A., Teis, D., and Emr, S.D. (2008). Assembly of a Fab1 phosphoinositide kinase signaling complex requires the Fig4 phosphoinositide phosphatase. Mol Biol Cell *19*, 4273-4286.

Cebollero, E., van der Vaart, A., Zhao, M., Rieter, E., Klionsky, D.J., Helms, J.B., and Reggiori, F. (2012). Phosphatidylinositol-3-phosphate clearance plays a key role in autophagosome completion. Curr Biol *22*, 1545-1553.

Delorme-Axford, E., and Klionsky, D.J. (2018). Transcriptional and post-transcriptional regulation of autophagy in the yeast Saccharomyces cerevisiae. J Biol Chem *293*, 5396-5403.

Duex, J.E., Nau, J.J., Kauffman, E.J., and Weisman, L.S. (2006a). Phosphoinositide 5-phosphatase Fig 4p is required for both acute rise and subsequent fall in stress-induced phosphatidylinositol 3,5-bisphosphate levels. Eukaryot Cell *5*, 723-731.

Duex, J.E., Tang, F., and Weisman, L.S. (2006b). The Vac14p-Fig4p complex acts independently of Vac7p and couples PI3,5P2 synthesis and turnover. J Cell Biol *172*, 693-704.

Foti, M., Audhya, A., and Emr, S.D. (2001). Sac1 lipid phosphatase and Stt4 phosphatidylinositol 4-kinase regulate a pool of phosphatidylinositol 4-phosphate that functions in the control of the actin cytoskeleton and vacuole morphology. Mol Biol Cell *12*, 2396-2411.

Gary, J.D., Sato, T.K., Stefan, C.J., Bonangelino, C.J., Weisman, L.S., and Emr, S.D. (2002). Regulation of Fab1 phosphatidylinositol 3-phosphate 5-kinase pathway by Vac7 protein and Fig4, a polyphosphoinositide phosphatase family member. Mol Biol Cell *13*, 1238-1251.

Gary, J.D., Wurmser, A.E., Bonangelino, C.J., Weisman, L.S., and Emr, S.D. (1998). Fab1p is essential for PtdIns(3)P 5-kinase activity and the maintenance of vacuolar size and membrane homeostasis. J Cell Biol *143*, 65-79.

Gire, V., Marshall, C., and Wynford-Thomas, D. (2000). PI-3-kinase is an essential anti-apoptotic effector in the proliferative response of primary human epithelial cells to mutant RAS. Oncogene *19*, 2269-2276.

Gire, V., Marshall, C.J., and Wynford-Thomas, D. (1999). Activation of mitogen-activated protein kinase is necessary but not sufficient for proliferation of human thyroid epithelial cells induced by mutant Ras. Oncogene *18*, 4819-4832.

Guo, S., Stolz, L.E., Lemrow, S.M., and York, J.D. (1999). SAC1-like domains of yeast SAC1, INP52, and INP53 and of human synaptojanin encode polyphosphoinositide phosphatases. J Biol Chem *274*, 12990-12995.

Hughes, W.E., Woscholski, R., Cooke, F.T., Patrick, R.S., Dove, S.K., McDonald, N.Q., and Parker, P.J. (2000). SAC1 encodes a regulated lipid phosphoinositide phosphatase, defects in which can be suppressed by the homologous Inp52p and Inp53p phosphatases. J Biol Chem *275*, 801-808.

Ichimura, Y., Kirisako, T., Takao, T., Satomi, Y., Shimonishi, Y., Ishihara, N., Mizushima, N., Tanida, I., Kominami, E., Ohsumi, M., et al. (2000). A ubiquitin-like system mediates protein lipidation. Nature *408*, 488-492.

Ikenoue, T., Kanai, F., Hikiba, Y., Obata, T., Tanaka, Y., Imamura, J., Ohta, M., Jazag, A., Guleng, B., Tateishi, K., et al. (2005). Functional analysis of PIK3CA gene mutations in human colorectal cancer. Cancer Res *65*, 4562-4567.

Isakoff, S.J., Engelman, J.A., Irie, H.Y., Luo, J., Brachmann, S.M., Pearline, R.V., Cantley, L.C., and Brugge, J.S. (2005). Breast cancer-associated PIK3CA mutations are oncogenic in mammary epithelial cells. Cancer Res *65*, 10992-11000.

Kang, S., Bader, A.G., and Vogt, P.K. (2005). Phosphatidylinositol 3-kinase mutations identified in human cancer are oncogenic. Proc Natl Acad Sci U S A *102*, 802-807.

Kihara, A., Noda, T., Ishihara, N., and Ohsumi, Y. (2001). Two distinct Vps34 phosphatidylinositol 3-kinase complexes function in autophagy and carboxypeptidase Y sorting in Saccharomyces cerevisiae. J Cell Biol *152*, 519-530.

Klionsky, D.J., Abdelmohsen, K., Abe, A., Abedin, M.J., Abeliovich, H., Acevedo Arozena, A., Adachi, H., Adams, C.M., Adams, P.D., Adeli, K., et al. (2016). Guidelines for the use and interpretation of assays for monitoring autophagy (3rd edition). Autophagy *12*, 1-222.

Lang, M.J., Strunk, B.S., Azad, N., Petersen, J.L., and Weisman, L.S. (2017). An intramolecular interaction within the lipid kinase Fab1 regulates cellular phosphatidylinositol 3,5-bisphosphate lipid levels. Mol Biol Cell.

Li, M., Rong, Y., Chuang, Y.S., Peng, D., and Emr, S.D. (2015). Ubiquitin-dependent lysosomal membrane protein sorting and degradation. Mol Cell *57*, 467-478.

Ma, M., Burd, C.G., and Chi, R.J. (2017). Distinct complexes of yeast Snx4 family SNX-BARs mediate retrograde trafficking of Snc1 and Atg27. Traffic *18*, 134-144.

Menant, A., Barbey, R., and Thomas, D. (2006). Substrate-mediated remodeling of methionine transport by multiple ubiquitin-dependent mechanisms in yeast cells. EMBO J *25*, 4436-4447.

Parrish, W.R., Stefan, C.J., and Emr, S.D. (2004). Essential role for the myotubularin-related phosphatase Ymr1p and the synaptojanin-like phosphatases Sjl2p and Sjl3p in regulation of phosphatidylinositol 3-phosphate in yeast. Mol Biol Cell *15*, 3567-3579.

Rodriguez-Viciana, P., Warne, P.H., Vanhaesebroeck, B., Waterfield, M.D., and Downward, J. (1996). Activation of phosphoinositide 3-kinase by interaction with Ras and by point mutation. EMBO J *15*, 2442-2451.

Rostislavleva, K., Soler, N., Ohashi, Y., Zhang, L., Pardon, E., Burke, J.E., Masson, G.R., Johnson, C., Steyaert, J., Ktistakis, N.T., et al. (2015). Structure and flexibility of the endosomal Vps34 complex reveals the basis of its function on membranes. Science *350*, aac7365.

Samuels, Y., Wang, Z., Bardelli, A., Silliman, N., Ptak, J., Szabo, S., Yan, H., Gazdar, A., Powell, S.M., Riggins, G.J., et al. (2004). High frequency of mutations of the PIK3CA gene in human cancers. Science *304*, 554.

Segarra, V.A., Boettner, D.R., and Lemmon, S.K. (2015). Atg27 tyrosine sorting motif is important for its trafficking and Atg9 localization. Traffic *16*, 365-378.

Stjepanovic, G., Baskaran, S., Lin, M.G., and Hurley, J.H. (2017). Vps34 Kinase Domain Dynamics Regulate the Autophagic PI 3-Kinase Complex. Mol Cell *67*, 528-534 e523.

Strunk, B.S., Steinfeld, N., Lee, S., Jin, N., Munoz-Rivera, C., Meeks, G., Thomas, A., Akemann, C., Mapp, A.K., MacGurn, J.A., et al. (2020). Roles for a lipid phosphatase in the activation of its opposing lipid kinase. Mol Biol Cell *31*, 1835-1845.

Sun, B., Chen, L., Cao, W., Roth, A.F., and Davis, N.G. (2004). The yeast casein kinase Yck3p is palmitoylated, then sorted to the vacuolar membrane with AP-3-dependent recognition of a YXXPhi adaptin sorting signal. Mol Biol Cell *15*, 1397-1406.

Suzuki, S.W., and Emr, S.D. (2018). Membrane protein recycling from the vacuole/lysosome membrane. J Cell Biol *217*, 1623-1632.

Taylor, S.S., Shaw, A.S., Kannan, N., and Kornev, A.P. (2015). Integration of signaling in the kinome: Architecture and regulation of the alphaC Helix. Biochim Biophys Acta *1854*, 1567-1574.

Teis, D., Saksena, S., and Emr, S.D. (2008). Ordered assembly of the ESCRT-III complex on endosomes is required to sequester cargo during MVB formation. Dev Cell *15*, 578-589.

Zhu, L., Jorgensen, J.R., Li, M., Chuang, Y.S., and Emr, S.D. (2017). ESCRTs function directly on the lysosome membrane to downregulate ubiquitinated lysosomal membrane proteins. Elife *6*.

# CHAPTER III

## Future Directions

Studies with hyperactive Vps34 revealed that elevating phosphoinositide (PPI) lipids selectively impact a subset of downstream processes that require a specific PPI. We find that hyperactive Vps34 can drive certain pathways, inhibit other pathways, and have no measurable effect on others. Our studies suggest that stimulus-induced elevation of phosphoinositides provides a way for these stimuli to selectively regulate downstream processes. However, there are still gaps in our understanding of the biological roles and regulation of PI3P.

### Evidence for another PI 3-kinase in yeast

Others have suggested that Vps34 is the sole enzyme responsible for generating PI3P from PI in yeast because of reports that no PI3P is detected in *vps34Δ* cells (Schu *et al.*, 1993). In my own studies, however, when examining elution profiles of PPI lipids separated by anion exchange chromatography in *vps34Δ* cells, a small peak elutes at the same location where the PI3P peak elutes in wild-type cells (Figure 3.1). I have not tried to analyze this peak further. If this peak is due to PI3P, this would raise the possibility that an as yet unidentified PI 3-kinase generates a small pool of PI3P in yeast. Tor1 is a potential candidate to have a small amount of PI 3-kinase activity, as it

contains a domain with significant sequence similarity to yeast and mammalian Vps34 (Cafferkey *et al.*, 1993).

**Gleaning mechanistic insights into the regulation of Vps34**

Previously, our lab generated hyperactive mutations in the PI3P 5-kinase, Fab1, by screening for mutants that rescued Fab1 function in strains where key Fab1 activators were knocked out (Duex *et al.*, 2006; Lang *et al.*, 2017). These mutants led to mechanistic insights into the regulation of Fab1 (Lang *et al.*, 2017). In this study, instead of knocking out genes encoding Vps34 regulators, we performed a screen based on rescuing growth of a hypomorphic Vps34 allele that was mutated near the active site of the enzyme. The mutants identified in this screen were concentrated near the active site of the kinase and most likely help favor an active conformation of the kinase, but may not be regulatory sites on the native enzyme. In support of this idea, we found that while mutations near the active site such as Y501C and D628V rescued the growth of the K759D mutant on several conditions tested, the R283E A287D mutants did not (Figure 3.2). Thus, these two different screening strategies appear to return mutations that provide insight into different aspects of PPI kinase function and regulation. These differences should guide the design of future screens for hyperactive PPI kinases. A screen that avoids crippling the active site of the kinase is more likely to yield mechanistic insights into the regulation of a PPI kinase. When regulators of PPI kinases are not known or when the sole goal of a hyperactive mutant is to determine downstream effects of elevating a PPI lipid, a screening strategy based on a hypomorphic PPI kinase allele is straightforward because catalytic site residues can be

readily identified. Going forward, to glean new mechanistic insights into the regulation of Vps34, it may be informative to screen for mutants that rescue Vps34 function in strains where key Vps34 activators are knocked out.

**Additional screens to identify hyperactive mutants in PI 3-kinase complex components**

We have begun the process of identifying screening conditions to generate hyperactive Vps34 mutants that can provide novel insights into the regulation of Vps34. We found that, unlike the Vps34-K759D mutant, all tested hyperactive Vps34 were able to rescue growth of *vps30Δ* cells grown at 33°C on plates containing 15mM $ZnSO_4$ (Figure 3.3). Using these new conditions, we performed an unbiased genetic screen for hyperactive Vps34 mutants that rescue growth of *vps30Δ* cells (Figure 3.4). Different from the previous screen, we performed random PCR mutagenesis on the N-terminal rather than C-terminal half of Vps34 and were able to isolate 25 mutants (Figure 3.5). Of the mutants generated, we were encouraged that we isolated mutations at amino acid R283 (orange), as the R283E mutant was already confirmed to be hyperactive. Additionally, we isolated mutations at nearby E285 and R286 (orange), suggesting that multiple mutations on this helix can result in hyperactive Vps34. Also encouraging was the isolation of two mutants on the alpha-C helix, Q633K and E644K, a region of Vps34 where hyperactive mutants D628V and M642V were already identified.

Interestingly, there were also two clusters of mutants in the helical domain of Vps34 that possibly represent novel regulatory sites on Vps34 (yellow and blue). However, a

number of these mutants included mutations to glycine and proline, amino acids with poor propensity to form helices and thus may be disrupting the folding of the helical domain rather than acting as a true regulatory site. If, however, these mutants were disrupting the binding of a Vps34 regulator to the helical domain, we reasoned that charge reversal mutations in charged residues on the surface of Vps34 in these regions would disrupt the binding of the Vps34 regulator, while not affecting the folding of the helical domain. Thus, we selected three mutations, E353K, R388E, and E417K on the surface of the helical domain in these clusters (Figure 3.6) and tested whether these mutants led to increased production of PI3P, finding that none of the three mutants resulted in significant increases in PI3P levels (Figure 3.7). While it is possible that these clusters do represent bonified regulatory sites for Vps34, this result suggests that the mutants identified in the screen may simply be disrupting the folding of the Vps34 helical domain.

Going forward, additional hyperactive mutant screens may be informative in understanding more about the regulation of the yeast PI 3-kinase complexes. It may be instructive to repeat the screen described above for Vps34 mutants that rescue growth of *vps30Δ* cells grown at 33°C on plates containing 15mM $ZnSO_4$. Alternatively, it may be useful to identify a different growth condition for the screen or to perform the screen with a different PI 3-kinase complex protein knocked out. One option would be to perform the screen in *vps38Δ* cells, which maintain PI3P levels similar to *vps30Δ* cells (Burda *et al.*, 2002). On the other hand, it may also be informative to identify conditions

to perform a screen in *vps15Δ* cells, which do not produce detectable levels of PI3P (Stack *et al.*, 1993).

It may also be informative to screen for hyperactive mutants in other members of the PI 3-kinase complex. We designed a screen to identify hyperactive mutations in Vps15 that elevate PI3P levels. The screen was based on rescued growth of *vps30Δ* cells grown at 33°C on plates containing 21 mM $ZnSO_4$. However, of the plasmids isolated from the 26 colonies that grew on 21 mM $ZnSO_4$ at 33°C, none were able to rescue growth on 21 mM $ZnSO_4$ at 33°C when retransformed into *vps15Δvps30Δ* cells. This result suggested that growth was rescued in these colonies by mutations at other places in the genome and raises the possibility that hyperactive mutations in Vps15 are difficult to generate. In the future, it may still be informative to repeat this screen to try to identify hyperactive mutations in Vps15 or to identify mutations in the genomes of colonies that rescue growth, but do not contain mutations in Vps15. Furthermore, it may also be instructive to identify a different growth condition for a Vps15 hyperactive mutant screen or to identify conditions to screen for hyperactive mutations in Vps30, Vps38, or Atg14.

**Evidence and potential roles for a third Vps34-containing complex**

There are a number of clues in the literature that Vps34/Vps15 maintain some functions independent of the other subunits in complexes I and II. In addition to defects in CPY and API maturation and autophagy, *vps15Δ* and *vps34Δ* cells exhibit temperature sensitive growth at 37°C and have defects in PrA and PrB maturation that are not present in *vps30Δ*, *vps38Δ*, or *atg14Δ* cells (Kihara *et al.*, 2001) (Figure 1.3).

Furthermore, while *vps30Δ*, *vps38Δ*, and *vps30Δvps38Δ* cells maintain about 30% of their normal PI3P levels (Burda *et al.*, 2002) and *atg14Δ* cells exhibit near wild-type PI3P levels (Kihara *et al.*, 2001), *vps34Δ* and *vps15Δ* cells have almost no detectable PI3P. These results raise two major possibilities: either Vps34 and Vps15 retain partial function that is independent of Vps30, Vps38, and Atg14, or Vps34 and Vps15 are members of an as yet unidentified third Vps34-containing complex in yeast.

The fact that *vps30Δ* and *vps38Δ* cells exhibit a defect in CPY maturation, but not PrA and PrB maturation is intriguing because *vps15Δ* and *vps34Δ* cells exhibit defects in PrA and PrB maturation and PrA and B and CPY follow a similar maturation pathway (Kihara *et al.*, 2001) (Figure 1.3). This difference potentially points to a role for a hypothesized third yeast PI 3-kinase complex. Vps10, a yeast mannose-6 phosphate receptor, acts as a sorting receptor for both CPY and PrA and cycles between the Golgi and endosomes (Westphal *et al.*, 1996). However, in a *vps10Δ* mutant, while most CPY does not mature, ~85% of PrA still matures. In *vps38Δ* cells, Vps10 mislocalizes from endosomes to the vacuolar membrane (Burda *et al.*, 2002). Retromer components Vps5 and Vps17 also mislocalize to the cytoplasm in *vps38Δ* cells. Taken together, this result suggests that the retromer is required for Vps10 cycling between Golgi and endosome and that disrupting this cycling affects CPY maturation. Mrl1, a relatively uncharacterized homolog of mammalian mannose-6 phosphate receptors, was identified as a partially redundant PrA sorting receptor. Simultaneous mutation of Vps10 and Mrl1 causes a much larger PrA sorting defect than mutation of Vps10 alone (Whyte and Munro, 2001). This result raised the possibility that Mrl1 will localize correctly in

*vps38Δ* and *vps30Δ* cells, but will mislocalize in a Vps34 mutant, suggesting a model in which Mrl1 recycles to the Golgi in a retromer-independent manner and in a manner that is independent of Vps30 and Vps38. However, I tested the localization of Mrl1 in PI 3-kinase complex mutants and found that Mrl1 localized normally in wild-type and *atg14Δ* cells, but mislocalized to the vacuole in *vps38Δ, vps30Δ*, *vps15Δ*, and *vps34Δ* cells (Figure 3.8). This result demonstrates that instead of being complex II-independent, Mrl1 localization depends on PI 3-kinase complex II.

In addition to temperature sensitive growth at 37°C and defects in Proteinase A and B maturation, *vps34Δ* and *vps15Δ* cells, but not *vps30Δ*, *vps38Δ*, or *atg14Δ* cells also exhibit a defect in pheromone signaling (Slessareva *et al.*, 2006) that could potentially be a role for a third yeast PI 3-kinase complex. Similarly, neither Vps30 or Vps38 are required for delivery of CPS to the vacuolar lumen (Burda *et al.*, 2002), suggesting that ESCRT function may be a complex I and II-independent role for Vps34. As further evidence, I determined that the ESCRT and PI3P-dependent internalization of the vacuolar cationic amino acid transporter Ypq1 (Zhu *et al.*, 2017) occurs in a complex I and II-independent manner (Figure 3.9). While Ypq1 is not internalized into the vacuole lumen in *vps34Δ* and *vps15Δ* cells, Ypq1 internalization is not affected in *vps30Δ*, *vps38Δ*, *atg14Δ*, and *vps38Δatg14Δ* cells.

Vps34 localization to autophagosomes is Atg14-dependent and the localization to puncta, which are postulated to be endosomes is Vps38-dependent. However, in addition to localizing to endosomes and autophagosomes, Vps34 also localizes on the

vacuole (Obara *et al.*, 2006). We hypothesize that a third PI 3-kinase complex could be required for Vps34 localization to the vacuole and might be required for the PI3P-dependent internalization of Ypq1, which occurs on the vacuole (Zhu *et al.*, 2017).

**A method of identifying the members of a third PI 3-kinase complex**

Identifying the members of a potential third PI 3-kinase regulatory complex is likely to be difficult and may require both biochemical and genetic approaches. Candidates for members of a third PI 3-kinase regulatory complex can be identified biochemically via immunoprecipitation of Vps34 and/or Vps15 and mass spectrometry of their interactors. A similar approach was recently used to identify the novel complex I interactor, Atg38 (Araki *et al.*, 2013). Immunoprecipitation of Vps34 and Vps15 and mass spectrometry of their interactors has also been performed by other groups (Graef *et al.*, 2013). Genetically, there are a number of ways one might narrow down candidates for members of a third PI 3-kinase regulatory complex. In my experience, *vps34Δ* and *vps15Δ* cells grow much slower than *vps30Δ*, *vps38Δ*, or *atg14Δ* cells. Thus, it is possible that a member of a third PI 3-kinase complex would exhibit a synthetic growth defect with Vps30. A member of a third PI 3-kinase complex would also likely be defective in a PI3P-dependent process that is independent of complex I and II, for example, a defect in pheromone signaling (Slessareva *et al.*, 2006) and/or ESCRT function (Burda *et al.*, 2002; Zhu *et al.*, 2017). Some genetic screens have identified mutations that disrupt ESCRT function. These mutants include the class E Vps mutants (Raymond *et al.*, 1992), which have been characterized as being defective for ESCRT function (Coonrod and Stevens, 2010). Additionally, a recent screen identified mutants

defective for PI3P and ESCRT-dependent Ypq1 degradation (Zhu *et al.*, 2017). Combining published biochemical and genetic data is potentially a powerful method of identifying members of a third PI 3-kinase complex, though there are no obvious candidates from published data. Additionally, the possibility that Vps34 and Vps15 can function in a binding partner-independent manner cannot be discounted.

**Testing hyperactive Vps34 mutants in mammalian cells**

Our studies have revealed that hyperactive Vps34 impacts some downstream pathways in yeast cells. Similarly, it will be informative to test the downstream effects of elevating PI3P in mammalian systems using hyperactive PIK3C3, the mammalian Vps34 homolog. Interestingly, despite the importance of PIK3C3 in a number of cellular processes, to my knowledge, there are not any well-documented instances of mutations in PIK3C3 that cause disease in humans. The lack of disease-associated mutations in PIK3C3 may be due to the fact that its proper function is critical for cellular homeostasis. Homozygous PIK3C3 null mice are embryonic lethal between E7.5 and E8.5 (Zhou *et al.*, 2011). Additionally, cell-type specific Cre-lox-mediated knockout of PIK3C3 leads to profound defects in cellular function of many cell types, including heart and skeletal muscle (Jaber *et al.*, 2012; Reifler *et al.*, 2014), sensory and pyramidal neurons (Zhou *et al.*, 2010; Wang *et al.*, 2011), T cells (Willinger and Flavell, 2012), kidney podocytes (Bechtel *et al.*, 2013), and liver cells (Jaber *et al.*, 2012). Inhibition of PIK3C3 has been proposed as a potential treatment for some types of cancer (Miaczynska and Zerial, 2002; Noman *et al.*, 2020), though PIK3C3 inhibitors are only in preclinical evaluation (Mulcahy Levy and Thorburn, 2020).

Despite the limited disease-relevance of PIK3C3, studying the downstream effects of using hyperactive PIK3C3 to elevate PI3P in mammalian systems is critical to understanding the role PI3P plays in regulating PI3P-dependent processes. From a published sequence alignment of yeast Vps34 with PIK3C3 (Miller *et al.*, 2010), the hyperactive mutants R283, A287, and Y501 in yeast Vps34 correspond with K272, S276, and Y492 in human PIK3C3. With Y501/Y492 being conserved and R283/K272 maintaining a basic side chain, it is likely that these mutations in human PIK3C3 will elevate PI3P levels in mammalian cells. Intriguingly, the fact that the negatively charged hyperactive A287D mutant in yeast Vps34 corresponds to S276 in human PIK3C3 raises the possibility that S276 has evolved as a phosphosite that regulates PIK3C3 activity. This possibility can be tested mammalian systems. Because many of the PI3P-dependent processes we tested in yeast are well-conserved in mammalian systems, including retrograde transport, ESCRT, and autophagy, if these mutations in PIK3C3 are hyperactive, we can test whether elevating PI3P has similar or different effects in yeast and mammalian systems.

Yeast Vps34 also has some homology with the helical and kinase domains of the mammalian $PI(4,5)P_2$ 3-kinases p110α (PIK3CA), p110β (PIK3CB), and p110γ (PIK3CG) that catalyze the phosphorylation of $PI(4,5)P_2$ to $PI(3,4,5)P_3$ (Miller *et al.*, 2010). p110α is of particular interest because multiple somatic mutations that activate p110α are associated with colorectal (Samuels *et al.*, 2004) and other forms of cancer (reviewed in (Samuels and Waldman, 2010)). Interestingly, using a sequence alignment of yeast Vps34 with p110α (Miller *et al.*, 2010), we noted that the hyperactive E505

mutant in yeast Vps34 identified in our screen is conserved as E674 in p110α. It is possible that mutation of E674 will activate mammalian p110α. Indeed, mutations at E674 in p110α have been identified in the COSMIC (catalogue of somatic mutations in cancer) database. However, we also generated mutations in yeast Vps34 at residues that correspond with mutations in human p110α that were listed multiple times in the COSMIC database, yet none of these mutants increased PI3P levels (Figure 3.10). This result suggests that the catalytic control of yeast Vps34 and mammalian p110α may differ significantly.

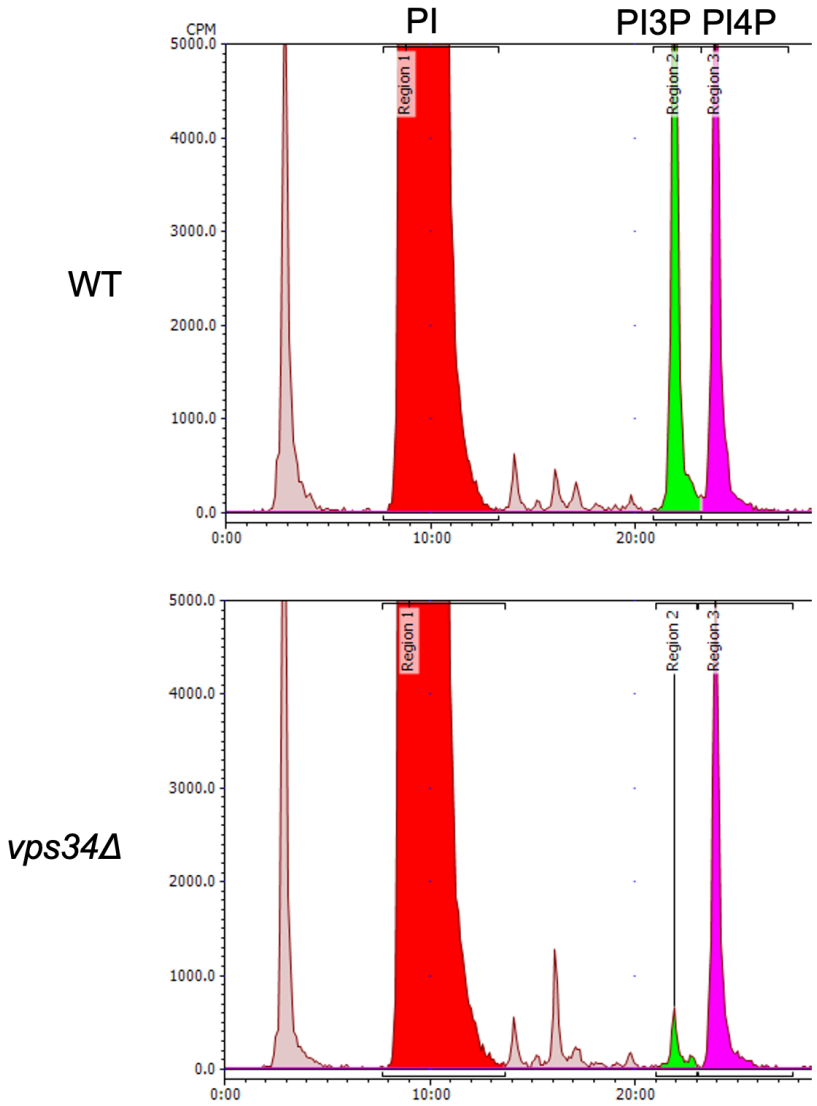


**Figure 3.1: Knockout of Vps34 may not lead to a complete loss of PI3P in yeast.** Comparing elution profiles of PPI lipids separated by anion exchange chromatography between wild-type and *vps34Δ* yeast cells. In *vps34Δ* cells, a small peak elutes at the same location where the PI3P peak elutes in wild-type cells. This small peak contains approximately 6% of the material contained in wild-type cells. Peaks are truncated at 5000 cpm so that all peaks can be visualized.

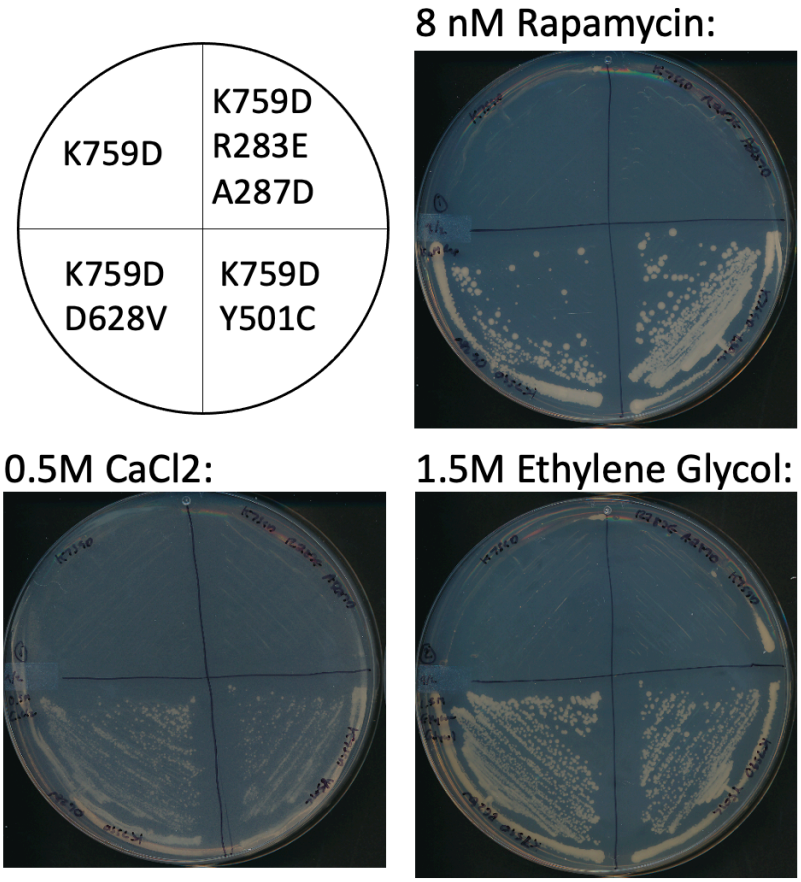


**Figure 3.2: Only some hyperactive Vps34 mutations rescue growth of the K759D mutant.** The Vps34-K759D mutant exhibits a growth defect at 33°C when grown on 8 nM Rapamycin, 0.5M $CaCl_2$ or on 1.5M Ethylene Glycol. This growth defect is rescued by adding mutations near the active site such as Y501C or D628V, but not R283E and A287D.

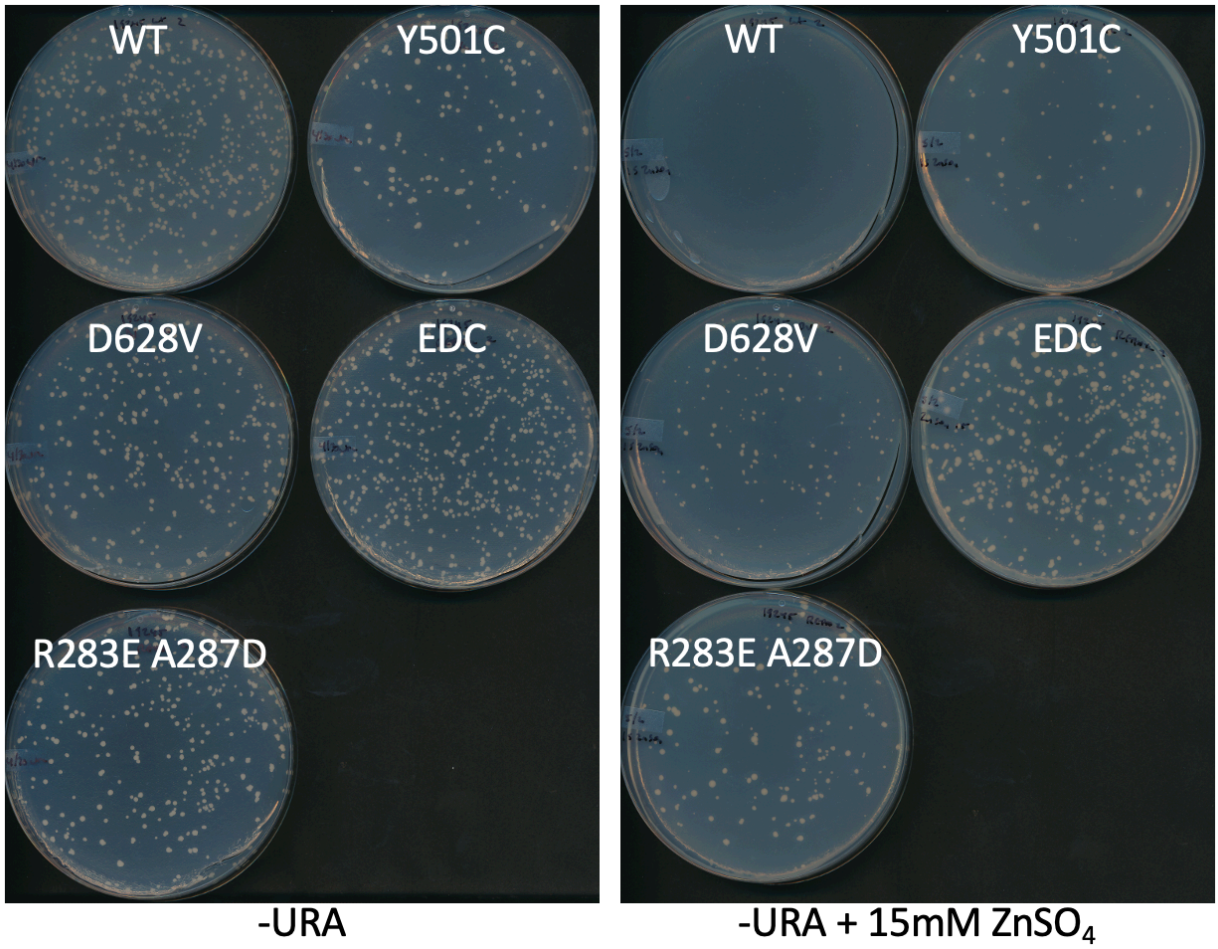


**Figure 3.3: All hyperactive Vps34 mutants tested are able to rescue growth of a *vps30Δ* yeast strain on 15mM $ZnSO_4$ at 33°C.** *vps30Δvps34Δ* cells were transformed with a wild-type or mutant Vps34 plasmid and plated on Sc-URA plates (left). These cells were replica plated to Sc-URA plates containing 15mM $ZnSO_4$ and grown at 33°C (right). While cells containing the wild-type Vps34 plasmid exhibit a growth defect, this growth defect is rescued by all hyperactive Vps34 mutants that were tested: Y501C, D628V, R283E A287D, and Vps34-EDC.

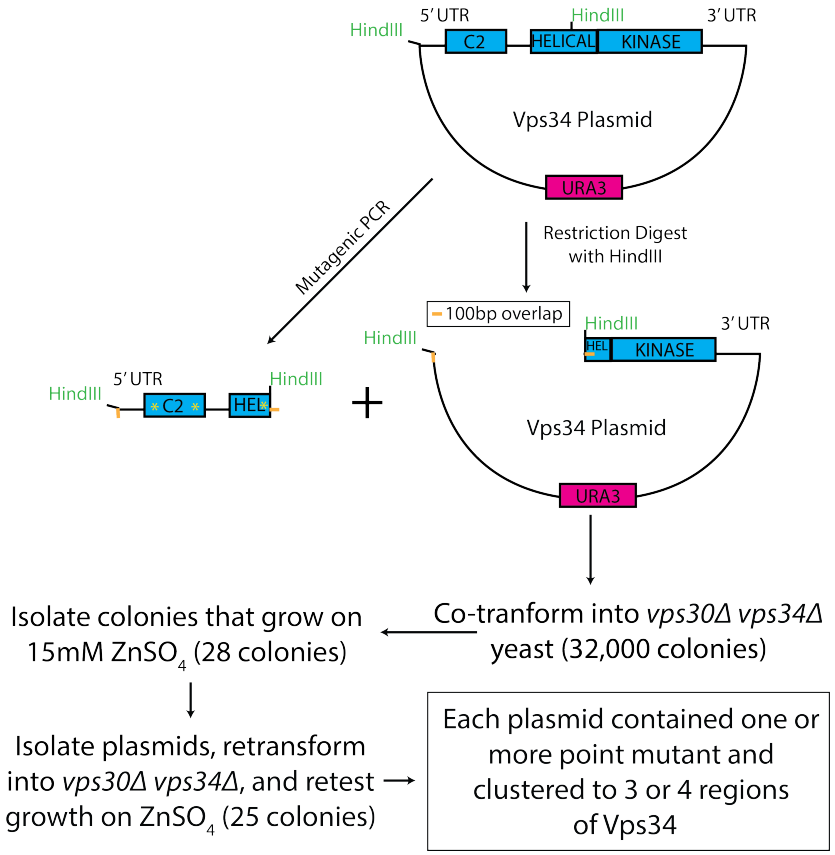


**Figure 3.4: New screening conditions for hyperactive mutations in Vps34.** A screen for hyperactive mutations in Vps34 was designed to identify mutants that rescue growth of *vps30Δ* cells. The N-terminal half of Vps34 was PCR amplified using mutagenic Taq DNA polymerase and a Vps34 plasmid was cut with restriction enzyme, HindIII, to remove the region of Vps34 that was mutated. The plasmid backbone and mutated PCR fragment were co-transformed into *vps30Δvps34Δ* cells. Two days following co-transformation, colonies were replica plated to plates containing 15 mM $ZnSO_4$ and grown at 33°C. Mutant Vps34 plasmids were isolated from colonies that rescued growth on $ZnSO_4$ at 33°C and retransformed into *vps30Δvps34Δ* cells to confirm rescued growth on $ZnSO_4$ at 33°C. Sanger sequencing was used to identify the mutations present in isolated plasmids.

| PCR Reaction number of each clone | Mutations Present | | |
|---|---|---|---|
| 4 | A->G K265R | T->C S445S | |
| 10 | G->A E279K | | |
| 1 | A->G R283G | | |
| 3 | A->G R283G | A->G E464G | |
| 5 | A->G E285G | T->C 5'UTR | |
| 1 | A->G R286G | A->G E26E | G->A P74P |
| 3 | A->G R286G | | |
| 4 | A->G R286G | G->A R195R | |
| 13 | A->G R286G | | |
| 6 | T->C L345S | | |
| 8 | T->C L350S | T->C S354P | |
| 9 | A->G E353G | A->G T136A | A->G D241G |
| 1 | A->G E355G | | |
| 10 | G->A E355K | A->T T431S | |
| 10 | A->G R356G | | |
| 7 | T->C S386P | A->G Y148C | |
| 4 | A->G R388G | | |
| 6 | A->G R388G | T->C F266L | |
| 10 | A->G R388G | | |
| 15 | A->G R388G | | |
| 2 | T->C S389P | C->T 5'UTR | |
| 5 | A->G Q409R | G->A V58V | |
| 5 | A->G E417G | | |
| 3 | C->A Q633K | | |
| 9 | G->A E644K | | |

**Figure 3.5: Mutations in Vps34 plasmids that were isolated from colonies that rescue growth of *vps30Δ* cells grown at 33°C on plates containing 15mM $ZnSO_4$.** Sanger sequencing was used to identify the mutations present in 25 Vps34 plasmids isolated from colonies that rescue growth of *vps30Δ* cells grown at 33°C on plates containing 15mM $ZnSO_4$. If multiple mutations were present in a plasmid, the mutation though most likely to be causative was listed on the left. Mutations that did not affect the Vps34 amino acid sequence are highlighted in green. Mutations highlighted in orange, yellow, and blue indicate mutations that were isolated more than once and/or are within 3 amino acids of another isolated mutation. Instances of the same mutation isolated from different PCR reactions indicate independent generation of the mutation, whereas instances of the same mutation isolated from the same PCR reaction are correlated.

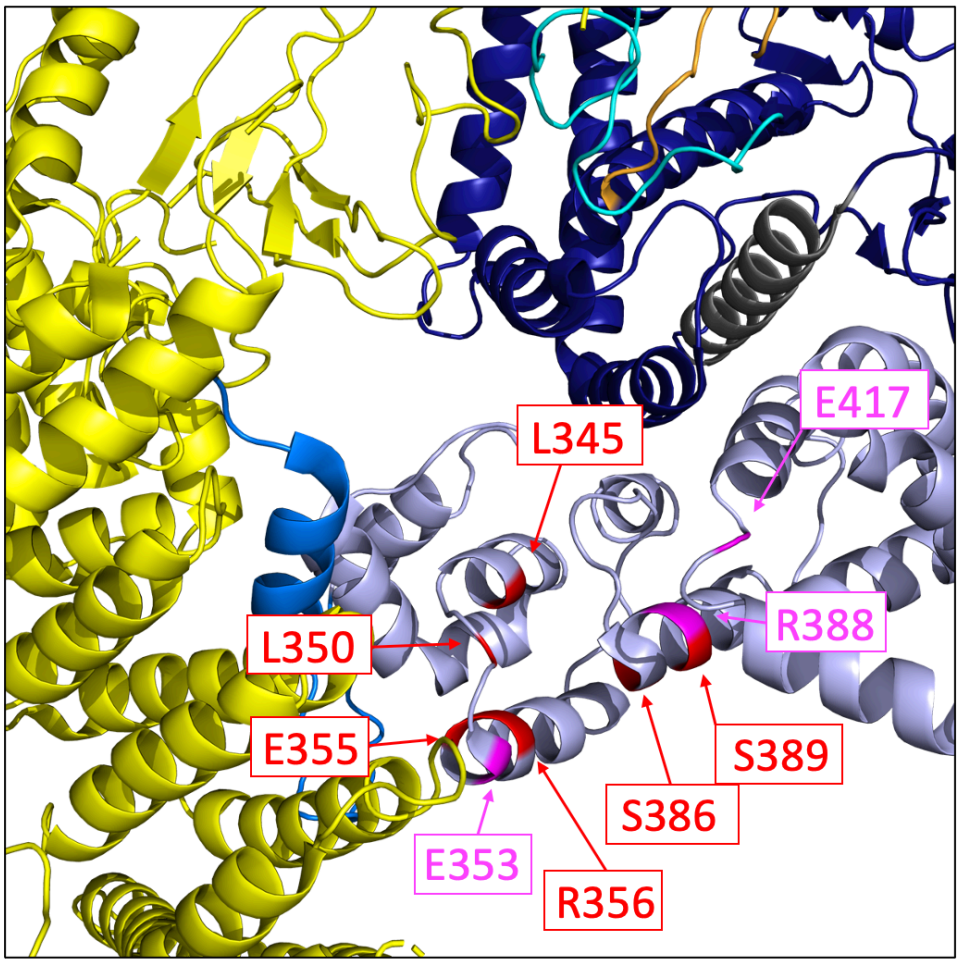


**Figure 3.6: Crystal structure of the helical and kinase domains of Vps34, indicating residues identified in the hyperactive Vps34 mutant screen.** Some of the residues identified in the screen for hyperactive Vps34 alleles are colored in red (L345, L350, E355, R356, S386, S389), while residues that were tested for changes in PPI lipid levels are colored in pink (E353, R388, E417). The alpha-C helix (gray) of the kinase domain (dark blue), the activation (cyan) and catalytic (orange) loops of Vps34 as well as the helical domain (light blue), and the alpha-helix N-terminal to the helical domain of Vps34 (neutral blue) are indicated. Vps15 is shown in yellow.

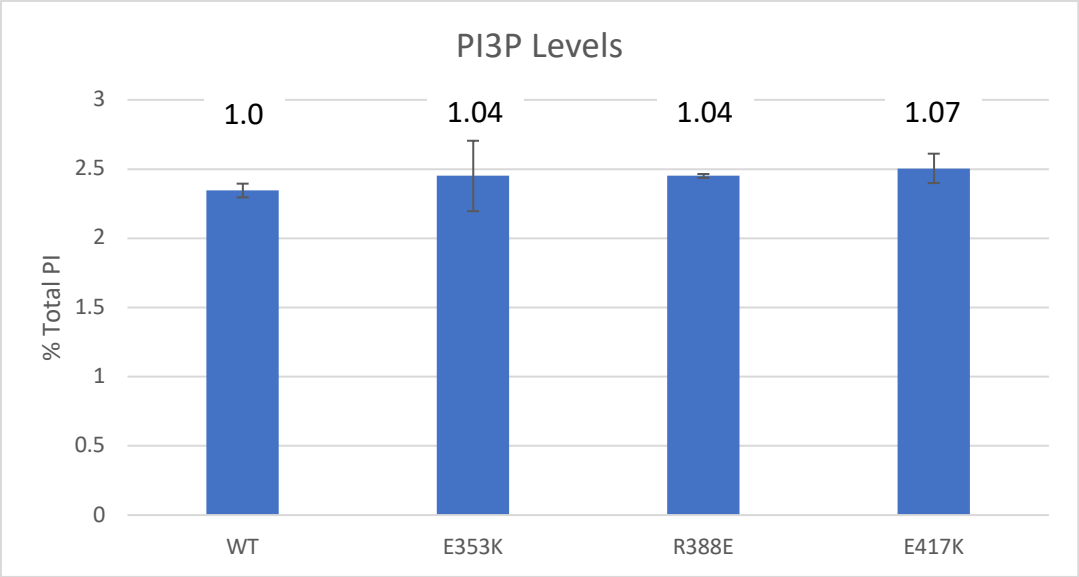


**Figure 3.7: Vps34 mutations based on mutants obtained from a hyperactive mutant screen do not elevate PI3P.** *vps34Δ* cells were transformed with a wild-type or mutant pRS416-Vps34 plasmid. PPI lipid levels were measured by metabolically labeling cells with myo-$^{3}$H-inositol for 16 h, harvesting cells, and separating PPI lipid head groups by anion exchange and HPLC. n=2. Error bars indicate standard deviation.

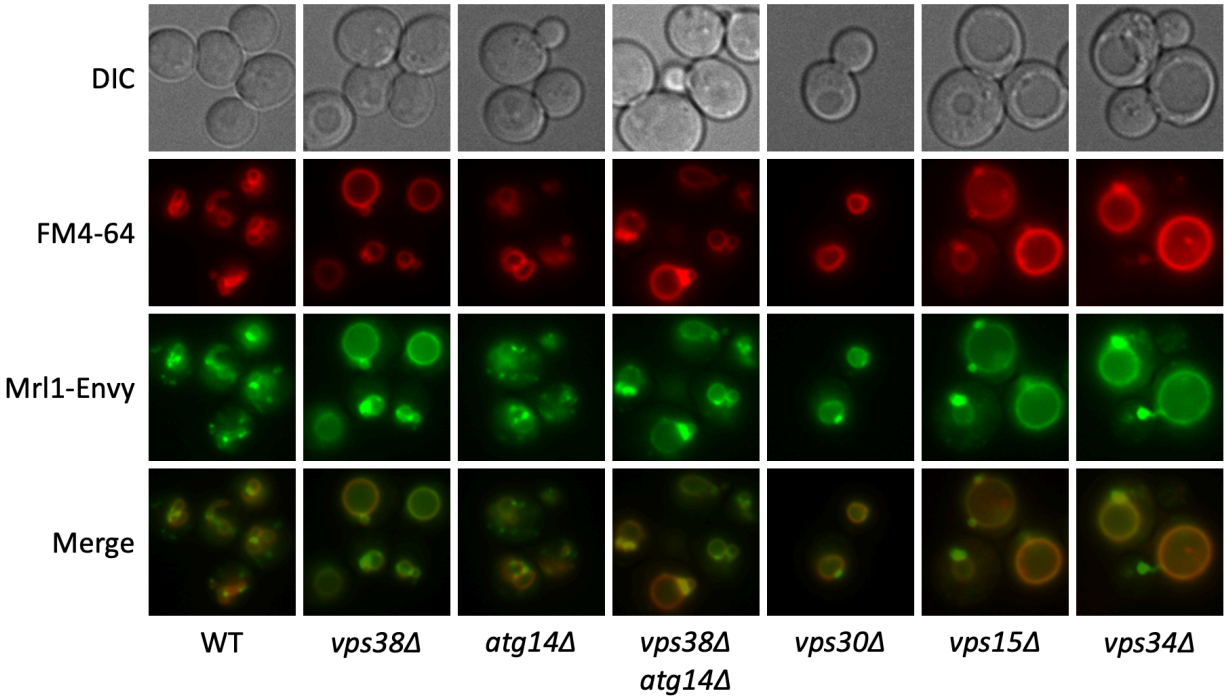


**Figure 3.8: PI 3-kinase complex II is required for proper Mrl1-Envy localization.** The mannose 6-phosphate receptor Mrl1-Envy localizes to Golgi in wild-type cells. Loss of PI 3-kinase activity in *vps15Δ* and *vps34Δ* cells resulted in a mislocalization of Mrl1-Envy to the vacuole. While Mrl1-Envy localizes normally in *atg14Δ* cells, it mislocalizes to the vacuole in *vps30Δ* and *vps38Δ* cells, indicating that its recycling depends on PI 3-kinase complex II.

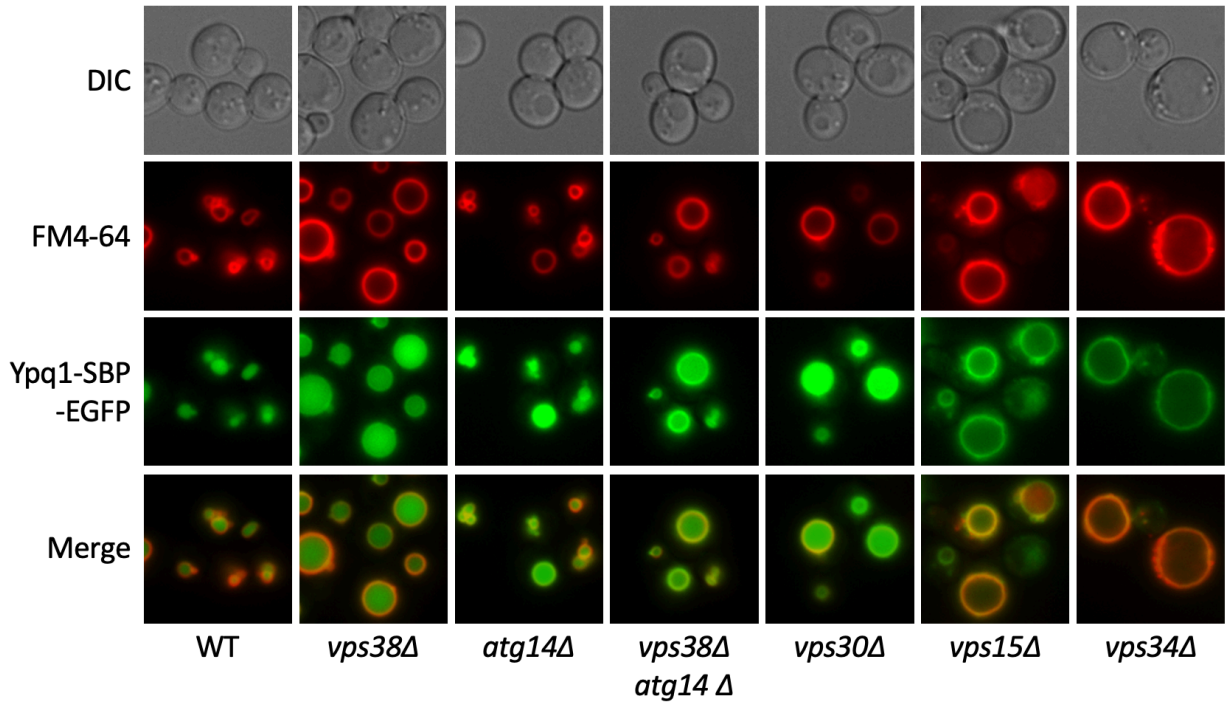


**Figure 3.9: While Vps34 and Vps15 are necessary for internalization of Ypq1-SBP-EGFP, neither PI 3-kinase complex I or II is required.** Ypq1 is a vacuolar cationic amino acid transporter. When tagged with SBP-EGFP, Ypq1-SBP-EGFP is constitutively sorted into the vacuole lumen in an ESCRT-dependent manner (Zhu *et al.*, 2017). In the absence of Vps34 or Vps15, Ypq1-SBP-EGFP is not delivered to the vacuole lumen, remaining on the vacuole membrane, suggesting that PI3P is required for this process. However, simultaneously disrupting PI 3-kinase complexes I and II by mutating Vps30 or Vps38 and Atg14 simultaneously did not affect the vacuole lumen localization of Ypq1-SBP-EGFP, suggesting a complex I and II-independent role for Vps34 and Vps15.

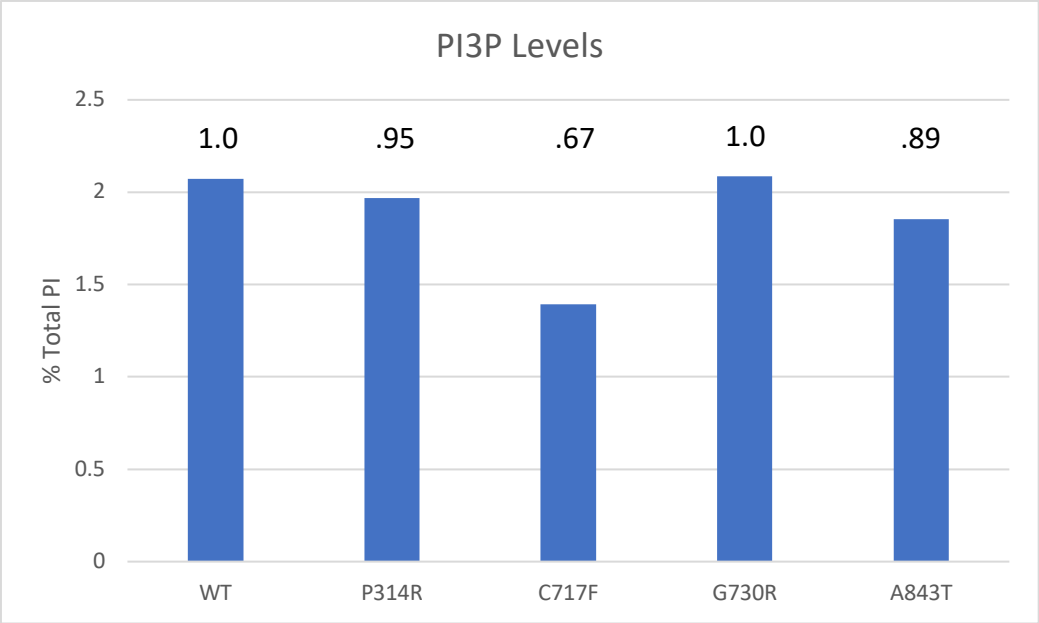


**Figure 3.10: Yeast Vps34 mutations at residues that correspond with mutations in human p110α that were listed multiple times in the COSMIC database do not elevate PI3P.** P314, C717, G730, and A843 in yeast Vps34 correspond with P539, C901, G914, and A1035 in human p110α. *vps34Δ* cells were transformed with a wild-type or mutant pRS416-Vps34 plasmid. PPI lipid levels were measured by metabolically labeling cells with myo-$^{3}$H-inositol for 16 h, harvesting cells, and separating PPI lipid head groups by anion exchange and HPLC. n=1.

**References**

Araki, Y., Ku, W.C., Akioka, M., May, A.I., Hayashi, Y., Arisaka, F., Ishihama, Y., and Ohsumi, Y. (2013). Atg38 is required for autophagy-specific phosphatidylinositol 3-kinase complex integrity. J Cell Biol *203*, 299-313.

Bechtel, W., Helmstadter, M., Balica, J., Hartleben, B., Kiefer, B., Hrnjic, F., Schell, C., Kretz, O., Liu, S., Geist, F., et al. (2013). Vps34 deficiency reveals the importance of endocytosis for podocyte homeostasis. J Am Soc Nephrol *24*, 727-743.

Burda, P., Padilla, S.M., Sarkar, S., and Emr, S.D. (2002). Retromer function in endosome-to-Golgi retrograde transport is regulated by the yeast Vps34 PtdIns 3-kinase. J Cell Sci *115*, 3889-3900.

Cafferkey, R., Young, P.R., McLaughlin, M.M., Bergsma, D.J., Koltin, Y., Sathe, G.M., Faucette, L., Eng, W.K., Johnson, R.K., and Livi, G.P. (1993). Dominant missense mutations in a novel yeast protein related to mammalian phosphatidylinositol 3-kinase and VPS34 abrogate rapamycin cytotoxicity. Mol Cell Biol *13*, 6012-6023.

Coonrod, E.M., and Stevens, T.H. (2010). The yeast vps class E mutants: the beginning of the molecular genetic analysis of multivesicular body biogenesis. Mol Biol Cell *21*, 4057-4060.

Duex, J.E., Tang, F., and Weisman, L.S. (2006). The Vac14p-Fig4p complex acts independently of Vac7p and couples PI3,5P2 synthesis and turnover. J Cell Biol *172*, 693-704.

Graef, M., Friedman, J.R., Graham, C., Babu, M., and Nunnari, J. (2013). ER exit sites are physical and functional core autophagosome biogenesis components. Mol Biol Cell *24*, 2918-2931.

Jaber, N., Dou, Z., Chen, J.S., Catanzaro, J., Jiang, Y.P., Ballou, L.M., Selinger, E., Ouyang, X., Lin, R.Z., Zhang, J., et al. (2012). Class III PI3K Vps34 plays an essential role in autophagy and in heart and liver function. Proc Natl Acad Sci U S A *109*, 2003-2008.

Kihara, A., Noda, T., Ishihara, N., and Ohsumi, Y. (2001). Two distinct Vps34 phosphatidylinositol 3-kinase complexes function in autophagy and carboxypeptidase Y sorting in Saccharomyces cerevisiae. J Cell Biol *152*, 519-530.

Lang, M.J., Strunk, B.S., Azad, N., Petersen, J.L., and Weisman, L.S. (2017). An intramolecular interaction within the lipid kinase Fab1 regulates cellular phosphatidylinositol 3,5-bisphosphate lipid levels. Mol Biol Cell.

Miaczynska, M., and Zerial, M. (2002). Mosaic organization of the endocytic pathway. Exp Cell Res *272*, 8-14.

Miller, S., Tavshanjian, B., Oleksy, A., Perisic, O., Houseman, B.T., Shokat, K.M., and Williams, R.L. (2010). Shaping development of autophagy inhibitors with the structure of the lipid kinase Vps34. Science *327*, 1638-1642.

Mulcahy Levy, J.M., and Thorburn, A. (2020). Autophagy in cancer: moving from understanding mechanism to improving therapy responses in patients. Cell Death Differ *27*, 843-857.

Noman, M.Z., Parpal, S., Van Moer, K., Xiao, M., Yu, Y., Viklund, J., De Milito, A., Hasmim, M., Andersson, M., Amaravadi, R.K., et al. (2020). Inhibition of Vps34 reprograms cold into hot inflamed tumors and improves anti-PD-1/PD-L1 immunotherapy. Sci Adv *6*, eaax7881.

Obara, K., Sekito, T., and Ohsumi, Y. (2006). Assortment of phosphatidylinositol 3-kinase complexes--Atg14p directs association of complex I to the pre-autophagosomal structure in Saccharomyces cerevisiae. Mol Biol Cell *17*, 1527-1539.

Raymond, C.K., Howald-Stevenson, I., Vater, C.A., and Stevens, T.H. (1992). Morphological classification of the yeast vacuolar protein sorting mutants: evidence for a prevacuolar compartment in class E vps mutants. Mol Biol Cell *3*, 1389-1402.

Reifler, A., Li, X., Archambeau, A.J., McDade, J.R., Sabha, N., Michele, D.E., and Dowling, J.J. (2014). Conditional knockout of pik3c3 causes a murine muscular dystrophy. Am J Pathol *184*, 1819-1830.

Samuels, Y., and Waldman, T. (2010). Oncogenic mutations of PIK3CA in human cancers. Curr Top Microbiol Immunol *347*, 21-41.

Samuels, Y., Wang, Z., Bardelli, A., Silliman, N., Ptak, J., Szabo, S., Yan, H., Gazdar, A., Powell, S.M., Riggins, G.J., et al. (2004). High frequency of mutations of the PIK3CA gene in human cancers. Science *304*, 554.

Schu, P.V., Takegawa, K., Fry, M.J., Stack, J.H., Waterfield, M.D., and Emr, S.D. (1993). Phosphatidylinositol 3-kinase encoded by yeast VPS34 gene essential for protein sorting. Science *260*, 88-91.

Slessareva, J.E., Routt, S.M., Temple, B., Bankaitis, V.A., and Dohlman, H.G. (2006). Activation of the phosphatidylinositol 3-kinase Vps34 by a G protein alpha subunit at the endosome. Cell *126*, 191-203.

Stack, J.H., Herman, P.K., Schu, P.V., and Emr, S.D. (1993). A membrane-associated complex containing the Vps15 protein kinase and the Vps34 PI 3-kinase is essential for protein sorting to the yeast lysosome-like vacuole. EMBO J *12*, 2195-2204.

Wang, L., Budolfson, K., and Wang, F. (2011). Pik3c3 deletion in pyramidal neurons results in loss of synapses, extensive gliosis and progressive neurodegeneration. Neuroscience *172*, 427-442.

Westphal, V., Marcusson, E.G., Winther, J.R., Emr, S.D., and van den Hazel, H.B. (1996). Multiple pathways for vacuolar sorting of yeast proteinase A. J Biol Chem *271*, 11865-11870.

Whyte, J.R., and Munro, S. (2001). A yeast homolog of the mammalian mannose 6-phosphate receptors contributes to the sorting of vacuolar hydrolases. Curr Biol *11*, 1074-1078.

Willinger, T., and Flavell, R.A. (2012). Canonical autophagy dependent on the class III phosphoinositide-3 kinase Vps34 is required for naive T-cell homeostasis. Proc Natl Acad Sci U S A *109*, 8670-8675.

Zhou, X., Takatoh, J., and Wang, F. (2011). The mammalian class 3 PI3K (PIK3C3) is required for early embryogenesis and cell proliferation. PLoS One *6*, e16358.

Zhou, X., Wang, L., Hasegawa, H., Amin, P., Han, B.X., Kaneko, S., He, Y., and Wang, F. (2010). Deletion of PIK3C3/Vps34 in sensory neurons causes rapid neurodegeneration by disrupting the endosomal but not the autophagic pathway. Proc Natl Acad Sci U S A *107*, 9424-9429.

Zhu, L., Jorgensen, J.R., Li, M., Chuang, Y.S., and Emr, S.D. (2017). ESCRTs function directly on the lysosome membrane to downregulate ubiquitinated lysosomal membrane proteins. Elife *6*.

# CHAPTER IV

## Methods[3]

### Yeast strains, plasmids, and media

Yeast cultures were grown in yeast extract peptone dextrose (YEPD) containing 1% yeast extract, 2% peptone and 2% dextrose or synthetic complete (SC) media lacking the indicated amino acid(s) at 24°C unless specified. For nitrogen starvation, yeast strains were cultured in SD-N medium containing 0.19% yeast nitrogen base, 2% glucose, and vitamins and lacking amino acids and ammonium sulfate (Formedium). Yeast strains and plasmids are listed in Tables 4.1 and 4.2, respectively.

### Phosphoinositide lipid labeling and quantification

Yeast *myo*-$^{3}$H-inositol labeling and total cellular phosphoinositide extraction, deacylation, and measurements were performed as described (Bonangelino *et al.*, 2002; Duex *et al.*, 2006). Briefly, cells were grown in the appropriate SC media to mid-log phase, washed with SC media lacking inositol, and used to inoculate 5 mL of SC media lacking inositol and containing 50 µCi of *myo*-$^{3}$H-inositol. Cells were grown for 16 h shaking at 24°C, harvested by centrifugation, and resuspended in 100 µL inositol-free

[3] This chapter is adapted from a published paper: Steinfeld, N., Lahiri, V., Morrison, A., Metur, S.P., Klionsky, D.J., and Weisman, L.S. (2021). Elevating PI3P drives select downstream membrane trafficking pathways. Mol Biol Cell 32, 143-156.

media. For hyperosmotic shock, 100 µL of inositol-free media with 1.8M NaCl was added to the sample for 10 min. For basal conditions, 100 µL of inositol-free media was added to the 100-µL sample. Cells were then killed via addition of ice-cold 4.5% perchloric acid. Cells were lysed using a mini-beadbeater for 2 min, then immediately put on ice for 2 min. This was repeated two more times for a total lysis time of 6 min. Cell extracts were centrifuged at 16,000 x g for 10 min at room temperature. Pellets were washed with 1 mL of 100 mM EDTA pH 8.0 then resuspended in 50 µL distilled deionized water ($ddH_2O$). Samples were deacylated with 1 mL methylamine reagent for 1 h at 55°C, then dried in a speed vac concentrator. Pellets were resuspended in 300 µL of $ddH_2O$, mixed with 300 µL of a 20:4:1 mixture of butanol/ethyl ether/formic acid ethyl ester, vortexed, and centrifuged for 2 min at 16,000 x g. The lower aqueous phase was then transferred to a fresh microcentrifuge tube. This sample extraction was repeated, and samples were dried in a speed vac concentrator. Dried samples were resuspended in 60 µL $ddH_2O$ and analyzed by HPLC using a SAX anion exchange column. Buffer A ($ddH_2O$) and Buffer B (1 M $(NH_4)_2HPO_4$, pH 3.8) are used to generate the following gradients run at a 1 mL/min flow rate: 1% Buffer B for 5 min, 1–20% Buffer B for 44 min, 20–50% Buffer B for 3.75 min, and 50% Buffer B for 8 min. To quantify scintillation counts from each sample, the raw counts in each peak were expressed as a percentage of total phosphatidylinositol-related species, calculated from summation of the counts of the five glycero-inositol peaks present in yeast (PI, PI3P, PI4P, $PI(3,5)P_2$, and $PI(4,5)P_2$). Background scintillation counts were calculated from adjacent regions and subtracted from all peaks.

**Screen for hyperactive Vps34 mutants**

Schematic of screen shown in Figure 2.3A. A pRS416-Vps34-K759D plasmid was gapped by digesting with XhoI restriction enzyme. The gapped plasmid was purified by agarose electrophoresis followed by DNA purification (Qiagen). Primers AM30 (5-GAATTCACTATTGTGGATGCCGTATCTTCG-3) and AM31 (5-GGGTAACGCCAGGGTTTTCC-3) were used to PCR amplify the gapped region along with approximately 100 bases upstream and downstream of the XhoI restriction sites using error-prone Taq DNA polymerase (Invitrogen). Gapped plasmid backbone and mutated PCR product were co-transformed into *vps34*Δ cells. Two days following co-transformation, colonies were replica plated to plates containing 10 nM rapamycin and grown at 33°C. From an estimated 12,000 colonies, mutant Vps34 plasmids were isolated from 59 single colonies that rescued growth on rapamycin at 33°C and amplified in *E. coli*. When mutant plasmids were retransformed into *vps34*Δ cells, 33 of the 59 plasmids rescued growth on rapamycin at 33°C. Sanger sequencing of those 33 plasmids revealed that 11 plasmids contained a mutation at the D759 locus. The 22 remaining independent mutants indicated 9 unique point mutations. Of those 9 mutations, changes at 5 of them elevated PI3P levels.

**Fluorescence microscopy**

Yeast cells were grown in the appropriate SC media to mid-log phase. Live cell images were obtained on a DeltaVision Restoration system (Applied Precision) using an inverted epifluorescence microscope (IX-71; Olympus) with a charge-coupled device camera (Cool-SNAP HQ; Photometrics) and processed in FIJI. When vacuoles were

visualized, cells were labeled with 12 µg FM 4-64 in 250 µl media for 1 h, then washed twice and grown in 5 ml fresh SC media for one doubling time (2-3 h) (Vida and Emr, 1995).

**Quantification of fluorescence microscopy images**

Quantification of the number of vacuole lobes, the number of cells with Atg27-2xGFP visible on the vacuole, the number of GFP-Atg8 puncta, and the colocalization of GFP-Atg8 puncta with Atg18-RFP puncta was performed by a scorer who was blinded to the genotype of the cells being quantified.

The amount of Envy-Vps34, Fab1-Envy, or Fig4-Envy that colocalized with the vacuole was measured using FIJI. Background fluorescence was subtracted using a 5.0 pixel rolling ball radius in the green channel and a 10.0 pixel rolling ball radius in the FM 4-64 channel. FM 4-64 images were thresholded such that pixels with signal present were set to 1 and pixels without signal present were set to 0 using the Otsu method. Total signal that colocalizes with the vacuole was calculated by multiplying the background subtracted green channel image by the FM 4-64 thresholded image and determining the integrated intensity of the resulting image. The total colocalized green signal was divided by the number of cells in the quantified images to give the green signal intensity on the vacuole per cell.

Colocalization of Atg27-2xGFP with FM 4-64, Sec7-mCherry, or Vps8-mCherry was measured using FIJI. Background fluorescence was subtracted using a 5.0 pixel rolling

ball radius and images were thresholded such that pixels with signal present were set to 1 and pixels without signal present were set to 0. The Otsu method was used, except for Vps8-mCherry where the Renyi Entropy method was used. Total Atg27-2xGFP signal was calculated by multiplying the background subtracted Atg27-2xGFP image by the Atg27-2xGFP thresholded image and determining the integrated intensity of the resulting image. The Atg27-2xGFP signal that colocalized with FM 4-64, Sec7-mCherry, or Vps8-mCherry was calculated by multiplying the Atg27-2xGFP thresholded image and the FM 4-64/Sec7-mCherry/Vps8-mCherry thresholded image. The resulting image was multiplied by the background subtracted Atg27-2xGFP image and integrated intensity of the resulting image was determined. Colocalized Atg27-2xGFP signal was divided by total Atg27-2xGFP signal to calculate percent overlap.

**Western blot analysis**

Yeast cells were grown in the appropriate SC media to mid-log phase. Before harvesting, cells were treated in the appropriate experiment-specific conditions. For Ypq1-GFP and Mup1-GFP degradation assays, cells were washed twice in lysine-free SC media before resuspending in lysine-free SC media or resuspended in SC media containing methionine, respectively (Zhu *et al.*, 2017). For Atg8–PE and GFP-Atg8 assays, cells were shifted to nitrogen-starvation media (-N) for autophagy induction. One OD of cells was harvested, and 100 µL urea lysis buffer was added (1% SDS, 8 M urea, 10 mM Tris, pH 6.8, 10 mM EDTA, 0.01% bromophenol blue, 0.2% β-mercaptoethanol, Roche complete protease inhibitor cocktail). One-half volume of 0.5 mm Zirconia glass beads were added and tubes were vortexed in a micro tube mixer for

10 min at 4°C. Supernatants were transferred to fresh tubes and samples were heated for 10 min at 75°C and run on an SDS polyacrylamide gel. Proteins were transferred to a nitrocellulose membrane at 60V for 16 h. Membranes were blocked in 5% milk before incubation with the indicated primary antibody. Membranes were washed 3 times for 5 min in TBST, incubated in secondary antibodies, washed again, developed with ECL prime (GE Healthcare, Pgk1) or Clarity Max (Bio-Rad, other antibodies), imaged on a Bio-Rad ChemiDoc imager, and quantified using FIJI. For immunoblot analyses, the following antibodies were used: mouse anti-GFP (1:1,000; Roche), mouse anti-Myc (1:1,000; clone 9E10 EMD, Millipore), mouse anti-Pgk1 (1:10,000; Invitrogen), mouse anti-Vph1 (1:1,000; Abcam), rabbit anti-Atg8 (described previously (Huang *et al.*, 2000)), mouse anti-Dpm1 (1:5,000; ThermoFisher), mouse anti-HA (1;1,000; Covance MMS-101P).

**Analysis of Mup1-GFP degradation**

Mup1-GFP levels were normalized to Pgk1. A linear mixed-effects model was used to assess the degradation rate of Mup1-GFP. The logarithmic transformation of Mup1-GFP levels was modelled as a linear function of time and allowed to vary by genotype. Replicate-specific intercepts were included to account for residual correlation between protein levels within the same replicate. A 95% confidence interval of the genotype by time interaction was used to determine whether there were statistically significant differences between wild-type and hyperactive Vps34-EDC.

**Hyperosmotic shock growth assay**

Yeast cells were grown to mid-log phase in SC media and then diluted to equal concentrations. An equal volume of SC media or SC media with 1.8 M NaCl was added to the culture to begin the time-course. ODs were measured immediately following the addition of SC media or SC media with 1.8 M NaCl and then every 4 h for 24 h. The time zero OD measurement for each sample was normalized to 1. A natural logarithmic transformation was applied to the normalized ODs so that exponential growth is represented linearly.

**Real-time quantitative PCR (RT-qPCR)**

Yeast were cultured in the appropriate SC media to mid-log phase and then shifted to nitrogen-starvation media (-N) for 30 min for autophagy induction. Cells were collected and flash frozen in liquid nitrogen. Total RNA was extracted using an RNA extraction kit (Clontech, Nucleo Spin RNA, 740955.250). Reverse transcription was carried out using the High-Capacity cDNA Reverse Transcription Kit (Applied Biosystems/Thermo Fisher Scientific, 4368814). For each sample, 1 µg RNA was used for cDNA synthesis. RT-qPCR was performed using the Radiant SYBR Green Lo-ROX qPCR kit (Alkali Scientific) in a CFX Connect (Bio-Rad, 1855201) real-time PCR machine. For all RT-qPCR experiments, melting curves were run after the PCR cycles to verify primer specificity. Relative gene expression was calculated using the $2^{-\Delta\Delta CT}$ method and normalized as indicated (Livak and Schmittgen, 2001).

**Nitrogen starvation survival assay**

Yeast cells were grown to mid-log phase in SC media. Equal numbers of cells were collected and rinsed twice in nitrogen-starvation media before resuspending in nitrogen-starvation media. Following 1 day and 14 days of nitrogen starvation, equal volumes of culture were serially diluted 1:5 and spotted on SC plates. Plates were imaged following 3 days of yeast growth.

**Table 4.1. Yeast strains used in this study**

| Strain | Genotype | Source |
|---|---|---|
| LWY13700 | *MATa, leu2,3-112, ura3-52, his3-Δ200, trp1-Δ901, lys2-801, suc2-Δ9, vps34Δ::KAN* | (Steinfeld *et al.*, 2021) |
| LWY19264 | *MATalpha, leu2,3-112, ura3-52, his3-Δ200, trp1-Δ901, lys2-801, suc2-Δ9, vps34Δ::KAN, Atg27-2xGFP::HIS3* | (Steinfeld *et al.*, 2021) |
| LWY19252 | *MATalpha, leu2,3-112, ura3-52, his3-Δ200, trp1-Δ901, lys2-801, suc2-Δ9, vps34Δ::KAN, Atg27-2xGFP::HIS3, snx4Δ::HYG* | (Steinfeld *et al.*, 2021) |
| LWY19306 | *MATa, leu2,3-112, ura3-52, his3-Δ200, trp1-Δ901, lys2-801, suc2-Δ9, vps34Δ::KAN, Atg27-2xGFP::HIS3, Sec7-mCherry::HYG* | (Steinfeld *et al.*, 2021) |
| LWY19358 | *MATa, leu2,3-112, ura3-52, his3-Δ200, trp1-Δ901, lys2-801, suc2-Δ9, vps34Δ::KAN, Atg27-2xGFP::HIS3, Vps8-mCherry::HYG* | (Steinfeld *et al.*, 2021) |
| LWY19146 | *MATalpha, leu2,3-112, ura3-52, his3-Δ200, trp1-Δ901, lys2-801, suc2-Δ9, vps34Δ::HYG* | (Steinfeld *et al.*, 2021) |
| LWY19144 | *MATa, leu2,3-112, ura3-52, his3-Δ200, trp1-Δ901, lys2-801, suc2-Δ9, vps34Δ::HYG, ymr1Δ::HIS3* | (Steinfeld *et al.*, 2021) |
| LWY19450 | *MATa, leu2,3-112, ura3-52, his3-Δ200, trp1-Δ901, lys2-801, suc2-Δ9, vps34Δ::HYG, Atg18-RFP::TRP1* | (Steinfeld *et al.*, 2021) |
| LWY19453 | *MATa, leu2,3-112, ura3-52, his3-Δ200, trp1-Δ901, lys2-801, suc2-Δ9, vps34Δ::HYG, Atg18-RFP::TRP1, vam3Δ::NAT* | (Steinfeld *et al.*, 2021) |
| LWY7235 | *MATa, leu2,3-112, ura3-52, his3-Δ200, trp1-Δ901, lys2-801, suc2-Δ9* | (Bonangelino *et al.*, 1997) |
| LWY19518 | *MATa, leu2,3-112, ura3-52, his3-Δ200, trp1-Δ901, lys2-801, suc2-Δ9, vps34Δ::KAN, Atg27-2xGFP::HIS3, Sec7-mCherry::HYG* | (Steinfeld *et al.*, 2021) |
| LWY19521 | *MATalpha, leu2,3-112, ura3-52, his3-Δ200, trp1-Δ901, lys2-801, suc2-Δ9, vps34Δ::KAN, Atg27-2xGFP::HIS3, Sec7-mCherry::HYG, vps35Δ::NAT* | (Steinfeld *et al.*, 2021) |
| LWY19503 | *MATalpha, leu2,3-112, ura3-52, his3-Δ200, trp1-Δ901, lys2-801, suc2-Δ9, vps35Δ::NAT* | (Steinfeld *et al.*, 2021) |

**Table 4.2. Yeast plasmids used in this study**

| Plasmid | Description | Source |
|---|---|---|
| pRS416-Vps34 | CEN, URA3 | (Steinfeld *et al.*, 2021) |
| pRS416-Vps34-R283E A287D | CEN, URA3 | (Steinfeld *et al.*, 2021) |
| pRS416-Vps34-Y501C | CEN, URA3 | (Steinfeld *et al.*, 2021) |
| pRS416-Vps34-EDC | CEN, URA3 | (Steinfeld *et al.*, 2021) |
| pRS414-Ypq1-GFP | CEN, TRP1 | Subcloned from (Li *et al.*, 2015) |
| pRS414-Mup1-GFP | CEN, TRP1 | Subcloned from (Lin *et al.*, 2008) |
| pRS414-GFP-Atg8 | CEN, URA3 | (Abeliovich *et al.*, 2003) |
| pRS414-pCup1-GFP-Atg8 | CEN, TRP1 | (Abeliovich *et al.*, 2003) |
| pRS413-GFP-Atg8 | CEN, HIS3 | Subcloned from (Abeliovich *et al.*, 2003) |
| pRS426-GFP-Vps34 | 2μ, URA3 | (Steinfeld *et al.*, 2021) |
| pRS425-Vps15-13xMyc | 2μ, LEU2 | (Steinfeld *et al.*, 2021) |
| pRS416-Vps34-D275K | CEN, URA3 | (Steinfeld *et al.*, 2021) |
| pRS416-Vps34-R283E | CEN, URA3 | (Steinfeld *et al.*, 2021) |
| pRS416-Vps34-A287D | CEN, URA3 | (Steinfeld *et al.*, 2021) |
| pRS416-Vps34-N292D | CEN, URA3 | (Steinfeld *et al.*, 2021) |
| pRS416-Vps34-H322A | CEN, URA3 | (Steinfeld *et al.*, 2021) |
| pRS416-Vps34-E323D | CEN, URA3 | (Steinfeld *et al.*, 2021) |
| pRS416-Vps34-F761Y | CEN, URA3 | (Steinfeld *et al.*, 2021) |
| pRS416-Vps34-I863D | CEN, URA3 | (Steinfeld *et al.*, 2021) |
| pRS416-Vps34- D275K R283E A287D N292D | CEN, URA3 | (Steinfeld *et al.*, 2021) |
| pRS416-Vps34-D275K R283E A287D N292D H322A | CEN, URA3 | (Steinfeld *et al.*, 2021) |
| pRS416-Vps34-K759D | CEN, URA3 | (Steinfeld *et al.*, 2021) |
| pRS416-Vps34-E505G | CEN, URA3 | (Steinfeld *et al.*, 2021) |
| pRS416-Vps34-S506P | CEN, URA3 | (Steinfeld *et al.*, 2021) |
| pRS416-Vps34-D628V | CEN, URA3 | (Steinfeld *et al.*, 2021) |
| pRS416-Vps34-M642V | CEN, URA3 | (Steinfeld *et al.*, 2021) |
| pRS416-5xHA-Vps34 | CEN, URA3 | (Steinfeld *et al.*, 2021) |
| pRS416-5xHA-Vps34-EDC | CEN, URA3 | (Steinfeld *et al.*, 2021) |
| pRS416-Envy-Vps34 | CEN, URA3 | (Steinfeld *et al.*, 2021) |
| pRS416-Envy-Vps34-EDC | CEN, URA3 | (Steinfeld *et al.*, 2021) |
| pRS413-Vps34 | CEN, HIS3 | (Steinfeld *et al.*, 2021) |
| pRS413-Vps34-EDC | CEN, HIS3 | (Steinfeld *et al.*, 2021) |
| pRS416-Fab1-Envy | CEN, URA3 | (Steinfeld *et al.*, 2021) |
| pRS413-Fig4-Envy | CEN, HIS3 | (Steinfeld *et al.*, 2021) |
| pRS416-GFP-Yck3 | CEN, URA3 | (Steinfeld *et al.*, 2021) |
| pRS416-Atg18-GFP | CEN, URA3 | (Rieter *et al.*, 2013) |

## References


Abeliovich, H., Zhang, C., Dunn, W.A., Jr., Shokat, K.M., and Klionsky, D.J. (2003). Chemical genetic analysis of Apg1 reveals a non-kinase role in the induction of autophagy. Mol Biol Cell *14*, 477-490.

Bonangelino, C.J., Catlett, N.L., and Weisman, L.S. (1997). Vac7p, a novel vacuolar protein, is required for normal vacuole inheritance and morphology. Mol Cell Biol *17*, 6847-6858.

Bonangelino, C.J., Nau, J.J., Duex, J.E., Brinkman, M., Wurmser, A.E., Gary, J.D., Emr, S.D., and Weisman, L.S. (2002). Osmotic stress-induced increase of phosphatidylinositol 3,5-bisphosphate requires Vac14p, an activator of the lipid kinase Fab1p. J Cell Biol *156*, 1015-1028.

Duex, J.E., Nau, J.J., Kauffman, E.J., and Weisman, L.S. (2006). Phosphoinositide 5-phosphatase Fig 4p is required for both acute rise and subsequent fall in stress-induced phosphatidylinositol 3,5-bisphosphate levels. Eukaryot Cell *5*, 723-731.

Huang, W.P., Scott, S.V., Kim, J., and Klionsky, D.J. (2000). The itinerary of a vesicle component, Aut7p/Cvt5p, terminates in the yeast vacuole via the autophagy/Cvt pathways. J Biol Chem *275*, 5845-5851.

Li, M., Rong, Y., Chuang, Y.S., Peng, D., and Emr, S.D. (2015). Ubiquitin-dependent lysosomal membrane protein sorting and degradation. Mol Cell *57*, 467-478.

Lin, C.H., MacGurn, J.A., Chu, T., Stefan, C.J., and Emr, S.D. (2008). Arrestin-related ubiquitin-ligase adaptors regulate endocytosis and protein turnover at the cell surface. Cell *135*, 714-725.

Livak, K.J., and Schmittgen, T.D. (2001). Analysis of relative gene expression data using real-time quantitative PCR and the 2(-Delta Delta C(T)) Method. Methods *25*, 402-408.

Rieter, E., Vinke, F., Bakula, D., Cebollero, E., Ungermann, C., Proikas-Cezanne, T., and Reggiori, F. (2013). Atg18 function in autophagy is regulated by specific sites within its beta-propeller. J Cell Sci *126*, 593-604.

Steinfeld, N., Lahiri, V., Morrison, A., Metur, S.P., Klionsky, D.J., and Weisman, L.S. (2021). Elevating PI3P drives select downstream membrane trafficking pathways. Mol Biol Cell *32*, 143-156.

Vida, T.A., and Emr, S.D. (1995). A new vital stain for visualizing vacuolar membrane dynamics and endocytosis in yeast. J Cell Biol *128*, 779-792.

Zhu, L., Jorgensen, J.R., Li, M., Chuang, Y.S., and Emr, S.D. (2017). ESCRTs function directly on the lysosome membrane to downregulate ubiquitinated lysosomal membrane proteins. Elife *6*.